Design & Reliability Assessment of AEA Propulsion Grid

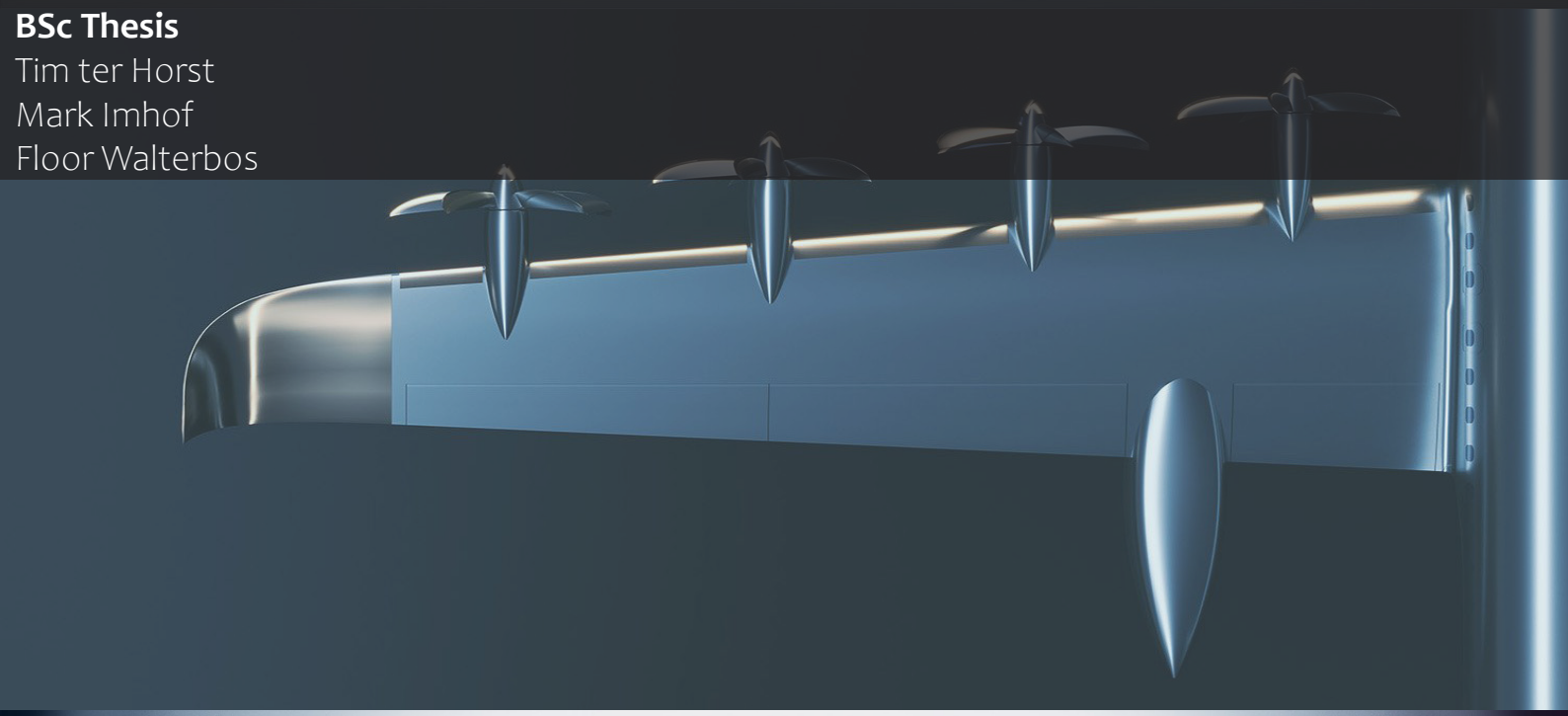

BSc Thesis

Tim ter Horst
Mark Imhof
Floor Walterbos

TU Delft

Bachelor Thesis

Design & Reliability Assessment of AEA Propulsion Grid

by Tim ter Horst, Floor Walterbos, Mark Imhof

to obtain the degree of Bachelor of Science
at the Delft University of Technology,
to be defended privately on Monday 24th of June, 2024 at 02:30 PM.

Student number:	Tim ter Horst	5105714
	Floor Walterbos	4962397
	Mark Imhof	4963040
Project duration:	April 22, 2024 – June 28, 2024	
Thesis committee:	Dr. Ir. M. Ghaffarian Niasar,	TU Delft, supervisor
	Dr. Ir. J. Dong	TU Delft, supervisor
	Prof. Dr. Ir. M. Popov	TU Delft, chair of committee
	Ir. A. Heidary	TU Delft, Advisor

TU Delft

Acknowlegdements

First and foremost, we extend our gratitude to our supervisor, Mohamad Ghaffarian Niasar, for his unwavering support and invaluable guidance throughout the duration of this project. His expertise and encouragement have been instrumental in the successful completion of our research. We also express our deep appreciation to our co-supervisor, Jianning Dong, whose contributions during our weekly meetings were crucial. His insightful feedback and rigorous approach kept us focused on the relevant subjects, ensuring the quality and precision of our work. Our sincere thanks go to Amir Heidary for his assistance in enhancing our understanding of physical electrical systems, particularly in the areas of circuit breakers and busses. His knowledge significantly enriched our technical comprehension and practical application of these concepts. Furthermore, we are grateful to Jundong Wang for his strategic advice on the broader aspects of AEA design. Lastly, we would like to thank our families and close friends for their patience, understanding, and unwavering support throughout this intense period. Their encouragement and belief in our capabilities were vital in enabling us to produce the best thesis possible within these ten weeks.

Preface

In this thesis, "Design & Reliability Assessment of AEA Propulsion Grid", the development of a reliable and efficient propulsion grid for All-Electric Aircraft (AEA) is investigated to reduce aviation emissions. Our primary objective is to design a lightweight Power Management and Distribution (PMAD) system that meets stringent reliability standards. By analyzing materials, heat transfer, and grid design, we propose optimized grid topologies that balance weight and reliability. The findings emphasize the importance of redundancy and suggest further research into subcomponent failure rates, control aspects, and real-world testing to enhance system reliability and performance. This thesis provides valuable insights into the future of electric aviation, highlighting the necessity for continued investigation and practical application to ensure ultra-reliable electric propulsion systems and make zero-emission flight a reality.

Tim ter Horst
Floor Walterbos
Mark Imhof
Delft, June 2024

Contents

1 Introduction

The electrification of air travel has been a topic of interest for the past years due to its huge potential to decrease emissions in this polluting industry. Every year, aviation produces over 900 million metric tons of CO_2 [1] in the United States alone. In 2019 this accounted for more than 2% of all global emissions. Transitioning into electric flight and letting go of traditional means of providing power to aircraft through fossil fuels can contribute significantly to the global sustainable development goals [2]. Although this emerging field has vast potential, there are still many challenges to address before being able to sustain commercially large air travel on electrical power only.

Traditionally, power in aircraft is generated by fuel-powered engines that convert it into four types of energy: electrical, hydraulic, pneumatic and mechanical. This energy drives the main systems of the aircraft needed to provide the thrust, actuation, instrumentation and overall control of the aircraft. In More Electric Aircraft (MEA), a non-propulsive, non-electrical subsystem is replaced by its electrical counterpart [3]. This is done for separate sub-systems, such as the hydraulics or the Wing Ice Protection System (WIPS) [2]. Such a (relatively) small change in the aircraft power system architecture will already result in a significantly higher burden on the Electric Power System (EPS) of the aircraft in the order of magnitude of several tens of kVAs for WIPS alone, for example. [2].

MEA are a step in the right direction, but the main difficulty in zero-emission flight lies in the propulsion system. The power needed for both take-off (25-30 MW) and thrust (2-3 MW per motor) is too demanding for current technologies to produce on a commercial scale, in terms of power generation and storage [2]. An All-Electric Aircraft (AEA) is an aircraft where all systems have been transitioned to electric power, the main difference with a MEA being that the whole propulsive system and drivetrain have also been electrified and no longer rely on conventional fuel but on Electrochemical Energy Units (EEUs) and high power electromotors.

This thesis is structured around the grid design for the propulsion drivetrain of a narrowbody, 90 pax, AEA, the E9X [4]. The aircraft has 8 motors that supply the required thrust for the propulsion system and uses battery packs to supply this power. Two backup generators are present in the design for fault scenarios. Figure 1.1 shows a sketch of the aircraft external outline compared to a standard commercial narrow-body aircraft and its dimensions and internal structure [4]. Further specifications of the aircraft are given in Section 2.1.

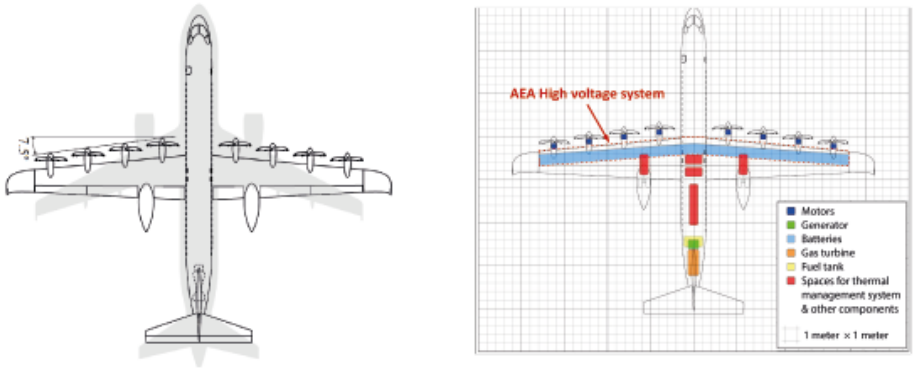

Figure 1.1: E9X external structure on the left. On the right its internal structural design for the propulsion grid.[4]

1.1. Thesis Objective

The objective of this thesis is to investigate and produce a reliable design for the grid powering the propulsion of an AEA. This paper is part of a larger project regarding electrical system protection of AEA, where the task division was the following:

- **DC Solid State Circuit Breaker for AEA**
- **Design & Reliability Assessment of AEA Propulsion Grid**

In this design, the weight of the system as well as its redundancy must be considered thoroughly in order for it to be successful. An in-depth study of the reliability of both the sub-components as well as the designed topology has to be done to be able to evaluate its effectiveness. This thesis will explore the transmission network of the grid in detail, evaluating the material choices of the cabling and their parameters in order to minimise the mass burden of the grid. Additionally, the grid design itself will be designed for redundancy while adhering to the mass restrictions placed on the system. The reliability assessment will consider different failure modes of the system, their impact on the system and how often they take place. These failure rates are then used to analyse the complete reliability of the system in the form of a critical failure rate, after which a final grid topology can be selected.

1.2. Thesis Structure

The thesis will start off by defining the programme of requirements set for the design and given specifications in Chapter 2. Consequently, the cabling structure, materials and weights will be discussed in Chapter 3. Next, in Chapter 4, the grid topologies will be explored, designed and structurally analysed. Chapter 5 will dive into the reliability aspect of the grid, looking at the sub-components of the grid and producing a critical failure rate for the grid. In Chapter 6 the results of the thesis will be presented, followed by an in-depth analysis of all the presented results, choices & estimations of this paper. Lastly, Chapter 7 will conclude the thesis and discuss possibilities to extend the work done in this thesis for future research.

2

Programme of Requirements

In order for the project to be successfully completed, it needs a frame of reference on which choices and system parameters can be tested on to effectively analyse the design. This will be structured by looking at the requirements set for the complete project and the requirements set for this thesis itself.

2.1. Intergroup requirements

As was stated in the introduction, the objective of this project is to design electrical power system protection of an AEA design. This includes the design of a reliable grid topology and its resulting weight, a reliability analysis for one part of the project and the design of a good functioning protection element fit for the AEA application. There are a number of set requirements on the aircraft that are of relevance for the whole project, specified to the project from [4] and listed below:

- The aircraft design is aimed for commercial launch and usage in 2033
- The aircraft is designed to carry a payload of 90 pax
- The aircraft is designed for a mission range of 800 km of battery-electric flight, with possible range extension to 1000 km
- Minimum cruising altitude of 7 km
- The aircraft thrust will be provided by 8 electrical motors, powering 8 turbo-props directly attached to the wing
- Every motor has a continuous power output of 1.36 MW and a peak power output of 1.50 MW (1.62 MW peak shaft power for 3 minutes)
- Two reserve generators are present in the back of the aircraft for covering reserves and emergency situations
- Each generator has a peak power of 5.8 MW
- The battery packs of the aircraft have an energy density of 360 Wh/kg
- The aircraft will have a cruise Mach number of 0.6
- The batteries of the aircraft are placed in the wings
- The battery packs are replaced every 1500 cycles

2.2. Intragroup Requirements

For this thesis, there are certain specific requirements formulated in order to test the design and structure of the design process. Specifically, it is structured around the weight constraints and optimisation of the transmission network, grid topology design and reliability requirements.

Transmission Network Requirements

- The weight of the cables used in the transmission network should be as low as possible
- Justified choice of cabling materials and sizing optimised for weight
- Detailed analysis of temperature considerations and high-voltage phenomena in the design of cables
- Thorough consideration of different voltage, current & power levels in systems and their effect on the transmission network & cable weights

Grid Topology Requirements

- The grid design has to be optimised in terms of length and components
- Balanced choice in component selection & quantity in grid
- The topology has to be designed for optimal reliability based on literature and balance between different options for every part of the grid
- Structural analysis of grid topology design in aircraft including parameters and location of components in aircraft
- Design of multiple different topologies to allow for rigorous comparison & balanced review
- Total mass of the grid topology has to be within 3860.6 kg [4]

Reliability Requirements

- Both the sub-components and the complete topology have to be evaluated in terms of reliability at the hand of balanced analyses
- Estimations of the failure rates of every component of the grid have to be made for different failure modes based on current literature and technology advancement projections
- Determining a critical failure rate for different architectures to assess reliability quantitatively
- Overall critical failure rate has to be within 10^{-9} per flight hour

3

Transmission Network

The critical design criteria that form a main restriction for (battery-electric) AEA in the current state of technology is the weight constraint. Current electrical motors are not able to provide enough power to generate the required thrust, caused largely because of the large mass of the battery packs supplying this energy [5]. Since reducing this battery mass is not an option, weight savings and optimisation must be done in other parts of the aircraft. For the propulsion drivetrain grid, this optimisation can mainly be done in the cabling system of the aircraft. Naturally, reducing weight by reducing the amount of cable will inherently reduce redundancy, meaning that it is very important that the cable mass itself is already optimised in the best way possible. This chapter will explore the design of the cable parameters used in the transmission network, by considering different conductor materials, analysing the heat losses through the cable in operation, the required size of the conductor based on voltage and power levels and the insulation required for the cabling system. Ultimately, a mass in kg per meter cable is presented for all the different power levels that will run over the grid. This will be used in the calculation of the complete mass of the topologies and their subsequent design further described in Chapter 4.

3.1. Material Considerations

In this section the cable structure will be explained and some considerations for the different materials of these components will be presented.

3.1.1. Cable structure

In order to be able to design the cable and optimise its weight, it first must be understood what components it is made out of and what variables can be changed in this consideration. The cables for the high-voltage transmission network of the aircraft consist of 5 different elements, listed below:

- Conductor
- Insulator
- Shield layer
- Semiconductor layer
- Outer jacket

Each of these layers has its own functions and properties. The conductor is responsible for carrying the main current and power from one place in the network to another, with the lowest losses possible. Its material considerations will be described further in Subsection 3.1.2. The insulator is responsible for isolating the high voltage conductor from the ground conductor. Furthermore, its sizing is important for mitigation of high voltage phenomena, such as partial discharging. This is explored in Section 3.3. The semiconducting layer is present in the cable in order to smooth out the conductor. This is done because sharper edges can cause the electric field to drastically increase in certain regions, meaning more (unwanted) stress on the insulation [6]. The metal sheath is present as a material that is able to

conduct a (discharge) current to ground or a return path to the source. Lastly, the outer jacket is used as a form of mechanical protection of the cable, against environmental factors such as humidity or rust [6]. The cable cross-section will correspond to Figure 3.1.

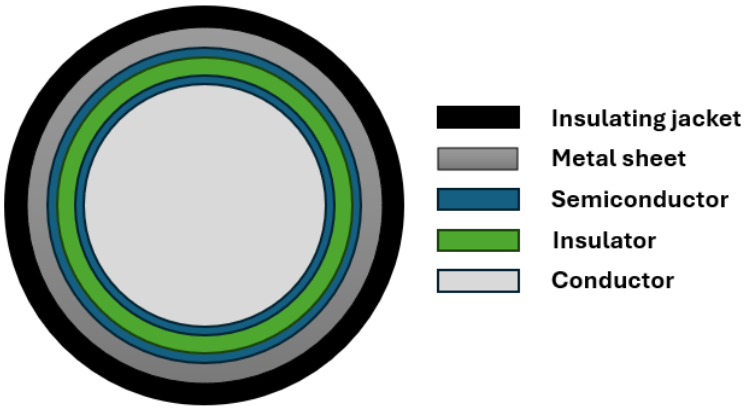

Figure 3.1: Cable cross section

In order to increase the flexibility of the wire, the conductor is often subject to 'stranding' where multiple conductor wires are wound together and create a wire structure as shown below in 3.2:

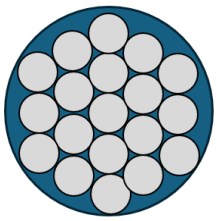

Figure 3.2: Conductor stranding

However, in order to simplify conductor radius calculations it is assumed the conductor wiring, together with the semiconducting layer, in the AEA is in one circular piece such as shown in Figure 3.1.

3.1.2. Conductor material

For the conductor layer in the cable there are two (common) options that are applicable for AEA lines. These are copper and aluminium. Both have varying material properties that are relevant for the discussion which of these is best for the cabling in this system. Copper is a better conducting material, and historically the preferred choice in cabling [6]. The conductivity of copper is $5.87 * 10^7 [S/m]$ while that of aluminium is $3.69 * 10^7 [S/m]$ [7]. Nevertheless, as was mentioned earlier in this chapter the weight constraints for AEA applications form a key element in the material considerations. Since copper is about three times more dense than aluminium ($8.96 [g/m^3]$ versus $2.70 [g/m^3]$) the mass per meter cable can also be expected to be much higher for copper. A weight comparison between both materials can be seen in Figure 3.3:

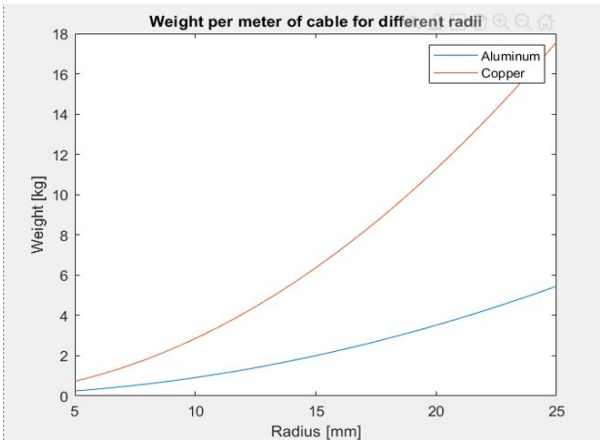

Figure 3.3: Weight comparison aluminium and copper

Especially for high radii, the mass differences become significant. This means that for the cables that carry the higher powers in the system the weight will become too high to adhere to the weight requirements set in Section 2.2. Seeing as the weight requirements are significantly more critical in this design than the efficiency of the conductor, it was decided that the conductor material should be aluminium.

3.1.3. Shield layer

The shield layer is composed of a metallic sheath that separates the outer jacket and the insulation. It has multiple functions in nominal operation. The main function the shield layer has is that it is responsible for the carrying of fault current or discharges to ground. Moreover, it provides a barrier for insulation moisture and a return path for capacitive charge currents [8]. It normally consist of several layers, especially for high current applications. For the sheath material aluminium was also used, for the same reasons as described in 3.1.2.

3.1.4. Semiconductor layer

The semiconductor layer is placed in two places; surrounding the conductor and surrounding the insulator. Especially for the conductor it fulfils a very important role; it has a smoothing effect on the conductor which lowers the electric field strength on the edge of the conductor and makes it uniform, by creating an equal voltage on the insulator edge [9]. Furthermore, due to the high currents that are passed through the conductor it reaches significantly high temperatures. The semiconducting layer is of importance here to mitigate the effect these high temperatures directly have on the insulating layer it separates [9].

3.1.5. Outer jacket

The outer jacket is a further layer that is mainly used as protection to external factors such as humidity. It is also a further insulating layer protecting the metallic sheath against corrosion, which is essential as aluminium is quite susceptible to corrosion. The material choice for this layer was Teflon, since it is a good, low-cost material for the jacket, but most of all has very good fire retardant properties [6].

3.2. Heat Transfer & Temperature Study

In order to determine the correct conductor radius, which essentially is the most important parameter of the cable, the temperature losses and parameters of the system have to be taken into account. These are all related to each other through thermodynamic laws. In this section these will be explored in order to determine the correct radius for the conductor to satisfy these relations and optimise the chosen parameters such that the cable has the lowest weight possible. This was mainly done through solving non-linear systems of equations through MatLab and using graphical methods to estimate solutions, as will be shown further on in this section.

3.2.1. Variables

There are a set of unknown parameters that need to be determined, some independent variables that can be changed in order to reach an optimum situation and some controlled variables that are known and kept constant. The following variables will be significant for the system and therefore are introduced here already for the reader to get familiar with:

Dependent variables/parameters to be found

- r_c - The conductor radius of the cable [mm]
- t_i - Insulation thickness [mm]

Independent variables

- T_s - The temperature at the surface of the cable [C°]
- T_c - The (inner) temperature of the conductor [C°]
- h - Heat transfer coefficient of convection [W/m^2K]
- V - System voltage level: either 800 or 3000 [V]
- P - Power level on cable [MW]

Controlled variables

- T_{amb} - Ambient temperature (surrounding temperature): 40 [°C]
- v - Kinematic viscosity of air: $2.65 * 10^{-5}$ at 10km [Pas]
- λ_{air} - Convection coefficient of air: $2.7 * 10^{-2}$ [W/mK]
- σ_{SB} - Stefan-Boltzmann constant: $5.67 * 10^{-8}$ [$Wm^{-2}2^{-4}$]
- ϵ - insulator emissivity (relative): 0.8

3.2.2. Heat losses

Since the currents that will be passed through the conductor are quite high due to the high powers it needs to transfer, the temperature the conductor reaches will also be significant. Therefore, the insulator needs to be able to mitigate these heat fluctuations well enough for the cable to stay operational, otherwise the risk of cable failure or even flammation risks becomes probable. Naturally, this should be avoided at all costs. The total heat loss due to convection and radiation through the cable can be equated to the total heat produced by the current running over the cable, and is shown in 3.1 [10]. All calculations and derivations are computed for 1 meter length of cable.

$$Q_c = Q_{convection} + Q_{radiation} = \frac{I^2}{\sigma_{Al} * \pi * r_c^2} \tag{3.1}$$

Where Q_c is the total heat produced by the conductor, I is the current over the cable, σ_{Al} is the conductivity of Aluminium and r_c is the conductor radius. The heat losses due to convection and radiation are described by the following two relations, 3.2 and 3.3 respectively:

$$Q_{convection} = h * 2\pi * r_{total} * (T_s - T_{Amb}) \tag{3.2}$$

$$Q_{radiation} = \epsilon * \sigma_{SB} * 2\pi * r_{total} * (T_s^4 - T_{Amb}^4) \tag{3.3}$$

Through these equations, it is possible to try to make an estimation of the heat loss through the cable. However, the h from Equation 3.2, requires a bit more attention. Before Equations 3.1, 3.2 and 3.3 can be used, this transfer coefficient value must be found. It is itself dependent on the surface temperature, making the system more complex. It is derived from the Nusselt relation [11]:

$$Nu = \frac{hL}{\lambda} = 0.12(Gr \cdot Pr)^{1/3} \tag{3.4}$$

Where Gr is the Grashof number and Pr is the Prandtl number, defined as Equations 3.5 and 3.6:

$$Gr = \frac{gL^3\beta\Delta T}{\nu^2} \tag{3.5}$$

$$Pr = \frac{\nu c_p}{\lambda} \tag{3.6}$$

Where g is the gravity constant, L the length of the cable (taken to be 1 as it is desired to obtain a mass per meter cable) and β in Equation 3.5 is the gas expansion coefficient, which for an ideal gas can be seen as the inverse of the average temperature [12]. Rewriting and combining these equations gives a final equation for the heat transfer coefficient of convection:

$$h = 0.12\lambda * (\frac{g}{\nu^2} * \beta * (T_s - T_{Amb}) * P_r)^{\frac{1}{3}} \tag{3.7}$$

In order to get a value for h that matches the correct value for the surface temperature, the surface temperature was plotted against h. As will be seen later, this plot will later be used in a loop that checked it for multiple surface temperature - heat transfer coefficient combinations in order to reach the correct value for h. The code for the generation of this plot and all further temperature and sizing calculations can be found in Appendix D.

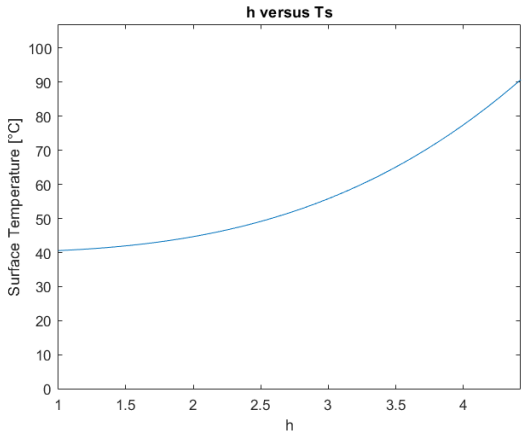

Figure 3.4: Heat transfer coefficient of convection, h, versus surface temperature according to 3.7 [11]

At steady state, the temperature differences between both conductor and the surface, and the surface and the surroundings (ambient temperature) are given by 3.8 and 3.9 [13]:

$$T_c - T_s = \frac{I^2}{\sigma_{Al}\pi r_c^2} * (\frac{1}{2\pi k_{tef}} * ln(\frac{r_c + t_{isc} + t_i + t_{osc}}{r_c}) + \frac{1}{2\pi k_{tef}} * ln(\frac{r_c + t_{isc} + t_i + t_{osc} + t_s + t_{oj}}{r_c + t_{isc} + t_i + t_{osc} + t_s})) \tag{3.8}$$

$$T_s - T_{amb} = \frac{I^2}{\sigma_{Al} * 2\pi^2 * r_c^2 * h * r_{total}} \tag{3.9}$$

Where t_{isc} and t_{osc} are the thicknesses of the semiconducting layers, t_s is the thickness of the aluminium sheath, and t_{oj} is the thickness of the outer jacket of the cable, k_{tef} and k_{PVC} are the thermal conductivity's of the polymer insulating layers (0.3 for Teflon and 0.12 for PVC [14]).

Equation 3.9 was used as the comparison tool in the loop mentioned earlier in order to verify the correct value for the h - T_s combination. Clearly, equations 3.2, 3.3, 3.8 and 3.9 cannot be explicitly solved. Therefore, MatLab was used in order to solve these non-linear set of simultaneous equations in a graphical manner through substitution.

In order to allow for comparison between different situations, a selection in the range of the independent variables was made. It was decided that the three cases for conductor temperature that would be tested are 90 [˚C], 120 [˚C] and 150 [˚C]. This is because the estimation of the operating temperature is around 120˚ for the conductor and in order to generate a fair reference and balanced choice for the conductor radius it is important that these are considered as well. Moreover, as mentioned in Subsection 3.2.1, there was a selection made between two system level voltages; 800 [V] and 3 [kV]. The specific reason for these levels is that they are commonly used for AEA designs [15]. A lower system voltage will inherently mean a higher mass of the cable since the currents run over the cable will be higher, while a higher system voltage increases the risk of insulation failure as will be explained in Section 3.3. In order to obtain a correct value for the surface temperature, both Equation 3.8 and 3.9 are plotted for a series of conductor radii and solved simultaneously. The resulting crossover point is then the solution of the equations; the required conductor radius and surface temperature combination. Seeing as Equation 3.9 is solely a function of the losses due to convection, these values are then checked by also considering the radiation as described in Equation 3.3 in order to complete the analysis.

The complete temperature analysis and subsequent plots can be found in Appendix A. As an example, the steady state (surface) temperature for 3 kV for a conductor temperature of 120˚ as a function of the conductor radius is shown below:

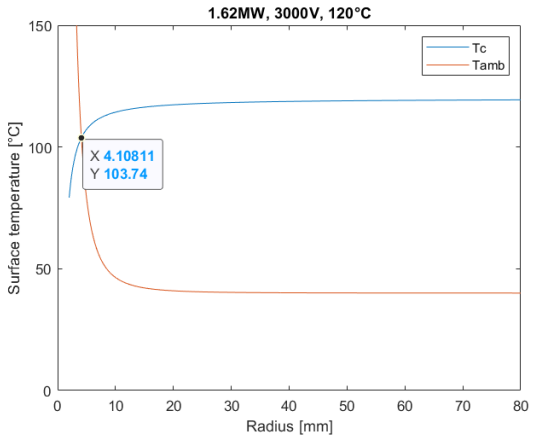

Figure 3.5: Surface temperature T_s as a function of conductor radius r_c for 3000V system voltage & 120˚ conductor temperature using Equations 3.8 (Tc) and 3.9 (T_{Amb})

Figure 3.5 shows that for this specific combination of the cable variables, the desired conductor radius would 4.11 [mm] and resulting surface temperature of 103.74 [˚C]. The remainder of the values found are presented in Section 3.2.4.

As mentioned before, the current analysis ignores the radiation losses in the cable. However, it has not been proven just yet that this indeed is a valid assumption. In order to verify this, Equations 3.1, 3.2 and 3.3 are rewritten to produce explicit functions in both T_s and r_c, shown below in Equations 3.10 and 3.11.

$$F(T_s) = h * (T_s - T_{Amb}) + \epsilon * \sigma_{SB} * (T_s - T_{Amb})^4 \tag{3.10}$$

$$F(r_c) = \frac{I^2}{\sigma_{Al} * 2\pi^2 * r_c^2 * r_{total}} \tag{3.11}$$

Nevertheless, it should be noted that the output of the functions (the 'y' values in the plots) is a quantity that is of no physical significance; it is purely used as a reference value to be able to verify whether the two equations are equal to each other and actually produce the correct output. It has unit $[\frac{W^2}{m}]$. For the 3000 V, 120˚ conductor temperature case the plots can be seen in Figure 3.6:

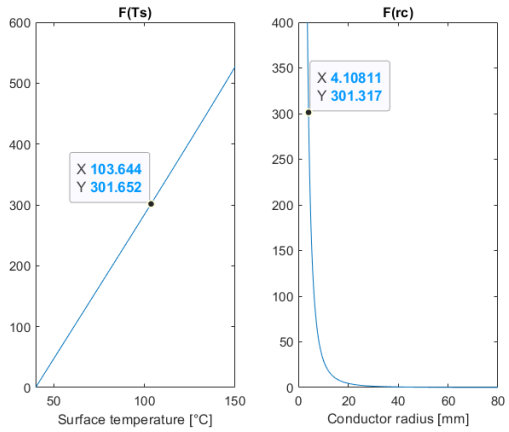

Figure 3.6: Radiation loss verification for 3000V system voltage & 120˚ surface temperature

As can be seen in the plots, the accuracy of the surface temperature is within 0.1 ˚C and the conductor radius even within the order 10^{-4} mm compared to the values found in the surface temperature and conductor radius obtained through 3.5. The comparison quantity 'y' falls within an acceptable accuracy of 0.2. Therefore, it can be assumed that the radiation contribution to the heat losses are negligible compared to the losses due to convection. The radiation verification plots for the other voltage-temperature pairs can be found in Appendix A.

3.2.3. Selection of parameters

So far we have considered quite a broad range of values for the variables present in the system. In order to build to a definitive cable sizing, the voltage level and (boundary condition) conductor temperature needs to be decided on. As mentioned in 3.2.2, the trade-off between these two voltage levels is found in two regions; weight (higher current on lower voltage means higher weight) and insulation considerations (higher voltage induces higher risk of insulation breakdown). Firstly, the weight comparison will be made, as it is forms an essential component of the requirements as defined in Chapter 2. Below a comparison can be seen between the conductor radius of the cable at conductor temperature of 120˚ for both voltage levels:

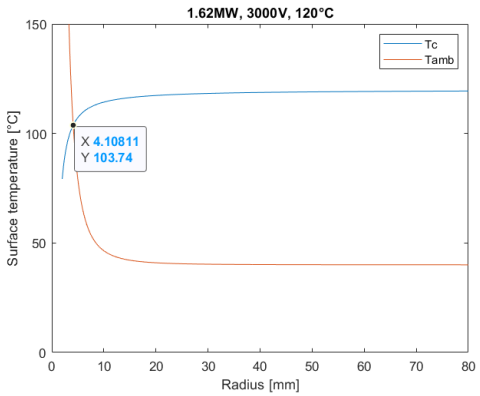

Figure 3.7: Surface temperature T_s as a function of conductor radius r_c for 3000V system voltage & 120˚ conductor temperature

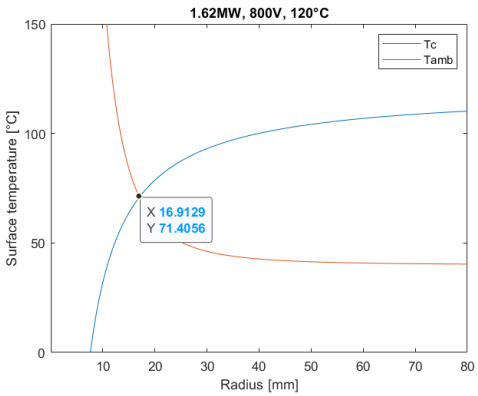

Figure 3.8: Surface temperature T_s as a function of conductor radius r_c for 800V system voltage & 120˚ conductor temperature

As can be seen in Figures 3.7 and 3.8 the difference in conductor radius is quite significant; about a factor 4 larger for the 800V cable. Qualitatively, it can be assumed that this means that the cable weight itself will be much higher. In Section 3.4 the calculation method for the weight per meter cable, and the

subsequent results will be explored in detail. However, in order to give a sustained reasoning for the voltage level considerations the weight comparison for the cables as defined in Figures 3.7 and 3.8 is shown in Figures 3.9 and 3.10:

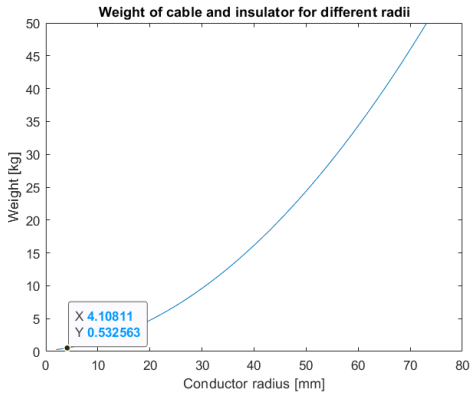

Figure 3.9: Weight per meter cable [kg] for 3000V system voltage

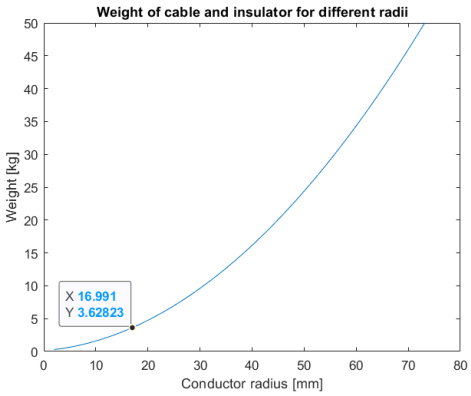

Figure 3.10: Weight per meter cable [kg] for 800V system voltage

The cable weighs significantly more per meter for the 3000 V system voltage level than for the 800 V level, as was expected (0.53 kg versus 3.68 kg). Henceforth, viewed purely from the weight standpoint, it should be evident that choosing a higher voltage level has the preference. As will be discussed in Section 3.3, the potential downsides of having the higher voltages for the insulation can be mitigated by properly designing the insulating layer.

Another consideration that is important to mention that was omitted until this point are the different power levels in the system. The minimum power every cable has to transfer in the system is 1.62 MW, which is the peak power demanded per motor. The specific details on loads and components in the system will be explored in more detail in the next chapter (Section 4.2). Nevertheless, it should be evident that some cables in the system need to be able to transfer more power, especially in fault scenarios where power has to be rerouted to supply more parts of the system. These power levels will be discussed further in Sections 3.4 and 4.3.6. Choosing a higher voltage level also means that for higher power a relative lower current will flow through the cable, which again significantly influences the radius of the conductor necessary (and therefore the weight). All in all, this led to the design choice of a system level voltage of 3000V.

Moreover, the conductor temperature the cables will be designed for has to be decided. Throughout this analysis three temperatures were be considered; 90˚ [˚C], 120˚ [˚C] and 150˚ [˚C] in order to evaluate the effect on conductor radius. However, in order to give a constraint to the design, one has to be chosen as a boundary condition. For this 120˚ was chosen, for the reason that this should be the worst case scenario for the cable (a higher temperature will not be realistic since the ambient temperature will heat up too much). In comparison to 90˚ the boundary case of 120˚ was preferred in order to give a more accurate estimate, and since the insulation allows such high temperatures (as will be explained in Section 3.3). Thus, the values for the 120˚ conductor temperature were used for the further weight calculations.

3.2.4. Conductor sizing

Table 3.1 shows what the radius of the conductor part would be for different temperatures and voltage levels at a power of 1.62 MW. The graph corresponding with these values can be found in Appendix A.

Conductor radii for different voltage levels and temperatures at 1.62 MW			
Voltage	**Conductor temperature**	**Surface temperature**	**Conductor radius**
3000 V	90 °C	80 °C	5.75 mm
	120 °C	103 °C	4.11 mm
	150 °C	130 °C	3.41 mm
800 V	90 °C	54 °C	22.53 mm
	120 °C	71 °C	16.91 mm
	150 °C	92 °C	14.1 mm

Table 3.1: Conductor radii

The biggest difference in conductor radius comes from the difference in voltage over the cable. The conductor radius of an 800 V cable is around 4 times wider than the radius of a 3000 V cable. In temperatures a small difference can be seen as well, but for conductor temperatures of 150 °C the surface temperature also becomes very high. This is why the choice of 120 °C and 3000 V is made. As can be seen from the table, this results in a radius of 4.11 mm for 1.62 MW of power. In Section 3.4, the final radius and weight are presented for every power level.

3.3. Insulation: Partial Discharge Mitigation

The insulation of the cable is very important for its function. As was introduced in 3.1.1, the insulation is put as a cover layer for the conductor in order to mitigate the thermal effects of the conductor current. It also has to be handle the high electric field it is exposed to induced by the current ran over the cable, due to the high voltages. These high voltages can damage the insulation significantly, due to a phenomenon called Partial Discharging [16]. This phenomenon and its implications will be explored in 3.3.2. This section aims at exploring the insulator material, properties and eventual sizing necessary to mitigate Partial Discharging and insulation breakdown.

3.3.1. Insulation material

Traditionally, polymers are used for insulator due to their good electrical properties. There are a lot of different polymers that are commercially used for insulating power cables. Seeing as the insulator in AEA cabling has to be able to withstand very high temperatures and has to be very fire resistant, it was decided that the insulating material was to be Polytetrafluoroetheylene (PTFE), more commonly known as Teflon [17]. Teflon can effectively insulate temperatures up to 200°, which gives a considerable margin for the maximum conductor temperature. Moreover, it has exceptionally good electrical quantities and a known lower void size; decreasing the risk of Partial Discharging [18].

3.3.2. Partial Discharge & Breakdown voltage

Higher operating voltages result in stronger electric fields, necessitating thicker insulation to prevent electrical breakdown. Partial Discharging is a phenomenon occurring in dielectrics when exposed to high voltages. This occurs when there are voids, mostly air gaps, in the insulating layer. During the manufacturing process of an insulator, small voids can form within the material. These voids come in two main types: spherical cavities within the insulation and fissures at the interface between the dielectric and the electrode. The electric field in these voids is higher relative to the dielectric by a factor of $\frac{3*\epsilon_r}{1+2\epsilon_r}$. If the electric field strength multiplied by the void distance exceeds a certain voltage, partial discharges will occur. This critical voltage is known as the breakdown voltage.

The breakdown voltage is related to the pressure that the cable is subjected to; meaning it is a very important factor to consider in the insulation design. At higher altitudes the pressure the cable is subjected to is decreased. This relation is known as *Paschen's Law*, given by the following equation [19]:

$$V_b = \frac{Bpd}{\ln(pd) + k} \tag{3.12}$$

where k is:

$$k = \ln\left(\frac{A}{\ln(1+\frac{1}{\gamma})}\right) \tag{3.13}$$

In 3.12 and 3.13 p is the gas pressure, d is the distance between electrodes, J is the secondary ionization coefficient, A is the saturation ionization in the gas at a particular E/p (electric stress/pressure)and B is related to the excitation and ionization energies [19]. It is out of the scope of this paper to go into further detail on these equation, but, 3.12 is used to generated the Paschen curve; visualising this relationship. Using the Pachen Curve, the worst case value for the breakdown voltage can be found. This is the edge case for which the insulating material should be resistant to electrical breakdown. The Paschen curve is shown in 3.11.

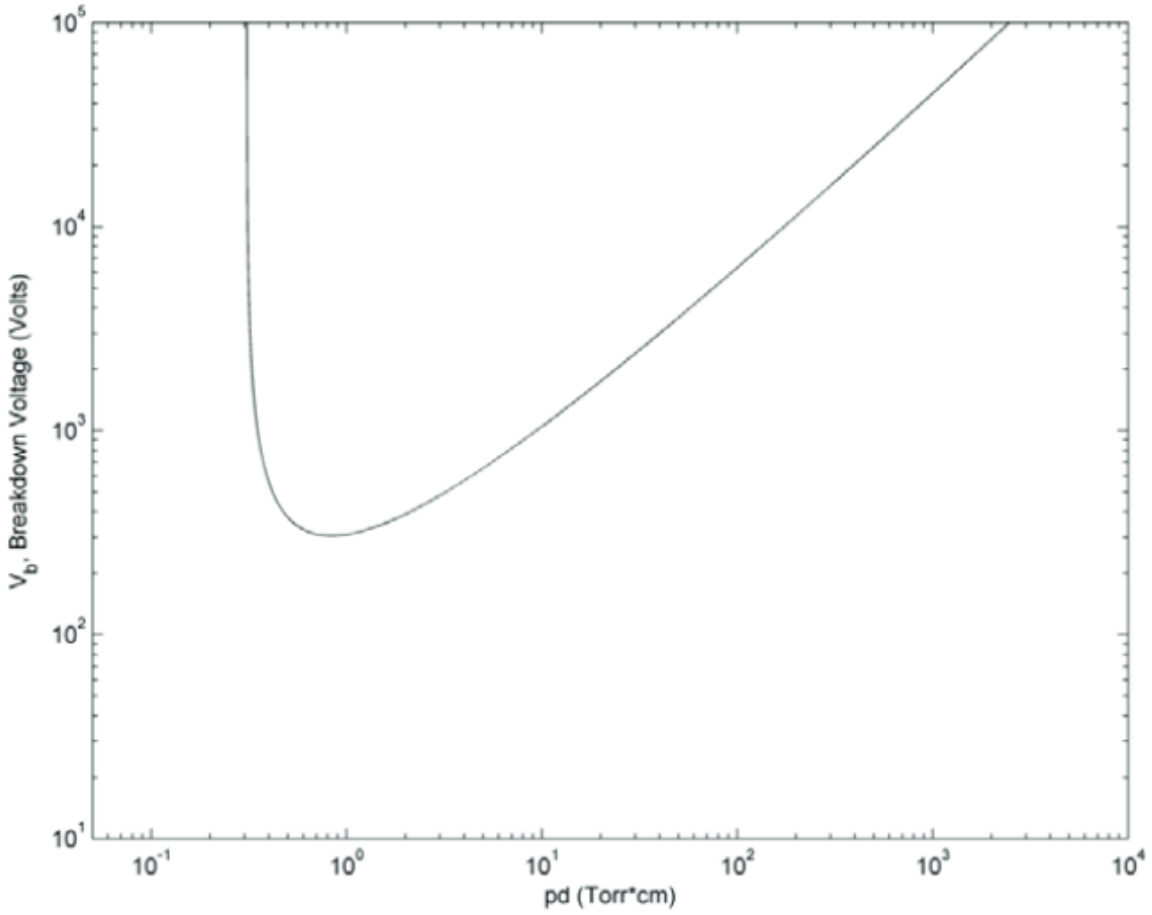

Figure 3.11: Paschen curve for air [19]

In Figure 3.11. The x axis of this curve has Torr*cm as its unit. Torr is a unit for pressure (1 bar ≈750 Torr). The unit cm corresponds to the distance between two electrodes, in this case the maximum size of a void (dV) in the insulator. As mentioned in 3.3.1, Teflon, the chosen insulator material, has a maximum void size of 33 μm, or 0.0033 cm.

The AEA is designed to have a cruising threshold of at least 7 km [4]. However, commercial short haul aircraft have a cruising altitude ranging between the 7 km and 10 km [20]. Therefore, in order to design the cable for the worst case scenario, the altitude must be selected that yields the lowest breakdown voltage. According to the curve, the breakdown voltage is at its lowest at around 0.75 Torr*cm. With the void size filled in, this corresponds to a pressure of 30.3 kPa, which corresponds to a cruising altitude of 9.1 km [21]. Since this falls within the operating range of the AEA, this value is taken to be

the worst case scenario. This yields an edge case value for the breakdown voltage of 300 V. In the subsequent sections, the breakdown voltage will be denoted by α.

3.3.3. Insulator sizing

The thickness of the insulating layer is designed based on several parameters, as discussed before. Thus, its sizing is very much dependant on the size of the conductor itself. In order to calculate the thickness of the insulator equation, the so-called *Single Void Dicharge* (SVD) method can be applied, leading to 3.14 [13]:

$$t_i = r_c * (\exp \frac{\frac{3*\epsilon_r}{1+2\epsilon_r} * V * dV}{\alpha * r_c} - 1) + C \tag{3.14}$$

Where V is the system voltage level, dV represents the void size and α the specified breakdown voltage of 3.3.2. The constant, C, added at the back of the equation is used to compensate for lower voltages under 20 kV. For voltages beneath the 20kV its value is 1 mm. Combing all the found parameters, 3.14 can be plotted to show the relation between the insulation thickness and the conductor radius. This is shown below in 3.12:

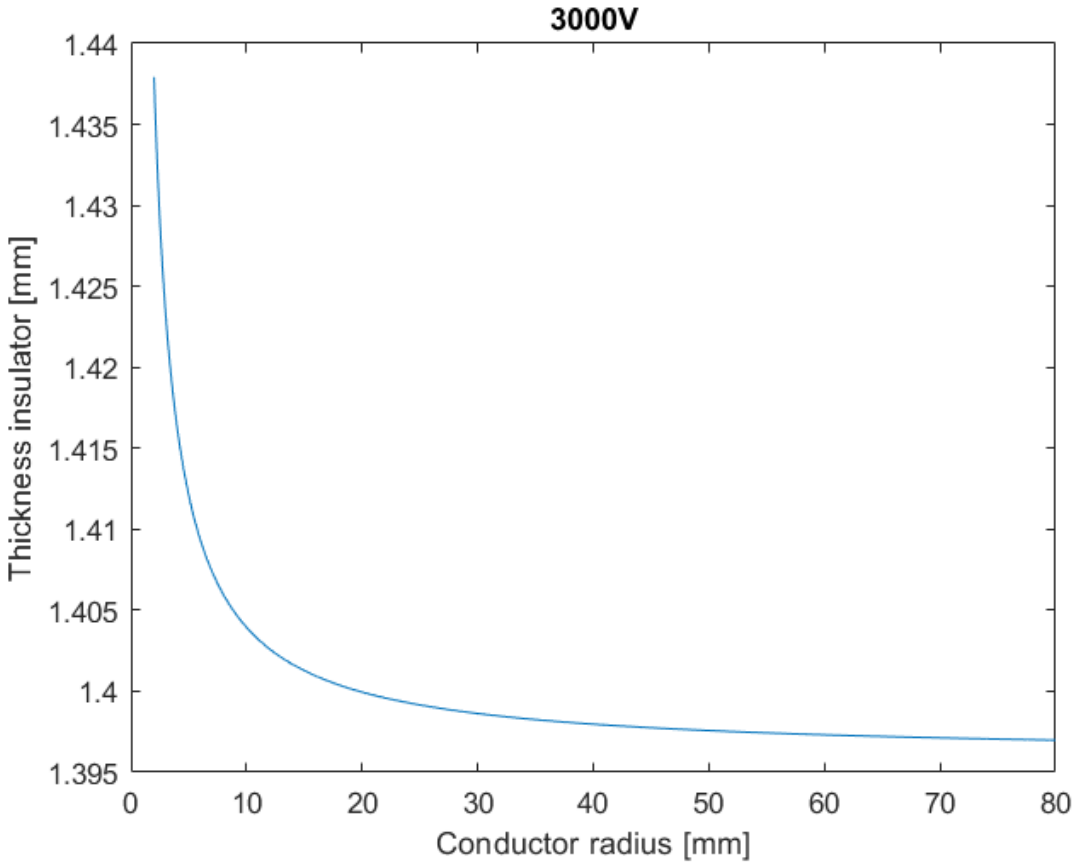

Figure 3.12: Insulation thickness t_i versus conductor radius r_c at 3000V system voltage

Figure 3.12 shows that the varying size of the conductor radius does not have a large impact on the insulator radius; especially for radii higher than 20 mm conductor radius.

3.4. Final Cable Parameters

Combining the results of this chapter, the final sizes of the layers and their subsequent weights can be determined. The sizes of the outer jacket (t_{oj}), semi-conductor layers (t_{isc} and t_{osc}, inside and outside) and metal sheath (t_s) are predetermined and taken to be 1 mm, 0.6 mm and 1 mm respectively [13].

The conductors sizing (r_c) was discussed in section 3.2.4. The insulator sizing (t_i) was discussed in Section 3.3.3. The final step is to calculate the weight of every material in the cable using their density and size, and add them up to get the final cable weights per meter cable. Equations 3.15, 3.16, 3.17 and 3.18 are used to make these calculations.

$$\text{Conductor mass} = \rho_{\text{Alum}} \cdot \text{length} \cdot \pi \cdot r_c^2 \tag{3.15}$$

$$\text{Insulator mass} = \rho_{\text{Insul}} \cdot \text{length} \cdot \pi \cdot \left((r_c + t_{\text{isc}} + t_i + t_{\text{osc}})^2 - r_c^2\right) \tag{3.16}$$

$$\text{Sheet mass} = \rho_{\text{Alum}} \cdot \text{length} \cdot \pi \cdot \left((r_c + t_{\text{isc}} + t_i + t_{\text{osc}} + t_s)^2 - (r_c + t_{\text{isc}} + t_i + t_{\text{osc}})^2\right) \tag{3.17}$$

$$\text{Jacket mass} = \rho_{\text{PVC}} \cdot \text{length} \cdot \pi \cdot \left((r_c + t_{\text{isc}} + t_i + t_{\text{osc}} + t_s + t_{oj})^2 - (r_c + t_{\text{isc}} + t_i + t_{\text{osc}} + t_s)^2\right) \tag{3.18}$$

Throughout this chapter the calculations were done per meter length, hence for the 'length' variable in Equations 3.15, 3.16, 3.17 and 3.18 we take 1 m. If all of the masses are added together, the total mass per meter cable for different conductor radii is given in Figure 3.13. As can be expected, the vast majority of the weight of the cable is dependent on the conductor sizing. Using Figure 3.13, the different weights can be calculated for every power level.

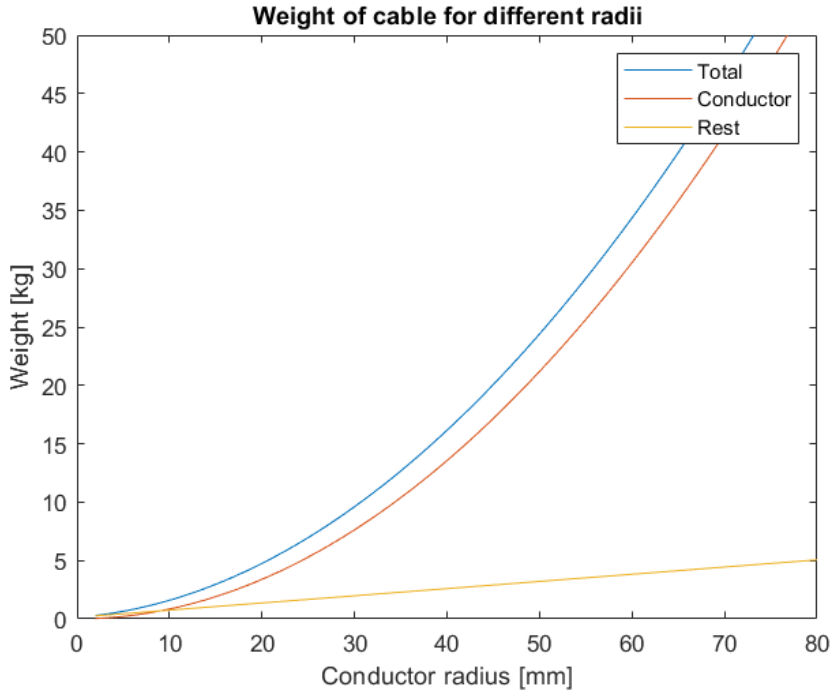

Figure 3.13: Weight per meter cable at different conductor radii

The different power levels in the system is dependent on grid topology & the location of the cable in the network. As will be seen in 4, there are 4 different (peak) power levels that the cables have to carry, these are 1.62 [MW], 3.24 [MW], 6.48 [MW] and in the worst case, 12.96 [MW]. For the system voltage level of 3000 V this changes the current that the cable transfers, and therefore also changes the radius of the conductor through the formulas and method described in 3.2.2. The final values for the cable radii, insulator thickness & the resulting weights per meter cable are listed in Table 3.2.

Weight for 3000V and 120°C at different power ratings			
Power [MW]	**Conductor radius [mm]**	**Weight [kg m^{-1}]**	**Insulator thickness [mm]**
1.62	4.11	0.56	1.42
3.24	7.93	1.17	1.41
6.48	17.07	3.67	1.40
12.96	44.94	20.06	1.40

Table 3.2: Cable weights

4

Grid Topologies

As was stated in the introduction, aircraft are driven by mechanical, electrical, hydraulic and pneumatic systems. Replacing the mechanical and hydro-mechanical for electrical systems reduces the weight of aircraft, while at the same time increasing the use of electrical power. These implementations reduce the weight and increase the efficiency of the power usage. However, the demand of the Electrical Power System (EPS) rises with the added elements [22]. This increase in required power ratings causes the current levels of the system to increase in order to meet the demand. Increasing the system voltage levels can mitigate this rise in current. As a result, the cables will be lighter, the feeder cable current can be reduced and higher efficiencies will be reached. For this reason, current and future electric aircraft are operating on a high-voltage grid. This chapter starts with an elaboration on the Electric Power Systems in AEA and MEA. It will explain why the high voltage (HV) distribution system is necessary for electric aircraft. Following this, an overview of the E9X and all its sub-components will be presented and an outline for the EPS created. With examples from literature study, the design steps and choices will be made clear and the resulting two grid topologies will be shown. The chapter ends with a structural analysis performed on both of these architectures, diving into the total weight of the grid topologies.

4.1. EPS in Electric Aircraft

The EPS in electric aircraft must be redesigned due to the required high reliability of aircraft and the added complexity of the grid. Reliability is a critical parameter for aircraft. As will be explained in Chapter 5, aircraft design is subject to strict regulations regarding safety (such as the EASA CS-25 regulatory set [23]). Thus, seeing as these novel grids are not that rigorously tested in the field (yet), the design of the EPS must already adhere to a high standard of reliability. Reliability in aircraft is measured in failures per flight hour and as mentioned in Section 2.2 for this thesis the goal is to have a critical failure rate of at most $10^{-9}\mathrm{h}^{-1}]$ The electric components that are used in the battery system, switching technologies, power electronics for the converters and passive components all have individual failure rates that need to uphold to the reliability standards [15]. The harsh conditions such as decreased air pressure, humidity and possible radiation influence the semiconductor technologies in many of these components [15] Accurate fault detection and prevention requires higher levels of control and clever grid design in order to mitigate the effects of such faults.

For AEA and MEA the motors are electric and provide a shaft with propulsive power for the rotation of the fans. Electric motors that are able to supply the amount of propulsive power required for current (2-motor) aircraft design, will probably not exist in the upcoming 20 to 30 years. The current ratings are in the range of 1 MW and the technology developments estimate that in the next twenty years, there will be some developments [24]. This requires the EPS of Electric Aircraft to be a distributed system, adding more motors to the powertrain, which in itself adds to the complexity and reliability challenges. In order to design a distributed HVDC grid an extensive literature study has been done regarding grid topologies of existing MEA and AEA. Specific structures will be highlighted in the upcoming sections that have been used for the design process in this project.

4.1.1. Grids in MEA

As mentioned in the in the introduction, MEA are aircraft that are partially electrified by replacing one or more of the non-electrical secondary systems by their electrical counterparts, such as the hydraulics or pneumatic systems. MEA grid topologies make use of electrical starter converters to start the turbines for which the electrical power is supplied by the Auxiliary Power Unit (APU), other turbine or External Power Supply. In Figure 4.1, a grid topology of an MEA based on the Boeing 787 is shown. These parts are depicted as the Generator, APU Generator and EXT-PWR. The jet engine is started by the APU or a ground vehicle. [15]. This is all made possible by replacing the bleed-air extraction system by electrical Variable Frequency Starter Generators (VGSFs), which in the case of this Boeing are able to supply a total of 1 MVA. In regular aircraft, this system is used numerous purposes, such as the the Wing Ice Protection System (WIPS) for example, where the bleed air is heated and pressurized by a (gas) engine. In MEA the VGSF's take over this function. In addition to the starter generators, the EPS supplies the power to loads such as the Environmental Control System (ECS) and the WIPS, which are secondary loads with a relatively high demand (especially the ECS). Navigation, avionics communication and control systems are not depicted in Figure 4.1 but are supplied by the EPS as well [15].

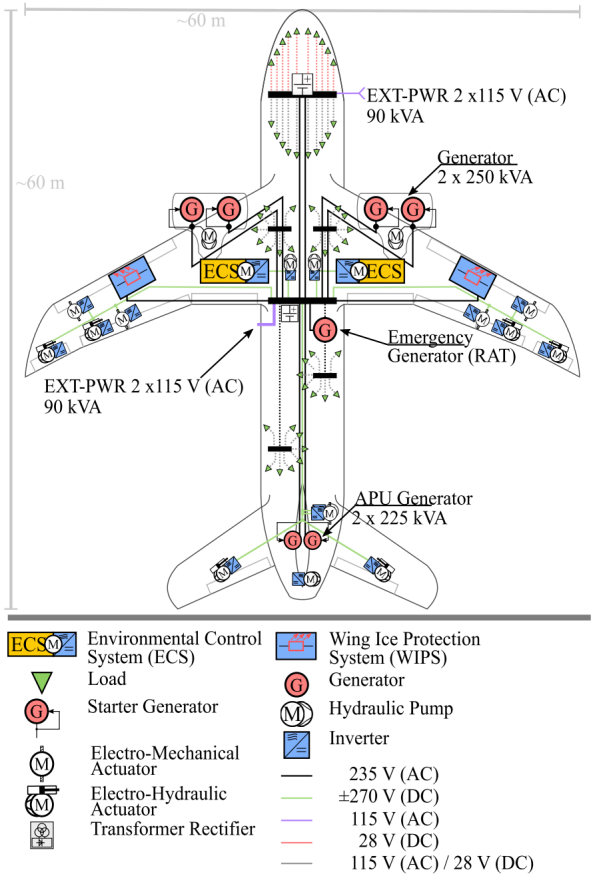

Figure 4.1: The EPS of a MEA, specifically the Boeing 787, with all the added loads and structural design [15].

Nodes in the grid where multiple cables come together are implemented with busses. For rerouting power and supplying loads with the correct voltage, current and power ratings these node connections are very important. Busbar function and implementation in the propulsion grid is discussed further in Sections 4.2 & 4.3.

The use of multiple motors in AEA and MEA leads to multiple propulsion channels in the EPS. These propulsion channels can be viewed as routes from the power source to the motors. As a standard, EPS grids use radial baseline architecture where the grid is divided into isolated propulsion channels, where the motors are connected to separate busbars. Considering that the motors in these electric systems have peak ratings of order size 1 MW as listed in 2.1, the size of a bus is much larger than for conventional aircraft, and inherently more susceptible to faults due to the higher powers it has to transfer and the more complex connections it facilitates [25]. Faults or problems in the bus can result in a loss of propulsion when the motors of that channel cannot be supplied with power. A method to mitigate this is to increase the size of the motors as a precaution. This principle is commonly referred to as 'oversizing' and is the safest method of making sure the propulsion system is able to function properly in case of motor failure [26]. Conversely, this significantly increases the weight of the aircraft and is not a very efficient design solution. Hence, reliability concerns in the power-train must be addressed in more effective placed; in the grid itself.

In a study conducted in 2023 [25] proposes two different ' loop' type structures of busses that can operate despite a fault at any location in the bus by operating the circuit breakers of the surrounding location of the fault to isolate it. Consequently, all connections to the bus will be able to operate continuously if, due to a fault, a part of the bus must be disconnected. Appendix F.3 shows an analysis of the grid for all cases of possible faults, shown in the figure as L1, L2, through L7. In this analysis, it can clearly be seen how fault scenarios are dealt with and how the implementation of the loop effectively mitigates the fault effects. One of the two architectures is shown in Figure 4.2, below:

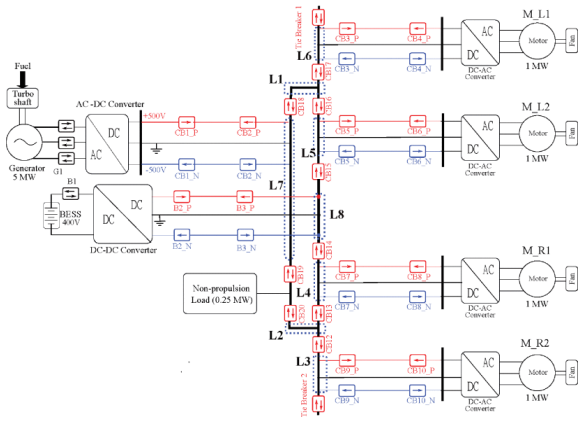

Figure 4.2: Loop-type structure for bus bars. From [25]

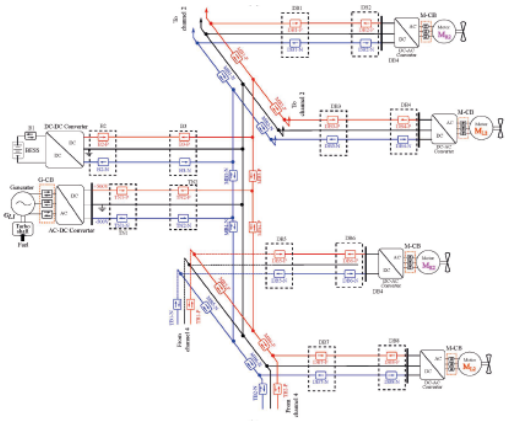

Figure 4.3: H-type structure for bus bars. From [27]

In a later paper using the gained knowledge from [25], an H-type structure for busbars is proposed and explored. In this structure the reliability of the grid is improved seeing as the 'H-structure' isolated the main bus from the motor bus, allowing the grid to be more fault-tolerant [27]. Figure 4.3 shows the grid structure. In Appendix F.3 the fault scenarios and their effects are shown again, including the operation of circuit breakers. This way of improving the redundancy of bus connections while also decreasing the complexity of the bus (and therefore also lowering the mass burden of the implementation) has numerous benefits for grid design.

Both papers compare the required over-sizing of the motors compared to radial baseline topologies. In both cases, the oversizing factor the motor design is subjected to is due to a fault case where two generators fail. Consequently, both structures are implemented to connect multiple propulsion channels to each other, displaying the benefits of interconnecting the busses compared to using structures with independent propulsion channels. In addition, in grids that use this structure the required (over)sizing of the motors is not influenced by the loss of one generator. This is because power can be re-rerouted in fault conditions and still properly distributed among the loads; requiring less oversizing.

The redundancy of these architectures is shown in how the architecture is able to disconnect in case of faults in different locations while the remaining connections operate continuously. Such connections are seen through literature to significantly enhance the reliability, and therefore these types of archi-

tectures will be used in the design of the grid topology in Section 4.3.

Besides increasing the reliability by improving the redundancy of the busbars structures in the grid, reliability can also be increased by improving the redundancy of the lines feeding the motors. A study conducted on turbo-electric distributed propulsion grids displayed this design method [26]. Using busses to connect multiple motors to the same bus is common practice in MEA grid design. Combining this with so-called 'multi-feeding' the motors drastically improves the reliability of the grid. Essentially, multi-feeding means every motor is connected to two lines, one main line and one secondary line connected to a different bus than its 'original bus'. Once there is a fault in either the main line or the bus supplying the main line, the power is diverted to the secondary line and the motor can resume nominal operation [26]. Due to this improvement in redundancy, the over sizing of the motors can also be reduced. Examples of such grids are shown in Figures 4.4 and 4.5:

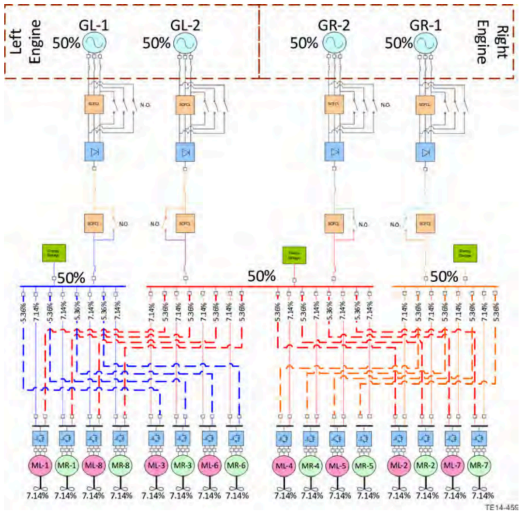

Figure 4.4: 3-Bus Multifeeder Topology [26]

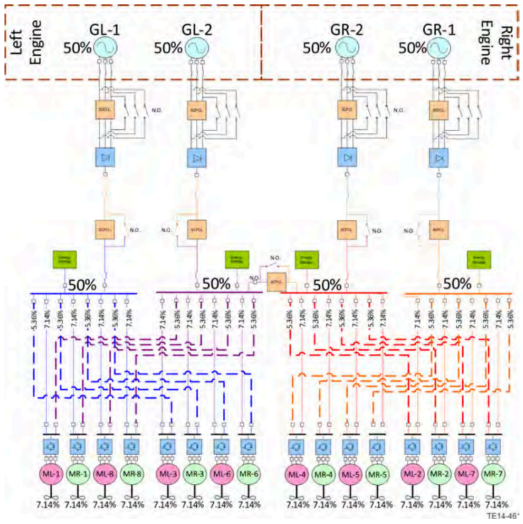

Figure 4.5: 4-Bus Multifeeder Topology [26]

Both designs significantly improve the reliability of the motor side of the grid, while inherently it also increases the total weight burden of the topology. Nevertheless, as will be further discussed in the relevant sections on grid design (Section 4.3) and reliability assessment of the grid (Section 5.3), using multi-feeding on the motor side has significant benefits in distributed propulsion grids.

4.1.2. Grids in AEA

In AEA the propulsion system is replaced by an EPS, removing all non-electric components from this system. As mentioned before, the challenge in this lies in minimising the mass of the grid from power source to load. Electric drive trains in EPS include everything from the power source to the load; in this case from the batteries to the motors used to power the propellers of the AEA. Clearly, this grid should be a distributed system, with multiple motors sharing the propulsion burden equally. The distributed EPS must be reliable which is achieved in the way the grid topology is organised, by using circuit breakers and making a control system for accurate fault-detection and fault-prevention. Furthermore, higher system voltage levels need to be used in order to be able to transfer the power at allowable weight values.

An example of an AEA distributed propulsion is the proposed design of the N3-X aircraft. Figure 4.6 displays the propulsion grid for this AEA. Here you can see the bus elements, cross-connections and distributed system of the grid. The grid operates at a system voltage level of 10 kV and incorporates some of the redundant design features mentioned in Section 4.1.1 such as multi-feeding of the motors.

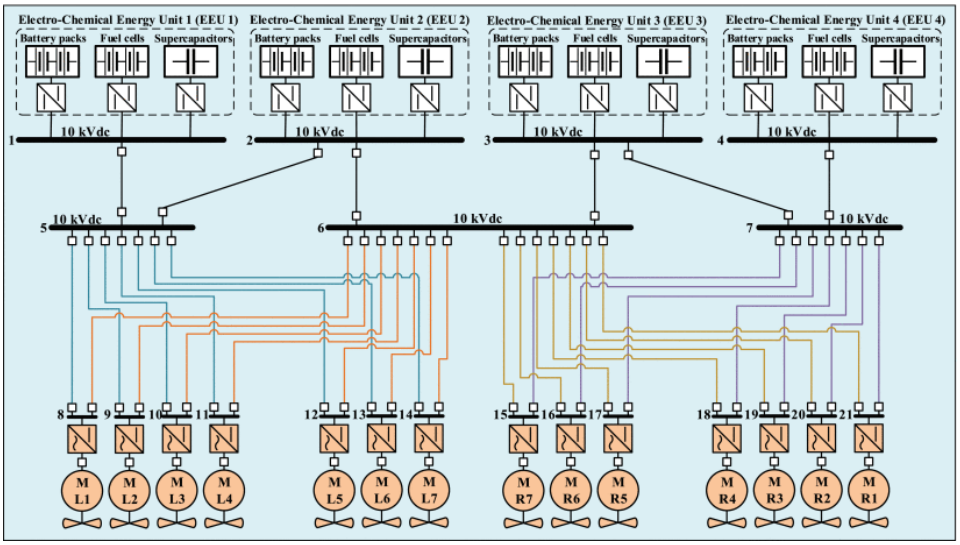

Figure 4.6: AEA propulsion grid design for NASA N3-X aircraft (from [28]).

In the following section the components of the grid will be listed in detail and the most important design choices are listed. Important to mention is that this thesis will focus on the design of the topology and inclusion of parameters of DC solid-state circuit breakers. In order to complete this grid design and allow it to be as effective as possible in mitigating fault cases, the control part of the topology is very important. However, this part is omitted in order to keep to the scope of this thesis. Further discussion of this subject van be found in Section 6.3.

4.2. Components of the Grid

This section will zoom into all the separate sub-components of the aircraft. The exact functionalities and characteristics of all electric components of the system are difficult to determine since the technology is relatively new and a lot of research must still be done. A quote from a publication from 2020 gives an insight into the timeline of electric aviation, ”A 150-passenger narrow body, single aisle AEA that properly operates over typical commercial missions can be considered an achievable target within the next 20-30 years.” [3, p. 169315]

The scope of this thesis is to design a reliable grid topology that falls into the weight budget available as listed in Chapter 2. The selection of motors, batteries and generators follows from the information available on the E9X from [5] and [4], which will be listed in the following subsections. Finally, the control of the detection and prevention of faults will not be discussed in this thesis. The same holds for the implementation of the WIPS, ECS, navigation, communication and other loads of the EPS. Both of these are present in the aircraft and will play a role in later design but due to time limits will not be included in this thesis, and will therefore also not be included in the program of requirements in Section 2.2. Further consideration of this subject can be found in 6.3.

4.2.1. Batteries

Where ‘normal’ aircraft use engines such as jet engines, turbines etc. that generate energy by the use of fuel and airflow the goal for the E9X is to fly fully on electric power. It is assumed that the battery packs will have an energy density of 360 Wh/kg [5]. This estimate is based on a review of studies on battery electric aircraft prior to the publication of this paper. For a higher range the battery densities will increase to 450 Wh/kg or 550 Wh/kg for 800 km and 1000 km [4]. The current research into battery technologies estimates the possibility of using lithium-ion chemistries such as lithium-air battery cells and packs with the required energy densities to be available between 2030 and 2035. [29].

In the case of the E9X, the total available weight for the battery cells and packaging is 34960 kg which is almost half of the total weight of the plane. Battery cells have a higher energy density but the packs make it possible and safe to install these cells in large quantities [4].

The packs are assumed to have the desired output voltage of the system level. However, in the topology, the option of using DC/DC converters for the batteries is discussed. The benefit of this would be a more stable voltage output level which is a requirement for the motors. These converters would implement a form of partial power processing that can also help if batteries due to degradation over time are unable to perform at the same levels. Partial processing in DC-DC converters involves only processing a portion of the total power through the converter, with the remaining power directly transferred from the input to the load, improving overall efficiency. This approach allows for better performance in applications requiring high efficiency, such as electric propulsion drivetrain systems [30]. With added control for these converters, possible differences between power and voltage ratings of two parallel battery packs could be nullified such that these levels are stabilised at the bus.

To conclude, the energy density of the batteries is 360 Wh/kg, a total weight of 34960 kg is available of which 25 % is used for overhead packaging. We consider non-isolated DC-DC converters that have a power density of 25 kW/kg [15]. Furthermore, a partial power processing factor of 33% was considered. As will be seen in Section 4.3, every battery pack will either supply 1.62 MW (in 8-battery structures) or 3.24 MW (in 4-battery structures) to the grid. Conversely, this means that the mass of the DC-DC converters considered are 21.6 kg (8-battery) or 43.2 kg (4-battery).

4.2.2. Generators

The generators are used as a back-up system in the plane in case of failure of the batteries or if all batteries are completely used up and a restart must be made. Two fuel generators are present in the tail of the plane that are able to supply the power to the EPS. A third generator is present that serves as a back-up system for the navigation, WIPS, ECS, communication systems and more. For this reason, the topologies will show the two generators that are a backup to the EPS.

The requirement for these backup generators comes from the possibility of a restart in case landing is not possible. These generators are also able to charge the batteries when they are turned on and are taken into account in the definitions of critical failure situations. Further elaboration on this can be found in Section 5.3.2. Additionally, it should be noted that the generators are purely meant as a back-up system and not for the purpose of range-extension, although it could serve this function without major changes to the grid [4]. For the scope of this project, the specifics of the generators are:

- Required range extender power of 11.3 MW
- Generator max power of 5.8 MW
- Generator and rectifier efficiency of 0.93
- Generator and rectifier mass of 536.6 kg

These values are taken as estimates from [5] and [4].

4.2.3. Motors

The motors used in the AEA are fully electric and are integral to the distributed propulsion system, which employs a total of eight motors. Each motor is directly connected to the wing, driving the propellers to provide the necessary thrust. These motors are connected to the aircraft's DC grid, with the assumption that the inverters required to convert DC voltage to the AC voltage for motor operation are integrated within the motors themselves [4].

The key parameters for the motors include an electric motor length and diameter of 0.56 meters each, a maximum continuous power of 1.36 MW per motor, and a peak power of 1.62 MW per motor for short durations (up to 3 minutes) [4]. The combined efficiency of the motor and inverter is 0.95, with a total mass of 326.4 kg per motor and inverter unit. It is crucial to note that the failure of more than one motor is considered a critical failure, emphasising the importance of the distributed propulsion approach in enhancing the reliability and safety of the aircraft. More detailed discussing of this will follow in Section 5.3.

4.2.4. Transmission network

The transmission network of the aircraft encompasses all components between the batteries, generators, and motors, including cables, buses, and circuit breakers. This entire network will henceforth be referred to as the Power Management and Distribution (PMAD) System.

Four different sizes of cables will be utilized, as detailed in Table 3.2, each tailored to handle different power levels. These sizes ensure efficient power transmission within the aircraft's system. It should be noted that the negative effects of harsh environmental conditions, such as radiation and low air pressure, on the cables are not considered in further design decisions.

The transmission network can be designed as either unipolar or bipolar. In a unipolar grid, a single voltage level of 3000 V is used along with a ground line. This configuration simplifies the design and can potentially reduce the overall weight of the system. On the other hand, a bipolar grid involves three lines: a ground line, a positive 1500 V line, and a negative 1500 V line. The bipolar configuration can offer advantages in terms of voltage stability and reduced electromagnetic interference, but it also adds complexity and weight to the system.

After careful consideration, the decision was made to implement a unipolar grid. This choice was primarily driven by the significant reduction in weight for the buses and breakers, which is a critical parameter in the aircraft's design, as specified in the program of requirements (see Section 2.2). The anticipated weight savings from using a unipolar grid are substantial, making it the more practical choice for this application.

4.2.5. Circuit Breakers

In the context of AEA, circuit breakers play a crucial role in ensuring the safety and reliability of the electrical grid. Circuit breakers are designed to protect electrical circuits from damage caused by overloads or short circuits. They achieve this by interrupting the flow of current when a fault is detected, thereby preventing potential hazards such as electrical fires or equipment damage [31]. The topology of the circuit breaker is typically conceptualised as switches arranged in parallel with a suppressor and a limiter in series. System voltage and current levels can significantly influence the characteristics of these circuits, potentially resulting in weight variations.

In an AEA, where electrical systems are paramount, the role of circuit breakers becomes even more critical. These devices must be capable of handling high power levels and responding quickly to faults. Solid-state DC circuit breakers are particularly suitable for this application due to their fast response times and ability to be controlled electronically, as well as low mass burden. An example of a Solid-state DC circuit breaker is displayed in Figure 4.7. Additionally, bidirectional circuit breakers enhance the flexibility and redundancy of the power management system, allowing for better fault isolation and system reliability. The reliability impact of circuit breakers in the grid will be further analysed in 5.3. By ensuring that circuit breakers are properly integrated and optimized within the grid, the overall safety, efficiency, and performance of the aircraft's electrical system can be significantly enhanced.

Figure 4.7: Solid-State DC Circuit Breaker [32]

For this design implementation, solid-state DC circuit breakers will be employed. While the precise design details will be handled by another team, certain choices and conditions will be established for the design of the overall topology. Most circuit breakers in the grid will be bidirectional, except those connected to the generator. Bidirectional circuit breakers are generally heavier and require more control signals compared to their unidirectional counterparts. This increased complexity arises because bidirectional breakers utilize two Insulated Gate Bipolar Transistors (IGBTs) to manage the switching operations of the circuit [31]. Although unidirectional breakers are typically preferred due to their simpler and lighter design, their feasibility depends on the specific implementation requirements. However, since reliability forms an even more important consideration, bidirectional breakers are preferred in the design. All in all, for this grid topology, a unipolar voltage level has been selected. However, if a bipolar grid is implemented, some components may be downsized due to the reduced voltage levels, leading to potential weight savings as well.

4.3. Design of Topologies

In this section all components and their connection possibilities to the grid will be explored. Through a bottom-up approach, the complete grid design will be developed. The grid topology can be divided into the four sub-systems listed in the above sections. Each of these sub-systems can be independently evaluated in terms of reliability and weight for different structures. When designing the full grid topology all the individually best-performing structures are laid out and combined to make the HVDC grid based on the requirements as defined in Chapter 2. In the following subsections, the results of these independent studies are shown and explained based on their characteristics. Next, a justified choice based on the set requirements and reliability vs weight concerns will be made to build to two final grid topologies in Section 4.3.5. The two designs will be specifically designed with a more reliability focus and a more weight focus in mind. Based on these two goals certain choices are made and can be justified. To conclude this section, the structural analysis of both topologies will give insight into their total masses and allow for quantitative comparison.

4.3.1. Design: Motor connections

The connection of the motors within the grid pertains to the interlinking between the motors and the buses of the interconnection network. In evaluating the redundancy of this system, the balance between the motors is a key consideration. The motors are connected in the most efficient manner, ensuring balance across either side of the aircraft (i.e., left to right), while minimizing the length of the cabling. Consequently, Motor ML1 (the leftmost motor on the left wing) is connected to the same bus as Motor MR4 (the leftmost motor on the right wing). As discussed in Section 4.1.1, several methods can enhance the redundancy of motor connections, which are listed below:

- Connecting all motors separately
- Using multi-feed connections or single connections
- Using multiple busses to connect the motors
- Balancing the motors

Considering the targets of the program of requirements and critical failure cases, the design must ensure that only one or two motors are permitted to fail during flight, thereby necessitating highly reliable motor connections. During the design process, multiple topologies were explored, combining the aforementioned elements in various configurations. Two of these topologies are illustrated in Figure 4.8 , both implementing multi-feed cabling to the motors, denoted by the dashed lines.

The topology employing three buses offers the advantage of supplying all motors with power from a single central bus in the event of a failure in either the left or right side buses. Despite this added reliability, this central bus becomes a critical point in the system. If the central bus or its power supply fails, the redundancy of the system is compromised, leaving only one connection to supply power to all motors. In the second topology, the central bus is replaced by four busbars. If any of these buses fail, only four motors lose their secondary connection to the system. This configuration enhances the overall reliability of the grid but also introduces a vulnerability by limiting the ability to supply one side

of the motors from a single side of the grid.

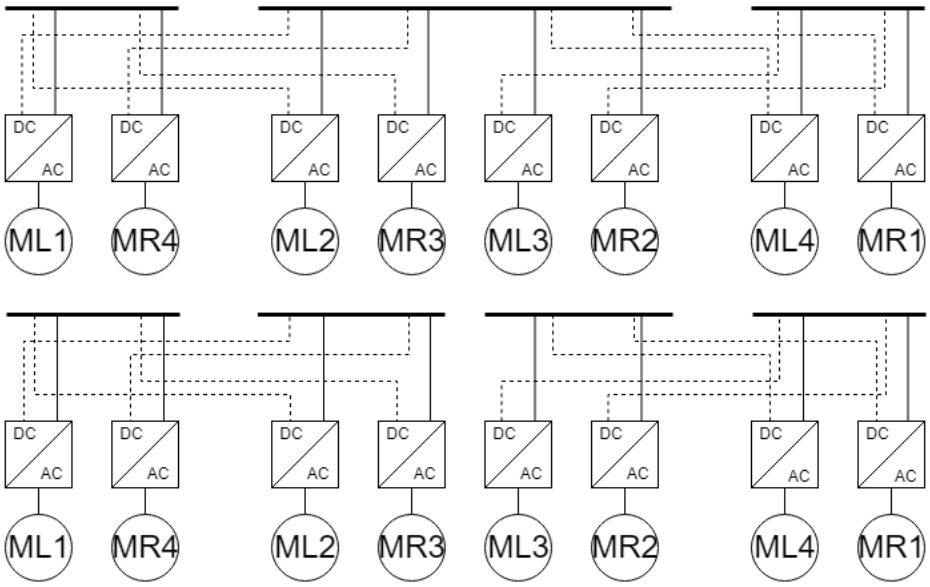

Figure 4.8: Grid schematics of two possible motor connections that use three of four busbars.

Evaluating these topologies based on weight, reliability, and complexity yields the following differences. The central bus in the three-bus topology must supply the full power demand of 12.96 MW, whereas the other buses need to supply only 6.48 MW each. When using copper busbars, this requirement increases the weight of the system. The thickness of the busbars must increase to accommodate the higher power rating, exemplified by the weight increase of a meter of cable from 3.67 kg to 20.06 kg for a doubling of power (which is over a factor 5 increase in weight). Both topologies utilize the same number of circuit breakers, totaling sixteen. In terms of reliability, the three-bus topology performs best, as detailed in Section 5.3. Evidently, the complexity difference between the topologies is not noteworthy. The balance in the three-bus topology is ensured by the central bus. While the four-bus topology does not inherently implement this balance, if balanced within the transmission network, its performance can be seen as equivalent to the three-bus implementation.

4.3.2. Design: Batteries

For the batteries, several design configurations are feasible, as outlined below:

- Configurations of four or eight battery packs
- Connection options with or without converters
- Arrangements in series or parallel
- Connections as single units or in groups to busbars

These design choices are influenced by the transmission network's parameters, which are detailed in Sections 3.2.3 and 3.4. The bus system voltage levels are anticipated to be 3 kV, and the batteries are expected to supply a total power of 12.96,MW. Configurations with four battery packs require higher energy density compared to those with eight. When connected in series, the batteries can produce different voltage output levels. DC-DC converters are used to elevate the voltage to necessary levels and provide stable supply control, as discussed in Section 4.2.1.

A critical failure scenario for the battery system occurs when more than half of the propulsion power is unavailable, resulting from faults in at least five of eight or three of four battery packs.

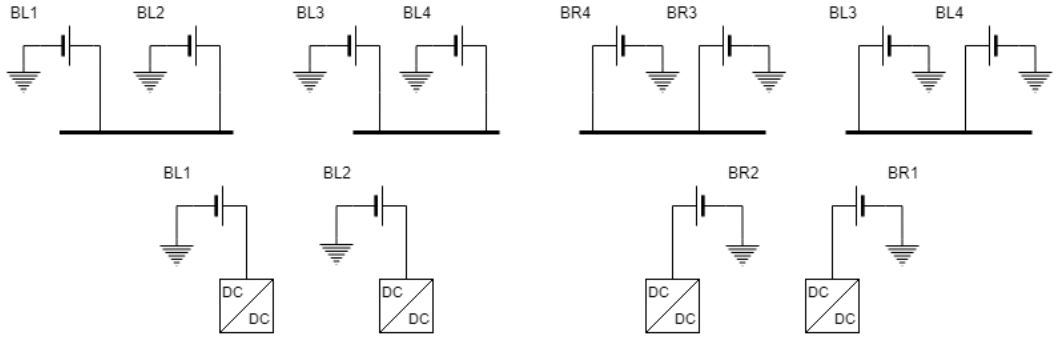

Figure 4.9: Two possible battery connections evaluating four or eight and the implementation of converters.

The grid connection options being evaluated include eight battery packs without converters connected to four busbars versus four battery packs with converters connected to two busbars; these setups are illustrated in Figure 4.9. The motors can accommodate voltage fluctuations of about 20 to 30% during nominal operation, indicating that DC-DC converters are not strictly necessary, thereby facilitating a comparison between the two designs.

The eight-battery pack configuration offers enhanced reliability against critical power loss that could lead to propulsion failure. In this setup, either four batteries or two busbars must fail to reach a critical state, whereas the threshold is lower with four battery packs. Although the cable and bus weights are comparable in both systems, the inclusion of converters in the eight-battery configuration provides advantageous weight characteristics. The possibility of connecting all batteries individually was rejected due to insufficient redundancy.

Ultimately, the selected topologies incorporate isolated connections to the bus, with a ring architecture that necessitates circuit breakers in between every bus connection, as explored in the subsequent section.

4.3.3. Design: Busbar structures

In AEA grid design, busbars play a crucial role in distributing electrical power efficiently across various systems. A busbar is essentially a conductive strip or bar that carries electricity within a distribution board, switchgear, substation, battery bank, or other electrical apparatus [25]. Its primary function is to consolidate incoming power from multiple sources and distribute it to outgoing feeders. In aircraft systems, busbars must accommodate dynamic changes in power demand and maintain system stability under different operating conditions.

As noted in Section 4.1.1, loop-type structures are critical for maintaining power distribution reliability in sensitive grid sections of electric aircraft. These loop structures can be configured in various ways, one common method being the ring structure, depicted in Figure 4.10. However, the ring structure has its limitations, such as potential overloading of circuit breakers if one fails, and challenges associated with adding additional loads or power supplies to the circuit. Practically, two other busbar topologies often employed are the dual bus and the transmission or auxiliary bus, as shown in Figure 4.11.

These systems both incorporate dual parallel busbars that connect to the loads and power supplies. The primary distinction lies in how these busbars are utilized. In the auxiliary system, the main busbar is employed during normal operations; if a fault occurs in a circuit breaker, load, or section of the busbar, the auxiliary busbar is activated. This switch is facilitated by a bus coupler—illustrated as a rectangle between the busbars—which allows the disconnected segment to maintain access to the main busbar.

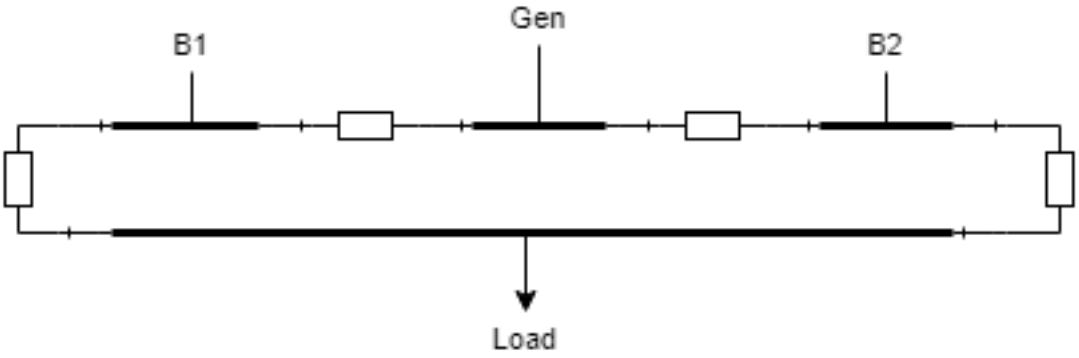

Figure 4.10: Bus-bar implemented as a ring structure

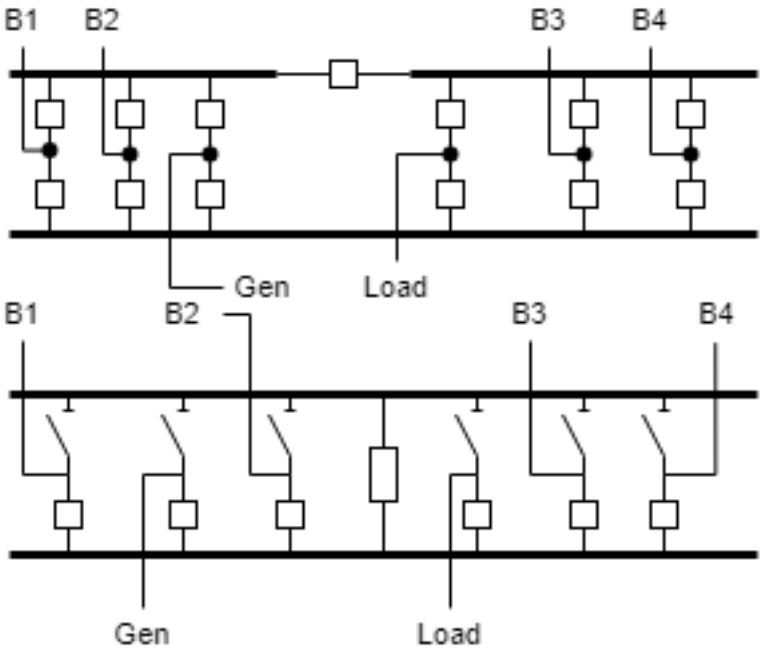

Figure 4.11: Dual busbar and main-auxiliary busbar implementation

Conversely, the dual bus-bar system distributes the load evenly across both busbars throughout operation, providing a more flexible power management system without the need for a transfer bus coupler. This setup offers significant advantages over the transfer bus system, particularly in terms of operational flexibility and the ability to adapt to varying electrical loads without the complexity of additional coupling mechanisms.

4.3.4. Design: PMAD network

The Power Management and Distribution (PMAD) network in aircraft is defined as comprising all components that connect the batteries to the motors. This network is central to the design of the EPS of the AEA, as it affects both the reliability and the weight of the aircraft. Various configurations can be explored for the PMAD network, each dependent on the interconnections chosen for the batteries, motors, and generators. Some of the possible configurations include:

- Implementing H-type, ring-type, or main bar bus structures
- Employing multiple central nodes or a single connection point
- Utilizing isolated single channels

It is important to note that these configuration options are more flexible compared to those available for batteries or motors. Two distinct transmission grid designs are illustrated in Figure 4.12 to provide a more detailed view of the possible configurations. It should be noted that the circuit breakers and their placements are omitted in these diagrams to allow create a clearer picture; naturally these are present in the actual design.

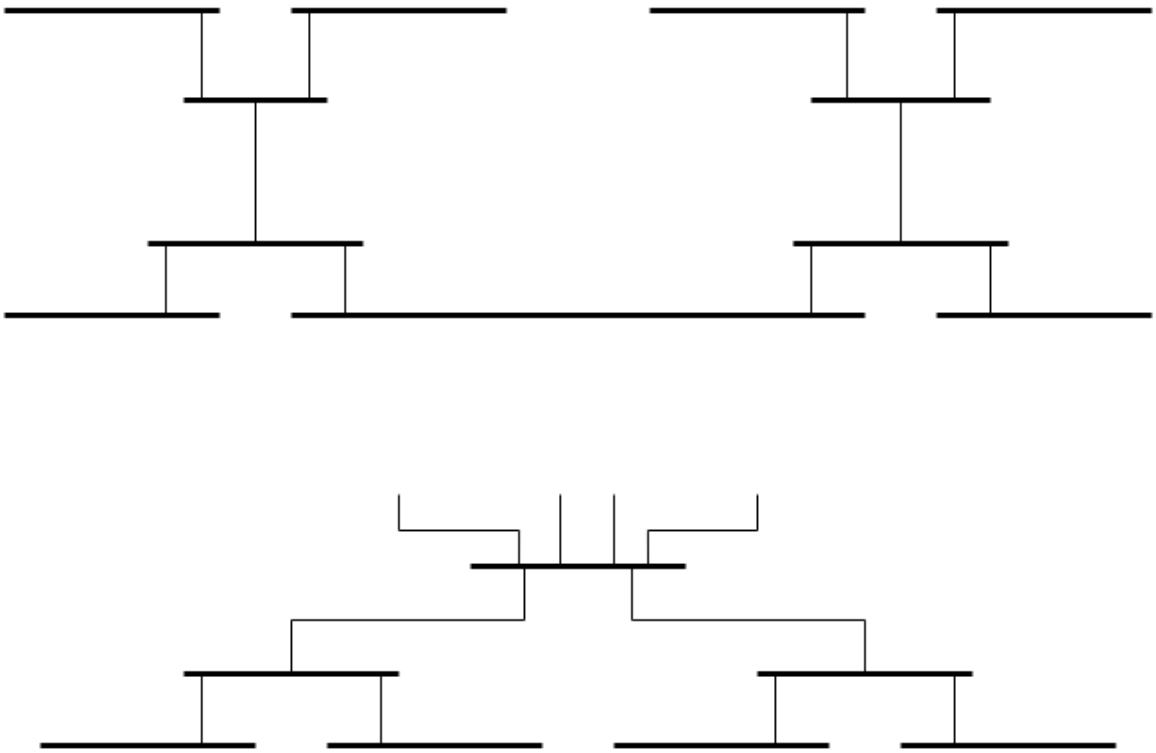

Figure 4.12: Different implementations for the transmission network.

One grid design features a single connection point using a ring-type bus, capable of connecting all motor channels to every battery pack via this bus structure. However, this configuration introduces a significant point of failure; a fault at the bus would result in a total power loss to the system. This grid is simpler and less complex, lowering the mass burden of the grid, but offers reduced reliability and redundancy.

The alternative grid design incorporates an H-type busbar system with three bus connections to the motors, featuring two main connection points at the battery interface. This arrangement does not allow every motor to be powered by all battery packs, but it enhances the overall system reliability.

The balance between reliability and weight is crucial in the design of the PMAD network. Increasing the network's complexity typically adds weight due to additional cabling but also improves reliability through enhanced redundancy. Thus, these aspects must be carefully evaluated both qualitatively and quantitatively, considering the trade-offs between weight increase and redundancy benefits.

A detailed weight comparison for these grids, based on the power ratings required at each connection point, is challenging to pinpoint accurately. Nevertheless, both grid topologies have been integrated into the chosen architectures, with total weights provided in Section 4.3.6. Additionally, Section

5.3.5 presents the calculated failure rates for these PMAD systems, providing further insights into their operational effectiveness.

4.3.5. Selected designs

The design process resulted in the selection of two distinct topologies, guided by the requirements detailed in the program of requirements (Chapter 2). Figures 4.13 and 4.15 illustrate these grid designs, which are crafted to balance the need for reliability with the technical constraints of the system, emphasizing optimal functionality within these bounds.

Design 1: 8 battery-3 bus grid

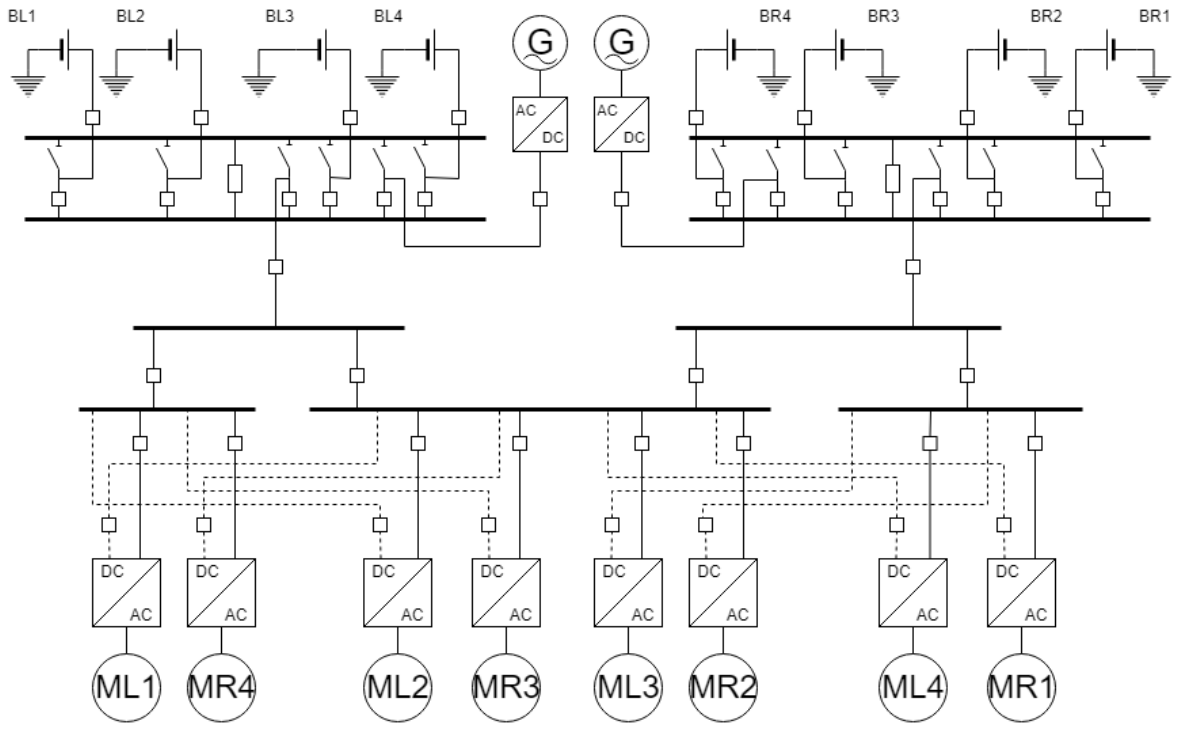

Figure 4.13: Grid architecture with 8 batteries and 3 bus-bars for the motor connections

This topology employs a main and auxiliary busbar connection for battery packs, each connected directly without converters. The motors are linked through a three-bus system combined with H-type busbars. Notable failure points include the connections between the battery busbars and the H-busbars. In the event of a failure in one of the battery busbars, the multi-feed cables ensure that all motors still receive power. The design allows for the middle bus of the motor connections to fail without a complete loss of power, although it would limit the ability of batteries on the right wing to power certain motors. The propulsion remains balanced despite these potential failures.

The weight of this topology is optimised to manage a total power of 12.96,MW, concentrated on the middle busbar of the motor connection, significantly reducing the weight requirements for other cables. However, a failure in a battery busbar also disrupts the connection to one generator, which could be mitigated by linking both generators to both battery busbars, albeit at the cost of increased cable weights. The total weights of all sub components and the total weight of the complete grid are depicted in Section 4.3.6.

Detailed failure scenarios and their management are depicted in Appendix F. An example fault scenario for this grid design is shown in Figure 4.14:
The fault in Figure 4.14 is depicted by the lightning symbol. After the fault event, the circuit breakers

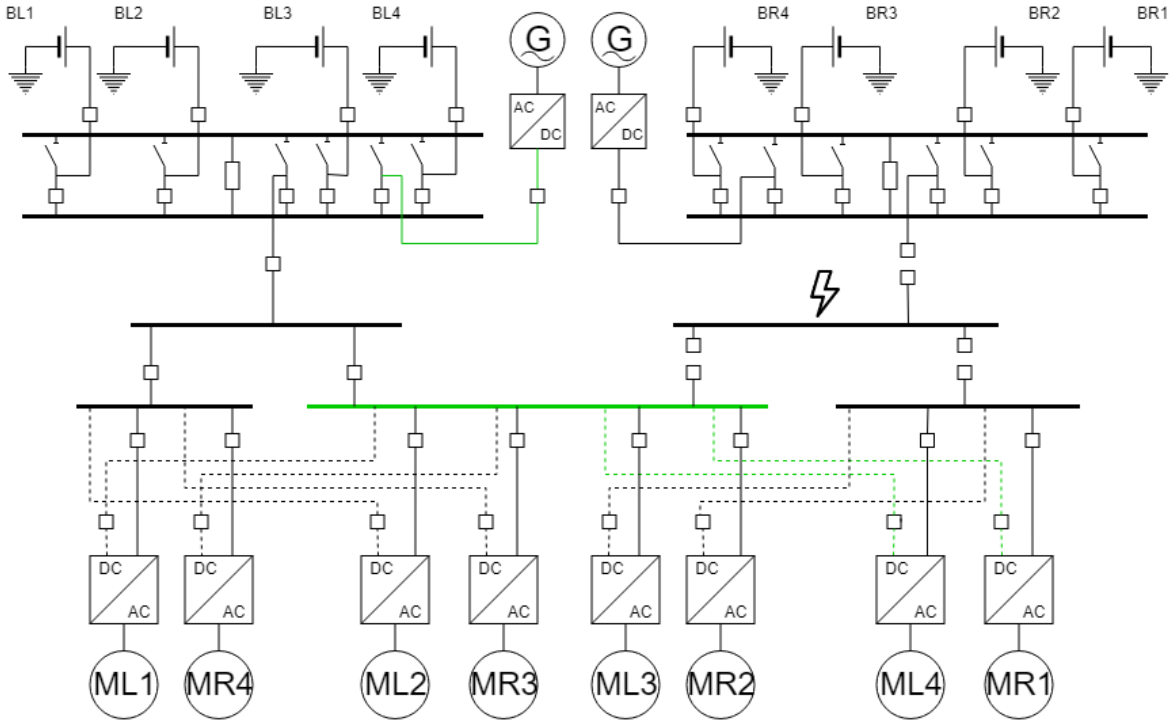

Figure 4.14: Bus failure in 8-battery grid & fault management

surround the bus are opened, disconnecting the right part of the grid (losing all right batteries). In order to mitigate the failure effect, the backup generator is turned on, supplying half of the power necessary to cover the loss of the batteries. The multi-fed lines from the central bus are turned on to keep continued power to Motors ML4 and MR1, allowing for the fault to be completed resolved and nominal flight operation to be continued. The additional operations required by the EPS (steered by the control systems) are highlighted by the green lines in the diagram.

Design 2: 4 battery-4 bus

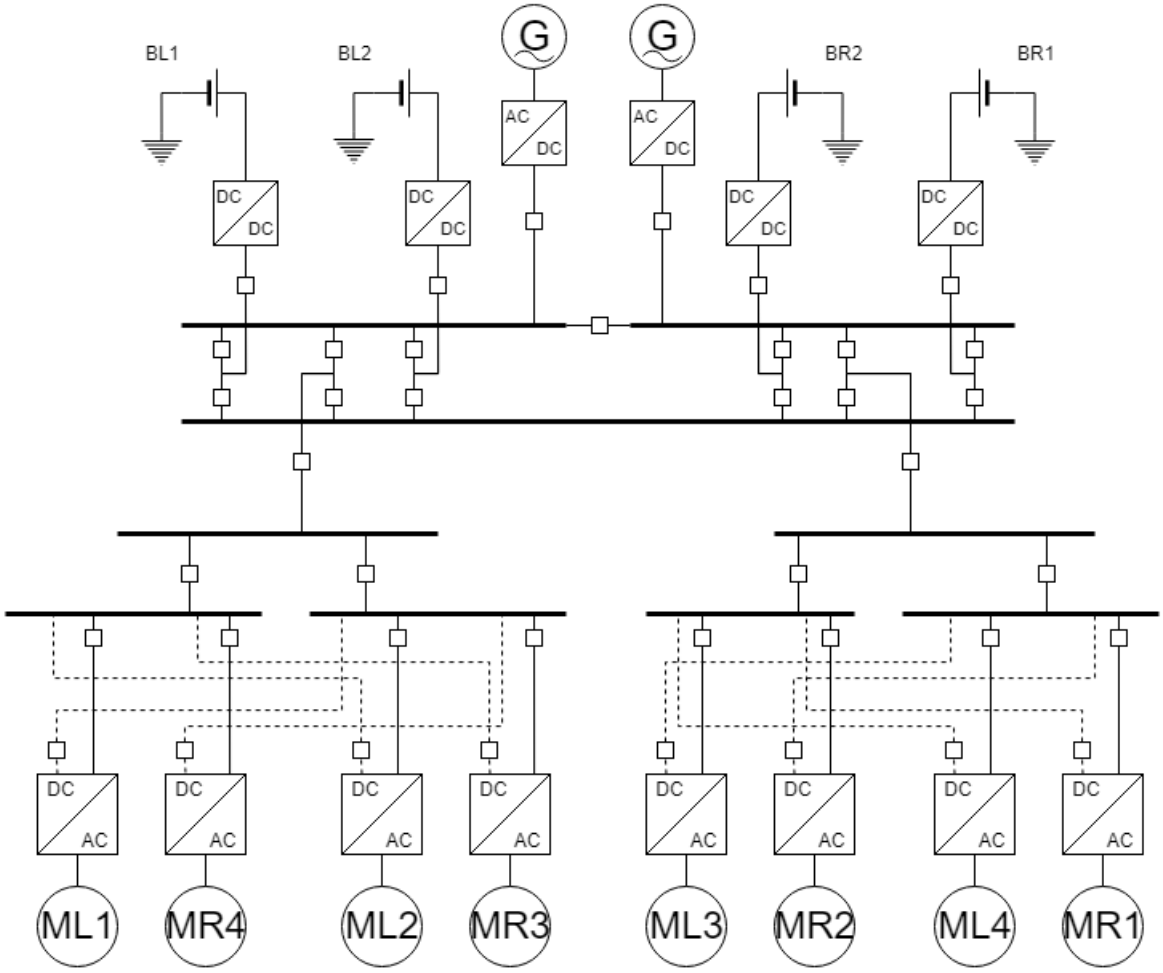

Figure 4.15: Grid architecture with 4 batteries and 4 bus-bars for the motor connections.

This design incorporates a sectioned dual busbar system, with four battery packs connected via converters. The motor connections utilize two H-type bus multi-feed structures. The primary failure risk is the bus for the battery connection, designed to allow disconnection of one half in case of failure, thereby still powering the grid with half the capacity. Other critical points include the connections to the H-busses; a fault here could mean half the motors would not be supplied. Fault management strategies and potential failure scenarios for this grid are outlined in Appendix F.2.

The total system weight is reported in Section 4.3.6. Most cables handle only half of the system's power, though the battery-side bus is subjected to higher loads. The inclusion of converters adds to the total weight, but for enhanced reliability, additional connections could be implemented between diagonal motor connections and generators.

It is crucial to underscore that the designs aim to ensure maximal reliability within the constraints imposed by system capabilities. One of the main reliability constraints, given by Section 5.3.1 (explored later in Chapter 5, is that no more than one or two motors may fail at any time. Therefore, while the grid could be designed to be more weight-efficient, the primary focus of this thesis has been to maximize redundancy and reliability to prevent any significant loss of propulsion or power, ensuring that the aircraft remains operational even under partial failure conditions. This design philosophy is critical in aligning with the overarching goal of this thesis to generate a weight efficient design optimised for reliability. This consideration will be further touched upon in Sections 4.3.6 and 5.4.

4.3.6. Structural analysis of grid

One of the primary objectives of the program of requirements is to maintain the weight of the grid topology within a total mass budget of 3860.6,kg, as outlined in Section 2.2. The components considered for this total mass are detailed below:

- Power electronics: DC-DC converters
- PMAD
  - Cables
  - Circuit breakers
  - Busses
- Transformers to low voltage

To achieve this goal, a Python code was developed to calculate the masses and lengths of cables and busbars, based on the locations of all components and busbars. The codes for both architectures are provided in Appendix C.2 and C.3.

Initially, the locations of motors, batteries, busbars, and their connections were defined. These locations were placed in a grid with dimensions relative to the aircraft. Figures 4.17 and 4.16 illustrate these orientations, where the symbols represent:

- **Blue diamond:** batteries
- **Blue dash**: battery bus
- **Black icon:** motor
- **Black dash:** motor bus
- **Green plus:** generator
- **Red dot:** main bus

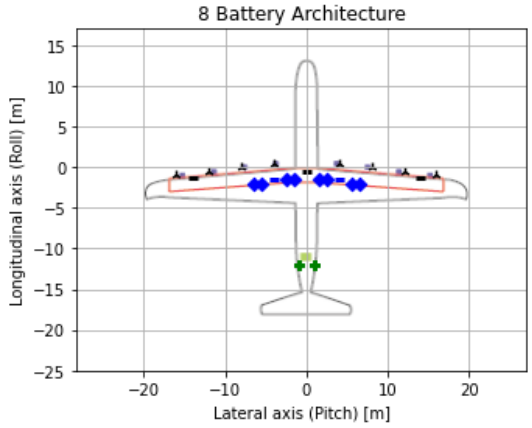

Figure 4.16: Structural analysis of 8 battery grid, including locations of components

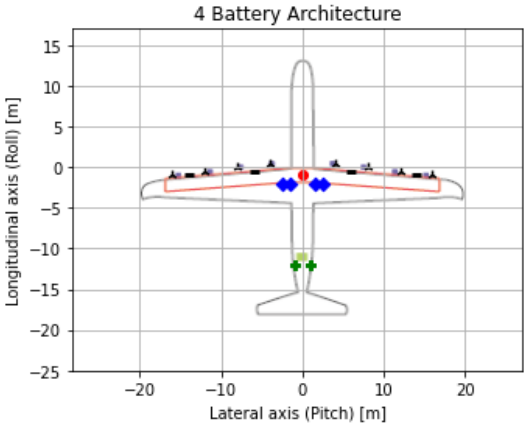

Figure 4.17: Structural analysis of 4 battery grid, including locations of components

The code comprises multiple separate functions for calculations. Two of these functions, `businfo` and `cablesitem`, are responsible for calculating the weight, length, and positions of the busbars and cables, respectively. The cables are categorized into four groups based on their maximum case power ratings, as shown in Table 4.1.

The calculations provide generalized and simplified estimates of the real-time situation. These estimates were done in order to be able to quantitatively compare both grid topologies for their weights. Cable lengths are determined based on the most direct paths between two locations, measured in a

two-dimensional plane. A correction factor of 1.2 is applied to account for unforeseen additions such as routing, bends, or mounting.

The weight of the busbars is calculated with a correction factor of 2.5 compared to the weight of the cable in the same power category. It is estimated based on the fact that busses can be considered to be simple nodes connecting pieces of cabling and by adding a factor 2.5 it allows for spacing between different lines attached to the bus and general up sizing. Naturally, for the calculations to become more accurate, this estimate needs to be refined based on the actual implementation of the busbars. The required length is based on the number of cables connected to the busbar, multiplied by estimated circuit breaker dimensions. The location of the busbars is considered the midpoint, although in reality, connections may vary.

These calculations could benefit from extra precision but provide an adequate basis for comparing different topology implementations.

Masses	**Architectures**			
	8 batteries		4 batteries	
Cables	2187.15 kg	317.11 m	793.40 kg	298.91 m
Busses	937.69 kg	15.05 m	204.59 kg	13 m
Circuit breakers	690 kg	46	615 kg	41
Converters	0 kg	0	172.8 kg	4
Total PMAD	3737.00 kg		1785.79 kg	
Battery system				
Cables	24.20 kg	21.6 m	33.70 kg	14.4 m
Busses	521.56 kg	5.2 m	0 kg	0 m
Circuit Breakers	330 kg	22	210 kg	14
Total	875.76 kg		243.70 kg	
Motor system				
Cables	241.92 kg	216 m	239.24 kg	213.6 m
Busses	217.91 kg	7.45 m	69.73 kg	7.6 m
Circuit Breakers	240 kg	16	240 kg	16
Total	699.83 kg		548.97 kg	
PMAD				
Cables	1716.16 kg	51.6 m	325.90 kg	44.4 m
Busses	120.36 kg	2.4 m	134.86 kg	5.4 kg
Circuit Breakers	90 kg	6	90 kg	6
Total	1926.52 kg		550.76 kg	

Table 4.1: Mass of Design 1 and 2, classified per subcomponent and system

Comparing the two grid designs, it is evident that the 8 battery design imposes a significantly higher mass burden on the grid, with a total PMAD mass of 3737.00 kg, compared to the 4 battery design's 1785.79 kg. Viewed purely from a weight perspective, the 4 battery design appears more optimal. However, both designs fall within the mass budget of 3860.6 kg, as defined in Section 2.2. Qualitatively, the 8 battery design is expected to offer greater reliability due to its redundant configurations, which enhance operational continuity even in the event of component failures. The reliability of these designs will be further investigated in the subsequent chapter, and it is important to note that the weight constraints outlined in Section 2.2 have been met.

Future enhancements for this code could include the development of a User Interface to simplify the creation of topologies. Users could specify the number of motors, batteries, generators, and the desired levels of complexity or reliability, which the program would then accommodate. A simple enhancement might involve optimizing weight versus location parameters based on the dimensions of the aircraft and the number of battery packs and busbars. A more complex addition could involve incorporating power distribution properties into the topology and evaluating the added weight of cables for higher power levels in terms of increased complexity. As discussed in Chapter 3, the weight per meter of cable in-

creases exponentially with power ratings. The program could calculate the added weight for a single cable with a higher power level connection compared to multiple smaller power level cables connected separately.

5

Reliability Assessment

Safety is and has always been an issue of paramount importance in aircraft. Large regulatory measures and bodies specify dimensions and parameters for aircraft to adhere to in order for air travel to be reliable and safe, where the most significant in the scope of this project is the EASA CS-25 [23]. Especially in AEA, where the propulsion drive-train is electric, safety has a large impact on the design of the system. The technical challenge in creating an EPS that is powerful enough to provide the thrust poses substantial difficulty on its own, while the reliability necessary in aircraft adds another dimension to the problem. Therefore, there should be a balance between optimising for propulsion power (i.e. weight optimisation) and adding reliability depth to the system in order for it to be significantly protected against potential failures. In the subsiding chapter a qualitative and quantitative reliability analysis on the designed grids of Chapter 4 will be presented, using a Failure Modes & Effects Analysis (FMEA) and a Fault Tree Analysis (FTA) to eventually build to a critical failure rate of the complete AEA propulsive drivetrain grid. Firstly, the FMEA will be structurally built up, identifying the critical failure modes of the sub components of the grid and leading to a set of failure rates per subsystem. Subsequently, the FTA framework will be used to quantitatively assess the reliability of the different grid topologies as presented in 4.3.5. Additionally, a Reliability Block Diagram (RBD) was created to assess the redundancy of the motor subsystem in 5.2. This was mainly done to give some insight in other reliability assessment methods that potentially could give more insight in the design of the grid and its safety. Concluding this chapter a balanced analysis of the two topologies in terms of reliability will be presented.

5.1. Failure Modes & Effects Analysis

The FMEA is a method to analyse the potential faults in a system and look at these both qualitatively and quantitatively [33]. It looks at the three core criteria that a fault's significance is assessed on; the severity of the fault (how bad is it?), the occurrence of the fault (how often does it happen?) and the control/detection of the fault (how can we detect and/or prevent it from happening?). These criteria are assessed *quantitatively*, by giving them a relative ranking from 1-10 (explained further in 5.1.2), which are combined to form the Risk Priority Number (RPN value). The RPN value ultimately determines how much risk a certain failure mode has in damaging the system significantly and thus how much attention the designer of the system should pay to mitigating this certain fault. Additionally, the potential causes and effects of the different failure modes are assessed *qualitatively* to complete the analysis and also give the numbers significance. In generating the FMEA a few initial choices were made, in order to be able to attain the requirements defined in Section 2.2 and to keep the analysis in the scope of the project.

5.1.1. Choices

The first and foremost choice that was made was that the quantitative control/detection part of the FMEA would be ignored. In order to be able to keep within the scope of the project it would be too detailed to dive into the control part of the system. However, it should be noted that the control in the EPS is of paramount importance, especially for the reliability. Further discussion of this subject can be found in Section 6.3.

Secondly, the analysis has a top-level approach in terms of the different failure modes; to be able to attain the requirement of an assessment of the complete grid as described in 2.2 the different failure modes would be structured per sub component of the system. These are the following:

- Batteries/EEUs
- Generators
- DC-DC converters ('Converters')
- AC-DC converters ('Rectifiers')
- DC-AC converters ('Inverters')
- Transmission lines
- Busbars
- Circuit breakers
- Motors

This will allow for a sound basis for the definition of the failure rates as needed by the FTA while also keeping the analysis within the purview of the grid.

Lastly, it was decided that the severity assessment in the FMEA would be separated into the three different stages of flight; take-off, cruising and landing. The reason is that faults in the propulsive system in aircraft have different levels of significance during different stages of flight [34].

5.1.2. Ratings

As mentioned in 5.1, the FMEA works with ratings from 1-10 to assess the severity, occurrence and control/detection of certain failure modes of a system. The severity ratings are based on the potential consequence a fault can have on the system; in this case the impact on the flight status of the AEA. Its scale is shown in Table 5.1:

Score	Description and Definition
10	**Extremely Dangerous** - Failure can result in catastrophic propulsion failure leading to potential loss of aircraft and life.
9	**Very High** - Failure results in severe propulsion damage, causing complete loss of propulsion and requiring emergency procedures.
8	**Very High** - Failure leads to significant propulsion damage, requiring major repairs and resulting in extended downtime.
7	**High** - Failure causes considerable propulsion degradation, leading to significant performance reduction and requiring extensive maintenance.
6	**Moderate** - Failure results in moderate propulsion damage, necessitating substantial repairs and leading to moderate downtime.
5	**Low** - Failure causes minor propulsion issues, requiring minor repairs with short-term impact on propulsion performance.
4	**Very Low** - Failure results in minor propulsion disturbances, causing brief performance hiccups but manageable with routine maintenance.
3	**Minimal** - Failure causes negligible propulsion disturbances, easily rectified with standard maintenance checks.
2	**Slight** - Failure has minimal impact on propulsion performance, with no significant maintenance required.
1	**None** - Failure is not noticeable and has no effect on propulsion performance or safety.

Table 5.1: FMEA Severity Ratings

The occurrence values in the FMEA are based on the probability a certain failure mode has of occurring. It has a predefined scale and is shown in Table 5.2.

Score	Description and Definition
10	**Extremely Frequent (failure is inevitable)** - More than once per day or a chance of more than 3 in 10.
9	**Very Frequent** - Once every three or four days or a chance of 3 in 10.
8	**Frequent** - Once per week or a chance of 5 in 100.
7	**Very Regular** - Once per month or 1 in 100.
6	**Regular** - Once every 3 months or 3 in 1000.
5	**Intermittent** - Once every 6 months to a year or 1 in 10,000.
4	**Occasional** - Once per year or 6 in 100,000.
3	**Low** - Once every one to three years or 6 in 10,000,000.
2	**Slight** - Once every three to five years or 2 in 1,000,000,000.
1	**Nil (failure is unlikely)** - Once every five or more years or less than 2 in 1,000,000,000.

Table 5.2: FMEA Occurrence Ratings

The RPN value is then calculated to be the multiplication of all the different ratings. It is a unit-less quantity and used as a relative comparison metric, given by the following equation:

$$RPN = O \cdot S \cdot C \tag{5.1}$$

Where ”S” is the severity rating, ”O” is the occurrence rating and ”C” is the control rating. As mentioned before, in this thesis the control is omitted and therefore the RPN rating is based solely on the ”O” and ”S” ratings, and Equation 5.1 is simplified to 5.2:

$$RPN = O \cdot S \tag{5.2}$$

However, as described in 2.2, the main objective of this paper is to eventually reach a value for the critical failure rate of the designed grid topology. In order to be able to calculate the critical failure rate, the failure rate of every subsystem has to be estimated. The RPN value is used in 5.1.4 for a relative comparison of the criticality of the different failure modes in the grid. The next section describes the different failure modes in more detail, including estimates for their failure rates.

5.1.3. Failure modes

As mentioned in Section 5.1.1, the failure modes were grouped per sub component of the system in this analysis. In total, this resulted in 21 failure modes in the FMEA. This section will briefly explain the different failure modes, after which the results of the analysis will be presented in Section 5.1.4. The complete FMEA table can be found in Appendix B.1. All failure rates are given in failure per flight hour.

Batteries/EEU’s

As mentioned in Section 4.2.1 the battery packs that the aircraft will rely on will be Lithium-Air batteries. Lithium-Air batteries are still in development, meaning that the failure modes, causes and rates are a broad estimation and it should be noted that these are taken for the current technology level [35]. Seeing as the target year for the design of the E9X is 2033, it can be assumed that this is significantly improved by the time of the production of the AEA [5]. For the batteries, three different failure modes were identified:

1. Partial Battery Failure
2. Temporary Battery Failure
3. Permanent Battery Failure

Partial Battery Failure (1): Degradation of performance due to wear-out of the battery. This failure is caused by over-usage of the battery and has an effect starting from a degradation of larger than 10% of the battery's original performance [35] [36]. It is estimated that the failure rate of such a failure is in the same order of magnitude as Temporary Battery Failure and therefore taken in this analysis as the same value: $9.25 \cdot 10^{-6}\,\mathrm{h}^{-1}$ [37]. This leaves an FMEA occurrence value of 3.

Temporary Battery Failure (2): Temporary loss of supply of the battery to the system. This could be caused by environmental of operational conditions, such as partial discharges or partial blockages of the (air) cathode [37]. The failure rate of this is estimated to be $9.25 \cdot 10^{-6}[h^{-1}]$ [37].

Permanent Battery Failure (3): Permanent loss of a battery. There are numerous causes for such a failure, such as Thermal Runaway (the most critical failure cause), short circuits and overcharging [37]. It is estimated that these faults occur once in every 500 cycles of the battery's usage [38]. The AEA is proposed to have an average cruising speed of $738\,\mathrm{km/h}$ and approach speed of $270\,\mathrm{km/h}$ [4]. The target mission range of 800 km leaves a mission time of about 1.5 hours to 2 hours (including take-off, taxing and landing). Assuming 1 full charge cycle per flight and an average of 4 flights a day for commercial short haul aircraft [20], this would lead to a theoretical failure rate of once every 125 days. However, seeing as the AEA does not always fly the designed range (only about 30% of flights are 'deep discharges'), the failure rate is estimated to be about $1 \cdot 10^{-4}[h^{-1}]$ [4]. Nevertheless, it should be noted that the battery packs are replaced once or twice a year as part of standard maintenance, corresponding to about once in every 1500 cycles [4], meaning that this failure rate estimate can be viewed as an absolute worst case scenario and a means to be able to numerically incorporate battery failure in the further analysis. This consideration is further discussed in Section 6.3.

Generators
The reserve generators function as a backup for the batteries in case they fail or are drained, so that they are able to provide power to the EPS when needed. During the take-off phase, but also during landing failures these can be considered very critical due to the potential of cascaded failures in the system [34]. For the generators, two failure modes were identified:

4. Failure to Start (FTS)/Temporary Generator Failure
5. Permanent Generator Failure

Failure to Start (FTS) (4): FTS in a gas-powered generator can have numerous causes, such as ignition failure, failures in the fuel supply system or control system faults [39]. It is estimated that for similar generators used in MEA the FTS rate is about $2.28 \cdot 10^{-7}[h^{-1}]$ [40], an occurrence rating of 3.

Permanent Generator Failure (5): If there is a permanent fault in the reserve generator it significantly poses a critical failure risk in case of battery failure. Such faults can be caused by short circuits in the stator core, winding faults or insulation faults [40]. The permanent failure rate of aircraft generators was estimated to be $7.54 \cdot 10^{-6}[h^{-1}]$ [41]. However, for these applications the generator is used constantly, while for the AEA it would only be made operational in specific (emergency) cases and cascaded failure modes, meaning that the actual failure rate is likely to be lower [4].

Power Converters
In the AEA there are different voltage levels, power levels and types of current needed for the different components of the grid as seen in Section 4.2. In order to facilitate this, three different types of power converters are used, DC-DC converters (Converter), AC-DC converters (Rectifiers) and DC-AC converters (Inverters). For simplicity and to keep the analysis concise, only one failure mode per type of power converter was considered; permanent failure. Faults in these can be quite critical, since they are placed after or before the three critical components of the EPS; the generators, the batteries and the motors. The failure rates estimated in this section were estimated using MEA research and general electronic component reliability data sheets as the MIL-HDBK-217F [42] and the NPRD-2016 [43] used by these studies. These led to the following failure modes:

6. Converter permanent failure

7. Inverter permanent failure
8. Rectifier permanent failure

Converter permanent failure (6): Converter faults can be caused by numerous factors, where short circuit faults in the circuitry are the most common ones. These can occur for example in the switches and transistors in the circuit [44]. Failure in a converter means the immediate loss of the battery pack feeding the converter, meaning that it is quite a critical point of the system. A reliability analysis of a MEA estimated the failure rate of the DC-DC converter in the grid to be around $4.54 \cdot 10^{-5}[h^{-1}]$ [45] [46]. This analysis focused on the Boeing 787 MEA, one of the more popular MEA in terms of its EPS. Although the voltage level in this study was significantly lower than the one in the AEA grid, the failure rate is assumed to be in the same order of magnitude for higher power converters for this thesis in order to be able to quantitatively assess the grid's reliability.

Inverter permanent failure (7): The inverters transform the power of the grid to AC in order to feed the motors. Failure in an inverter means the loss of the motor and directly a loss of propulsive power, enhancing the criticality of the fault. Common faults in inverters are faults in the switches, such as open or short circuit faults [47]. Seeing as inverters are not yet applied in many MEA cases, especially for the power scale required by the motors of the given AEA, it was estimated that the failure rate was in the order of magnitude of the DC-DC converter analysed in the study on the aforementioned Boeing 787, and taken as $4.54 \cdot 10^{-5}[h^{-1}]$ [46].

Rectifier permanent failure (8): The rectifier converts the generated AC power from the two reserve generators to DC power required by the grid at the 3 kV level. Failure in either of these means the loss of the generator itself, relating back to the effects of Failure Mode (5). A potential cause of critical rectifier failure can be commutation failure [48]. The failure rate for the rectifier was estimated to be in the same range as for the DC-DC converter, yielding a rate of $4.54 \cdot 10^{-5}[h^{-1}]$ [46]. However, studies show that its reliability can be considered to be lower due to the higher complexity of the component as well as the higher power rating it has in the AEA grid as opposed to MEA application [48].

Busbars

The busses in the system are used as node connections to connect several parts of the system together in a central place, as explained in 4.2.4. The reliability and inherent criticality of this component of the system depend on its location and the parts of the system it feeds. Therefore, it was decided to structure the failure modes as a single type of failure, in different locations of the grid, yielding the following failure modes:

9. Busbar permanent disconnect (Battery)
10. Busbar permanent disconnect (Motor)
11. Busbar permanent disconnect (Generator)

Busbar permanent disconnect (Battery) (9): Faults in the busses by definition mean that multiple lines and/or parts of the system will be disconnected. In terms of the batteries, this failure mode is likely to mean the loss of one or more battery packs, enhancing its criticality. A cause for critical busbar failure can be environmental issues such as humidity or sealing issues [49]. It was estimated that critical busbar failure, for aircraft applications was around $3.96 \cdot 10^{-9}[h^{-1}]$ [46]. The bus component is very reliable due to its simplicity and robustness [50].

Busbar permanent disconnect (Motor) (10): For this failure mode, the same causes can identified as the previous mode, seeing as the only difference is the effect the failure has on the system. Without assuring proper redundancy, the loss of the motor busbar could mean multiple motor failures and inherently this makes it a very severe fault. For completeness, the failure rate of this mode is $3.96 \cdot 10^{-9}[h^{-1}]$ as well. It should be noted that there could be small variations with the failure of the battery busbar in fault cases with the different power levels on the motor busses.

Busbar permanent disconnect (Generator) (11): Again, the generator busbar fault has the same causes as identified before in this section. The generator bus is very critical, seeing as its failure could mean the backup for the batteries is completely faulted. The same failure rate is then yielded for this mode: $3.96 \cdot 10^{-9}[h^{-1}]$. However, seeing as the usage of this bus is far lower than the other busses (it is only used in edge cases where the generators are turned on) [4], the failure rate of this component can be considered to be lower and the given rate to be the worst case scenario.

Transmission lines/Grid
The cables of the system, their structure, parameters and usage are described in much detail in Chapter 3. Similarly to the argument given for the busses, the failure modes for the transmission lines of the grid itself are structured on their location in the grid since this determines their criticality. The following failure modes were identified:

12. Transmission line failure (Generator)
13. Transmission line failure (Interconnection network)
14. Transmission line failure (Battery connections)
15. Transmission line failure (Motor connections)

Transmission line failure (Generator) (12): Faults in one of the transmissions lines in the grid can have significant impact on the system. Line failure can be caused by numerous faults, such as short circuits, humidity, insulation faults or wear out [51]. Faults in the generator line can be viewed as critical seeing as it directly impacts the availability of the generator to the grid, similarly to the criticality of the rectifier and the generator itself. The failure rate of standard cables in MEA was estimated to be $8.09 \cdot 10^{-7}[h^{-1}]$ [46]. Naturally, similarly to the argument around the generator busbar, this line will not constantly transfer power and thus is likely to have a lower failure rate. However, it should still be considered that this line carries a significantly greater amount of power than in MEA, and therefore the failure rate could be worse in reality than its estimated value.

Transmission line failure (Interconnection network) (13): Comparable to the failure modes of the busses, the transmission lines have the same fault causes and occurrences independent of their location in the grid. Therefore, for this failure mode the failure rate is also estimated to be $8.09 \cdot 10^{-7}[h^{-1}]$ [46]. However, a fault in the interconnection network can have more severe consequences depending on the location of the fault. Further analysis of this subject will be done in Section 5.3.

Transmission line failure (Battery connections) (14): Line faults in the battery connection will inherently mean that one of the battery packs will be lost, meaning it is a high-priority fault in terms of criticality. Especially since this stored energy would then be lost and rendered useless, this line failure is quite severe. Its failure rate is $8.09 \cdot 10^{-7}[h^{-1}]$ [46].

Transmission line failure (Motor connections) (15): Failure in the motor connections will mean that the system is not able to feed the motors, sparking the risk of loss of propulsion. Seeing as this is the main function of the grid, this is considered quite a high-risk failure mode. A large part of the grid design and reliability analysis is centred around this, as discussed in Sections 4.2.3 and 5.3. Its failure rate is $8.09 \cdot 10^{-7}[h^{-1}]$ [46].

Circuit Breakers
Circuit Breakers are the protection elements that allow faults to be contained to one part of the system and isolate certain faults from the rest of the system in order for the system to remain operational [52]. More in-depth information about the type and function of the circuit breakers can be found in 4.2.5. As part of the intergroup requirements (found in 6.1), it was decided that the following failure modes of circuit breakers were analysed:

16. Circuit breaker: Failure to open
17. Circuit breaker: breaks while disconnecting

18. Circuit breaker: failure to re-close after opening

However, in order to keep the analysis within the scope of the project, the failure rates of each of these were based on an estimation of general 'circuit breaker failure', through the already referred to reliability assessment on the Boeing 787 MEA. Therefore, for these failure modes, the failure rates are not specifically estimated per mode but rather kept general for the subcomponent itself such that it can be taken into account in the critical failure rate calculation in the FTA. Nevertheless, as will be discussed in 7.2, a potentially useful addition to this analysis can be to investigate the occurrence of these different modes in order to further increase the reliability of the designed topology. The failure rate for circuit breakers in the MEA grid was estimated to be $5.28 \cdot 10^{-6}[h^{-1}]$ [46].

Circuit breaker: failure to open (16): Circuit breakers are the essential elements in preventing a fault from cascading further into the system and causing critical failure. Potential critical faults that a circuit breaker has to be able to handle can for example be a large overcurrent that could damage the rest of the system. If the breaker fails to open, potential effects can be that there is a short circuit in the AEA, significant ignition risks and cascaded system failure [31]. The causes of such a failure can be incorrect detection of the fault or control system issues. In many ways, this can be considered the most critical failure mode and highlights the importance of protection in MEA and AEA [53].

Circuit breaker: breaks while disconnecting (17): If the component fails while attempting to disconnect, it is most likely due to the fault being more severe than the breaker is built to handle. This will most likely result in the permanent failure of the component the breaker is placed on; line failure [31]. This can have significant impact on the grid, as described in failure modes 12-15.

Circuit breaker: failure to re-close after open (18): In some cases, a circuit breaker will have tripped due to a fault and after the fault is resolved will fail to close again. This can be due to control system failures, improper handling of the fault itself or failure in the breaker [54]. This can cause a line to being disconnected from the grid, either temporarily if the circuit breaker fault can be resolved or permanent if it is more critical. The further impact of this failure mode are the same as for failure modes 12-15.

Motors
The high-power electro motors that power the 8 turbo-propellers that are responsible for the propulsion are critical in the system, although their design and parameters themselves are predefined and out of the scope of this thesis. Every motor is designed to carry around 1.62 MW peak power, as described in Section 4.2.3. Failure in this part of the system directly impacts flight performance, meaning its criticality should be considered thoroughly. Three different failure modes were analysed:

19. Temporary motor failure
20. Permanent motor failure
21. Partial loss of motor propulsion

Temporary motor failure (19): Temporary failure of the motor means the motor temporarily does not deliver power to the propeller, effectively losing part of the propulsion. A cause of this can be overheating or failure in control systems, for example [47]. This fault can be quite severe in critical stages of flight, mainly the take-off phase before decision speed and the final stage of landing [34]. Currently, motors of the required size are not yet commercially available and tested. However, Battery-Electric Vehicles (BEVs) are already in a further stage and there have been done numerous studies into the reliability and potential failures of their drive-train systems. Therefore, in order to estimate the failure rate of this mode an analysis of similar motors available in other BEVs and already available reliability research into potential electrical motor applications for AEA was used. The temporary motor failure rate was therefore estimated to be around $1.5 \cdot 10^{-6}[h^{-1}]$ [55].

Permanent motor failure (20): Permanent engine failure can be considered a highly critical failure mode. In itself, losing thrust is the first and foremost event the grid's reliability is tested on and forms a central part of the EASA CS-25 regulations for aircraft design [23]. As will be touched upon in further detail in Section 5.3.1, this also forms a central part of the further reliability study of this paper. There are

quite some potential causes for permanent motor failure, in areas such as electrical faults, mechanical faults, sensors faults or faults in the control system [55]. Electrical faults are more common and can be faults such as inter-turn short faults (ITSFs), phase faults or demagnetisation [47]. The failure rate was estimated using a similar method as for temporary battery failure and found to be around $5.9 \cdot 10^{-6}[h^{-1}]$ [55] [47].

Partial loss of motor propulsion (21): Partial power loss of the motors means that the motors lose part of their output power due to a fault in the motor. This failure means that the propeller cannot provide the thrust it is designed to deliver, which will not impact the flight status as severely as the other two motor failure modes as it still produces output power. However, in critical stages this can have more impact, especially if this fault fails to be detected. Causes of this mode can be worn bearings in the motor, poor contact of the motor connections or reduced isolation of the motor for example [47]. The failure rate of this mode was estimated using a reliability study on BEVs, since this failure mode is subject to extensive usage and therefore it was decided that an estimation based on real data was better than using theoretical results for motors for AEA applications such as the ones described in [55]. The rate was estimated to be $3 \cdot 10^{-5}[h^{-1}]$ [56].

5.1.4. Results

The results of the sums of all the ratings of the different failure modes are shown in Figure 5.1 below:

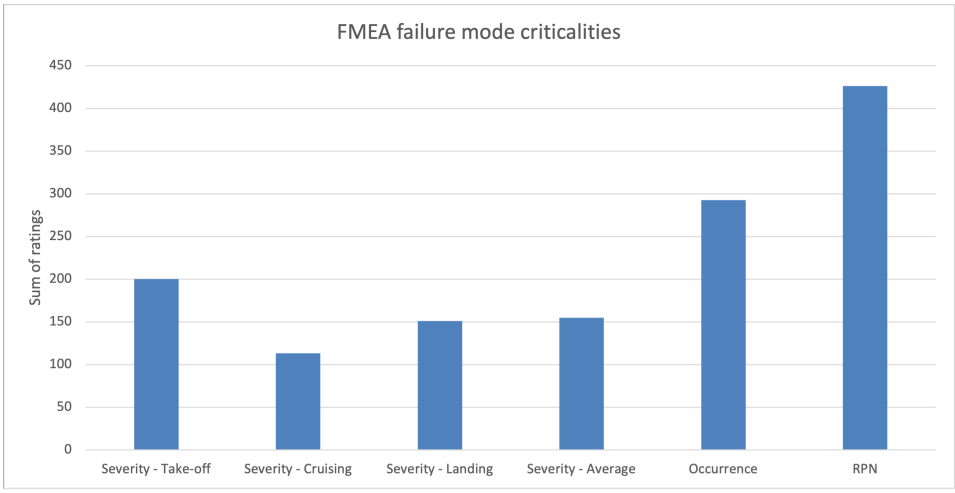

Figure 5.1: FMEA: Sum of all mode criticality values

The x-axis represents the different criteria the assessment was based on, and the y-axis is the sum of all the rating values as described in Subsection 5.1.2. As can be seen in Figure 5.1, the severity of all modes is most critical during take-off, while cruising faults are significantly less critical. The landing phase is the second most critical. This is mainly due to the fact that there is far less margin for error in the take-off and landing phases [34]. Furthermore, as part of the CS-25 regulations for aircraft design, commercial aircraft are legally bound to be designed to safely being able to return to the ground if there is a failure in cruising [23]. There is an average RPN value of 20.3 per mode (using average severity), meaning that the faults in the system require significant attention especially for aircraft applications where safety thresholds are high [33].

Secondly, a Pareto chart was created in order to visually demonstrate the most critical failure modes as based on the FMEA. This is shown in Figure 5.2. The code for generating this distribution and chart can be found in Appendix C.1.

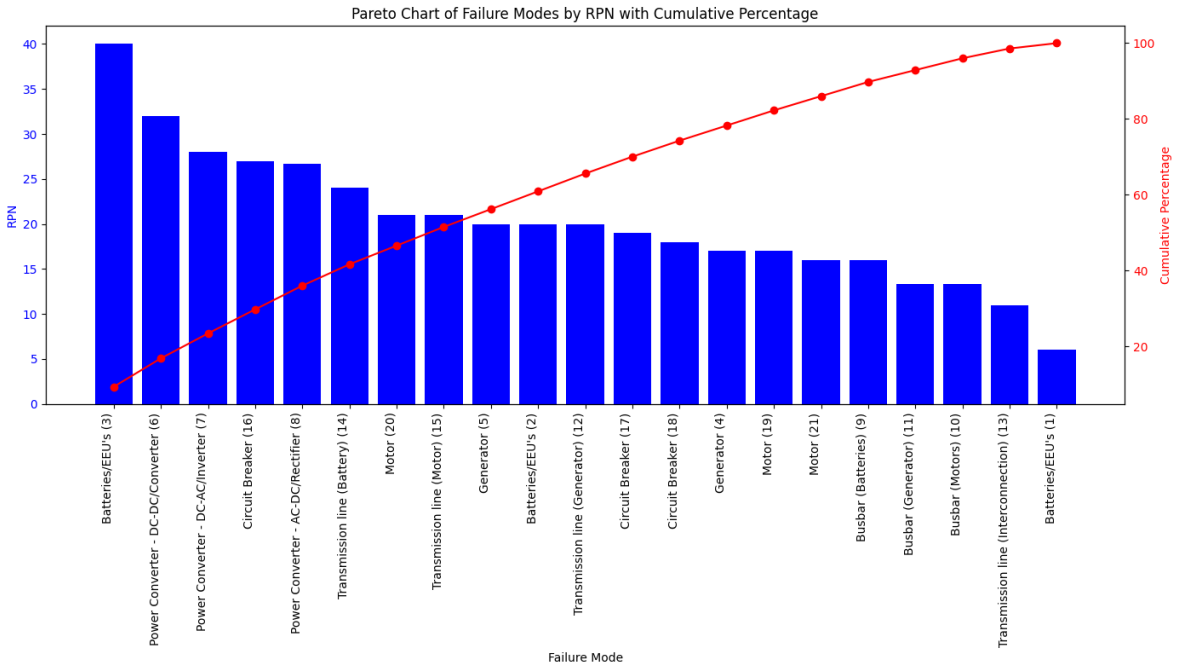

Figure 5.2: FMEA: Pareto chart of failure modes

This demonstrates the most critical failure modes of the FMEA, which are modes 3, 6, 7, 16 and 8 in descending order. For the specific breakdown of the different ratings of these modes, the reader is referred to the complete FMEA table in B.1 and the respective explanation of the modes in Subsection 5.1.3. However, it should be noted that for mode 3 the occurrence rating is a very high estimate resulting in a very high RPN value, which is likely to be lower.

5.1.5. Failure rates

All in all, through the FMEA a list of definitive failure rates per sub-component of the system can be identified. These are summarised in the table below:

Fault	λ	Failure rate per flight hour
Power system failures		
Battery fault	λ_{BF}	$1 \cdot 10^{-4}$
Converter fault	λ_{CF}	$4.54 \cdot 10^{-5}$
Failure to start	λ_{FTS}	$2.28 \cdot 10^{-7}$
Permanent failure	λ_{PF}	$7.54 \cdot 10^{-6}$
Rectifier fault	λ_{RF}	$4.54 \cdot 10^{-5}$
PMAD system failures		
Bus fault	λ_{Bus}	$3.96 \cdot 10^{-9}$
Cable fault	λ_{Cab}	$8.09 \cdot 10^{-7}$
Circuit breaker fault	λ_{CB}	$5.28 \cdot 10^{-6}$
Motor system failures		
Motor fault	λ_{MF}	$5.9 \cdot 10^{-6}$
Inverter fault	λ_{IF}	$4.54 \cdot 10^{-5}$

Table 5.3: Failure rates

These form the basic building blocks the FTA will be structurally build up from in Section 5.3.

5.2. Reliability Block Diagram

The Reliability Block diagram, or RBD, is a graphical representation of subsystems or components and their correlation in a system when looking at reliability [57]. An example of a RBD is given in Figure 5.3, this is the RBD of the motor side of the aircraft architecture mentioned in Chapter 4. A block in the diagram represents a subsystem or a component. This diagram shows what combinations of failures can lead to a critical failure. When a block fails, it is removed from the system. If the system still functions, meaning seven out of eight motors are fed, then there will be no failure. When this is not the case anymore, the system has failed. The circle with 1/2 in it on top of the motors means that one of the two cables has to minimally power the motor for it to function. When for example the middle bus should fail together with two cables from the other busses, a critical failure will occur.
Within this project, the possible combinations of failures are as well as possible included in the FTA. Therefore, only a small part of a RBD is investigated. A RBD could, however, give even more useful information in the future, more about this is mentioned in Section 7.2.

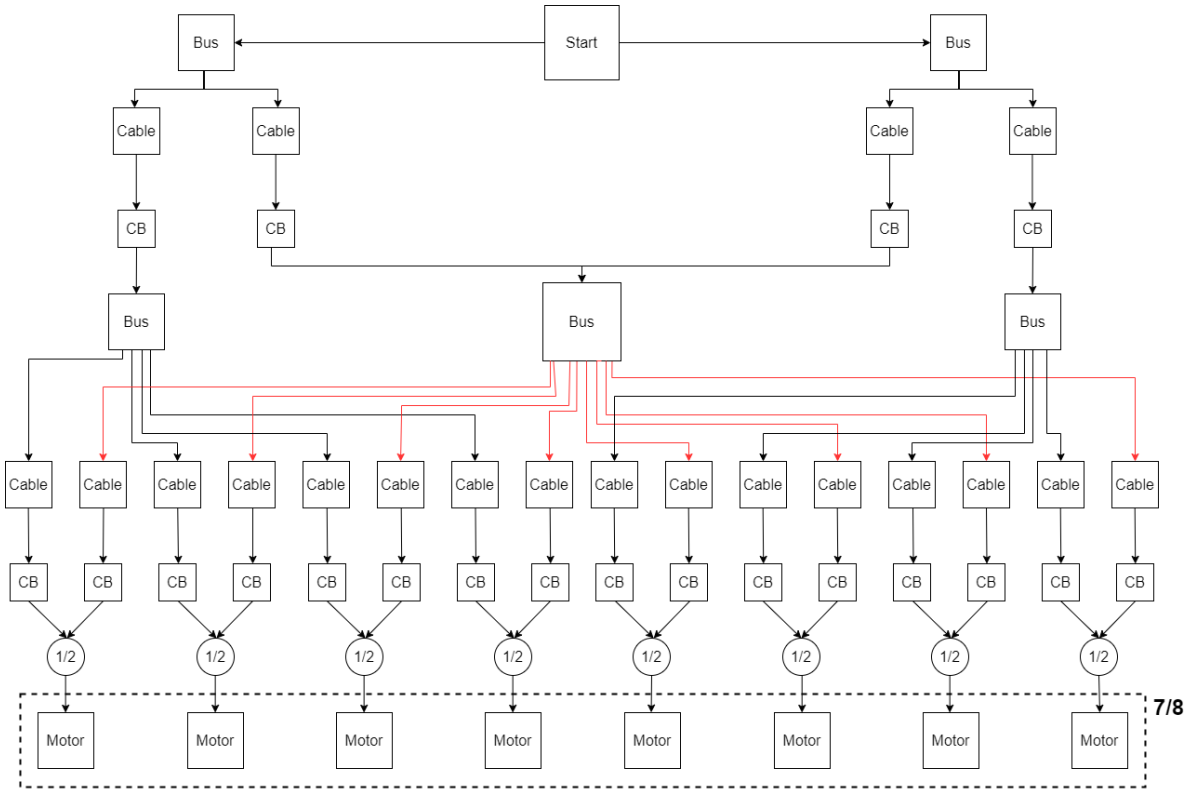

Figure 5.3: RBD of the motorside

5.3. Fault Tree Analysis

Fault tree analysis, or FTA, is a failure analysis method to analyse an unwanted event in a system using Boolean logic to combine lower-level events [58]. It is mostly used to calculate the probability of such an unwanted event. A top-down approach is used where the top-level event is the worst event that can occur. In the case of an all-electric aircraft, this is chosen to be ”Loss of propulsion”. In this section, FTA is used together with the failure rates mentioned in Table 5.3 to calculate the probability of loss of propulsion of the overall topology mentioned in chapter 4.

5.3.1. Critical Failure Conditions

Creating a FTA can be done in numerous ways. There are however five steps that are frequently used to model a FTA [59]:

1. Defining the undesired event

2. Obtaining an understanding of the system
3. Constructing the fault tree
4. Evaluating the fault tree
5. Controlling the hazards

As mentioned before, the undesired event is loss of propulsion. The top events that can lead to a loss of propulsion can be listed right below the main event. These events are:

- Power failure, i.e. Battery and/or generator failure
- Motor failure
- Fault in the PMAD

A view of the top of the fault tree is given in Figure 5.4. This is the same for both the 4 battery as for the 8 battery system, it changes however once the subsystems are divided into smaller branches.

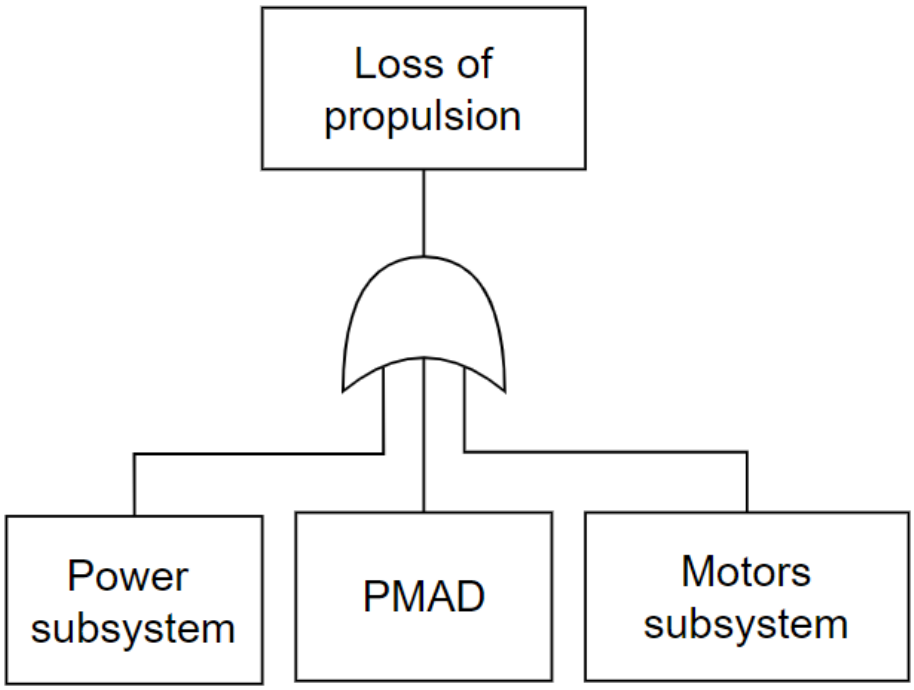

Figure 5.4: Top level FTA

The OR-gate means that if an error occurs in any of the systems, the main fault of loss of propulsion will happen if any of the lower subevents. If an AND gate is placed, every lower event will have to stop working to trigger an error. A visualisation of this is shown in Figure 5.5. In an AND gate, the failure rates of the input events are multiplied, for two entries this means that the output is $\lambda \cdot \lambda$. In an OR gate, the failure rates are added together, so $\lambda + \lambda$. When dealing with probabilities, every number λ is between zero and one. This means that when they are multiplied, the probability becomes smaller and when they are added together, it becomes larger. For a probability of failure, the goal is to get the probability as low as possible. So more AND gates are preferable.

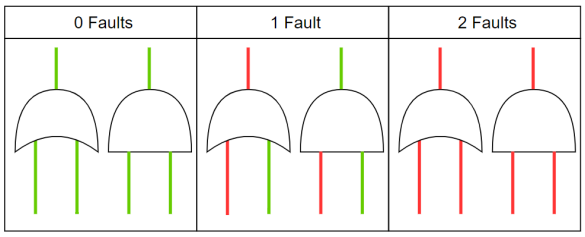

Figure 5.5: OR/AND gate comparison

A fault tree for the entire system can get big and complex very quickly, this is why a fault tree is often divided into smaller fault trees of subsystems. The values that roll out of the subsystems combined are the total critical failure rate of the system.
In the following subsections, the subsystems and their failure rates will be discussed. To, in the end, find the failure rate of the entire system. Due to the size of some of the fault trees, only a few visualisations are given in the text.

5.3.2. Power subsystem

The power subsystem includes the generators and the batteries of the system. For one of the architectures it consists of 4 battery packs and 2 generators and for the other one 8 battery packs and 2 generators.
There are three ways in which a critical failure occurs in the power side.

- All batteries fail
- All generators fail
- A combination of 1 generator and half of the batteries fail.

In these cases there is not enough power in the system to supply the motors.
The FTA of the 4 battery subsystem is shown in Figure 5.6.

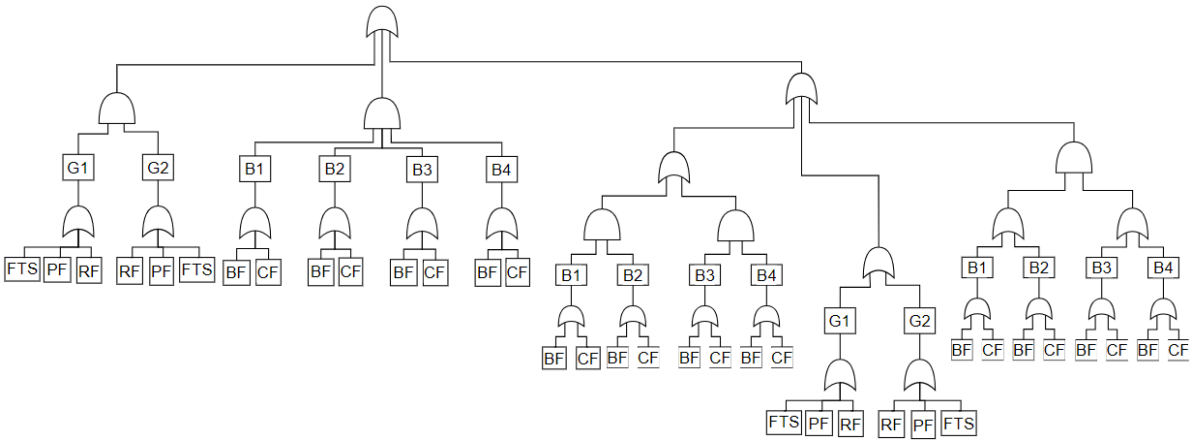

Figure 5.6: Power subsystem fault tree of 4 battery pack architecture

There are three lines that go into the top OR gate, these lines represent the three above-mentioned failure events. The left side is the case that all generators fail, the middle is when all batteries fail and the right is when half of the batteries fail together with one of the generators.

The failure rates used for the power side are mentioned in Table 5.3, these are called the basic events. The basic events are the events in the bottom of the fault tree. The intermediate events are the events that follow up. One of these intermediate events is the failure of the battery pack. In the case of the 4 battery pack architecture, if there is a battery fault or a converter fault, the battery pack fails as a whole. This

means that a battery pack failure rate per flight hour is equal to $\lambda_{BF}+\lambda_{CF} = 1.45 \cdot 10^{-4}$. For the 8 battery pack architecture there are no converters, so the failure rate is equal to $\lambda_{BF} = 1 \cdot 10^{-4}$. Another intermediate event is failure of the generator. If the generator has a failure to start, a permanent failure or a rectifier fault, the generator fails. Thus, the generator failure rate is equal to $\lambda_{FTS}+\lambda_{PF}+\lambda_{RF} = 5.32 \cdot 10^{-5}$ per flight hour. This is the case for both the 4 battery pack and 8 battery pack architectures. A visualisation of these basic and intermediate events for the 4 battery architecture is given in Table 5.4.

Intermediate event	λ	Failure rate [h^{-1}]	Basic event	λ	Failure rate [h^{-1}]
Power system failures					
Battery pack fault	λ_B	$1.45 \cdot 10^{-4}$	Battery fault	λ_{BF}	$1 \cdot 10^{-4}$
			Converter fault	λ_{CF}	$4.54 \cdot 10^{-5}$
Generator fault	λ_G	$5.32 \cdot 10^{-5}$	Failure to start	λ_{FTS}	$2.28 \cdot 10^{-7}$
			Permanent failure	λ_{PF}	$7.54 \cdot 10^{-6}$
			Rectifier fault	λ_{RF}	$4.54 \cdot 10^{-5}$

Table 5.4: Failure rates power side

With these intermediate events and the FTA given in Figure 5.6, the eventual failure rates of the power side can be calculated. The eventual calculation for the 4 battery pack power side failure rate is given in Equation 5.3.

$$\lambda_{4\text{Power}} = \lambda_G^2 + \lambda_B^4 + 2 \cdot \lambda_G \cdot 6 \cdot \lambda_B^2 = 2.84 \cdot 10^{-9}[h^{-1}] \tag{5.3}$$

The equation for the 8 battery pack architecture is shown in Equation 5.4. The FTA for this system is impossible to show because of its size due to the extra batteries, but an explanation of the equation is given below.

$$\lambda_{8\text{Power}} = \lambda_G^2 + \lambda_{Bat}^8 + 2 \cdot \lambda_G \cdot 70 \cdot \lambda_{Bat}^4 = 2.83 \cdot 10^{-9}[h^{-1}] \tag{5.4}$$

The big difference in the calculation of the two reliability values is that there are a lot more combinations of batteries that can fail in an 8 battery pack compared to a 4 battery pack topology. This is why the final part of Equation 5.4 is multiplied with '70' instead of the '6' that is used in Equation 5.3. Still, the numbers that roll out of both equations are almost equal. This is because the probability that two generators fail (λ_G^2) is already equal to $2.83 \cdot 10^{-9}$ and the other probabilities in the formula are way smaller than this number and can be neglected. Thus, it can be concluded that the highest probability of a critical fault in the power system of both architectures is that two generators will fail.

5.3.3. PMAD subsystem

The power management and distribution subsystem (PMAD) is the most intricate part of both of the architectures. They also differ heavily from each other. There are a lot of ways in which the PMAD can create a critical failure, these ways are described in this section. Because of the intricacy of the PMAD, it will be divided into smaller subsystems, namely a power and propulsion side. First, the top parts of both architectures will be calculated using FTA and the critical failure rates will be given. There are a lot of equations involved to calculate the failure rates for this subsystem. To give a clear view of all of the calculations, a table is given at the end summarising all critical failure rates.

Propulsion side

The propulsion part is similar for the two architectures. It consists of the motor connections, the lower busses and the lines that give these busses power. Firstly, the critical failure rate of the propulsion part of the four battery pack architecture will be calculated. After this, the calculations for the eight battery architecture critical failure rate will be presented.

Four battery pack topology:
The four battery pack architecture has four lower busses and a multi-feed cable network. Three events that cause a critical failure can occur in this case:

- Both connections of two separate motors fail. (λ_{F1})
- Two busses of one side of the PMAD fail.(λ_{F2})
- One bus of a side combined with two lines of the other bus connected to the same motors can fail.(λ_{F3})

Figure 5.7 shows the FTA for the propulsion part of the PMAD:

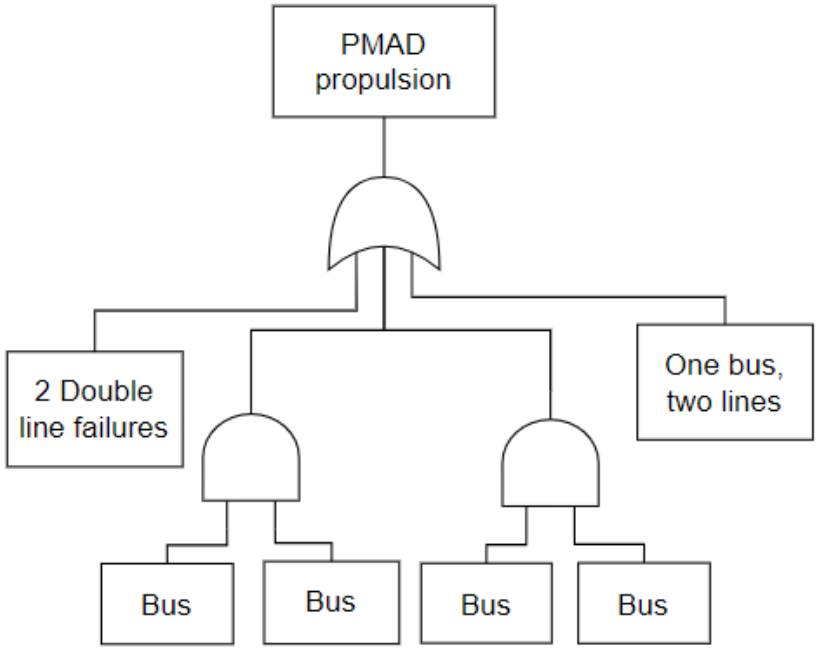

Figure 5.7: Fault tree of faults in propulsion side of four battery architecture

The FTA is simplified to show one of the failures in detail, the failure of two busses. The other failures are too extensive to show in the report, but the outcome of the probabilities is given in the equations below.

The first event should actually be the event that not only two, but two or even more motor connections fail. However, since the probability of three or more motor connections failing is already much smaller than the case of two failing this can be neglected. These faults can be calculated using the failure rates of the PMAD components given in Table 5.5.

Fault	λ	**Failure rate per flight hour**
PMAD system failures		
Bus fault	λ_{Bus}	$3.96 \cdot 10^{-9}$
Cable fault	λ_{Cab}	$8.09 \cdot 10^{-7}$
Circuit breaker fault	λ_{CB}	$5.28 \cdot 10^{-6}$

Table 5.5: Failure rates

The probability that both cables of two separate motors break is a difficult calculation to make. Using the binomial coefficient (Equation 5.5), the number of total connections can be calculated. If two (k) lines out of the sixteen (n) different connections to the same motor can fail, the total number of combinations is 120.

$$\frac{n!}{(n-k)! \cdot k!} \tag{5.5}$$

If these two lines fail, there is a 16/120 probability that those lines are connected to the same motor. This process is now repeated for the next two lines. Now there are fourteen connections remaining and again two cables that need to be connected. The probability that these cables are paired together is now 14/91. The probability that two lines fail is the probability that a circuit breaker or cable fails to the power of two ($(\lambda_{Cab} + \lambda CB)^2$).

The final calculation of the probability that both cables fail is given in Equation 5.6.

$$\lambda_{F1} = \frac{16}{120} \cdot (\lambda_{Cab} + \lambda_{CB})^2 \cdot \frac{14}{91} \cdot (\lambda_{Cab} + \lambda_{CB})^2 = 2.82 \cdot 10^{-23}[h^{-1}] \tag{5.6}$$

The probability that two busses of one side of the PMAD can fail is the probability that two busses fail times two for the two out of four busses that can fail. The connection to this bus is taken into account as well. The probability for this is given in Equation 5.7.

$$\lambda_{F2} = 2 \cdot (\lambda_{Bus} + \lambda_{Cab} + \lambda_{CB})^2 = 2.02 \cdot 10^{-10}[h^{-1}] \tag{5.7}$$

The final probability for the event that one bus of a side fails together with two lines that connect to the motors of this bus. Equation 5.8 shows the calculation for this probability.

$$\lambda_{F3} = 24 \cdot (\lambda_{Cab} + \lambda_{CB})^2 \cdot (\lambda_{Cab} + \lambda_{CB} + \lambda_{Bus}) = 5.42 \cdot 10^{-15}[h^{-1}] \tag{5.8}$$

The equation is multiplied by 24. This is because when a bus fails, there are four cables left that can power the motors on one side. Using Equation 5.5, two broken cables can have six different connections. There are two busses per side and 2 sides in total so this six is multiplied by four to get the eventual 24 that is given in the Equation.

The total critical failure rate of the bottom of the PMAD for the four battery pack architecture (λ_{Tot1}) is given in Equation 5.9.

$$\lambda_{Tot1} = \lambda_{F1} + \lambda_{F2} + \lambda_{F3} = 2.02 \cdot 10^{-10}[h^{-1}] \tag{5.9}$$

Eight battery pack architecture:
The eight battery pack architecture has two lower busses and one middle big bus and, just like the four battery pack architecture, a multifeed cable network. Figure 5.8 shows the global FTA for the eight battery pack system. Three events that cause a critical failure can occur in this case:

- The double connection of two separate motors can break. (λ_{F1})
- One of the side busses break together with two cables from the mid bus.(λ_{F4})
- The mid bus breaks together with two cables or together with another side bus. (λ_{F5})

For these events, a fault tree can be designed. The simplified fault tree is given in Figure 5.8

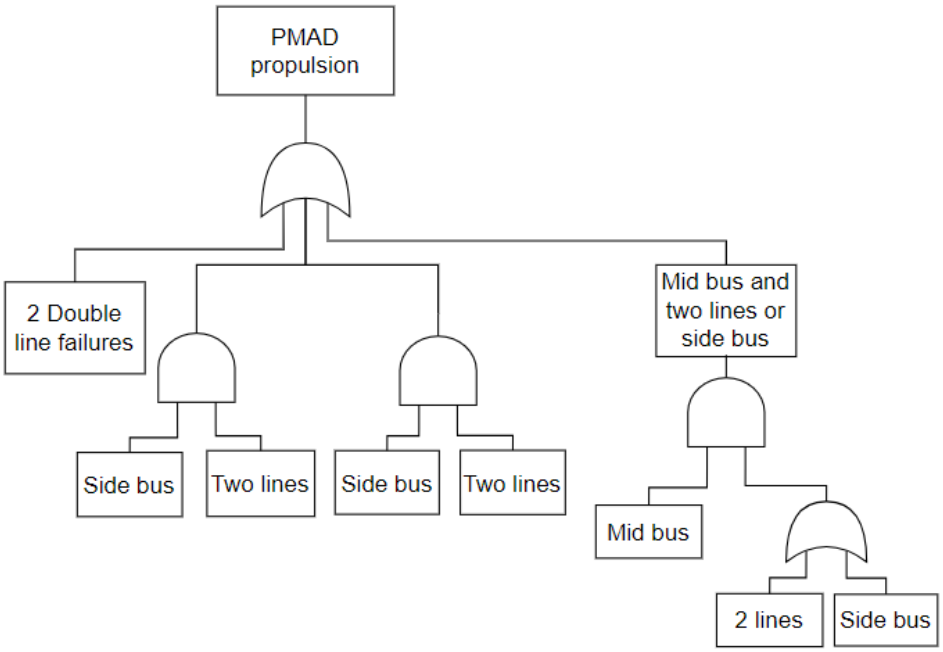

Figure 5.8: Fault tree of faults in ppropulsion side of eight battery architecture

Just like for the other architecture, the values mentioned in Table 5.5 are used to calculate the failure rates of these events.

The event that two double connections break is the same as for the other architecture, so this value is $\lambda_{F1} = 2.82 \cdot 10^{-23}$ (Equation 5.6). The second event is when a side bus breaks in combination with two cables from the mid bus. When a side bus breaks, four of the motors only have one cable remaining that feeds the power to them. If two of these four cables also fails, two motors will not be fed and thus, causing a critical fault. The probability of this happening is given in Equation 5.10.

$$\lambda_{F4} = 12 \cdot (\lambda_{Bus} + \lambda_{Cab} + \lambda_{CB}) \cdot (\lambda_{Cab} + \lambda_{CB})^2 = 2.71 \cdot 10^{-15}[h^{-1}] \tag{5.10}$$

The equation is multiplied by twelve, because there are six different possible connections of the two broken cables that give a critical fault. There are also two side busses, so the entire equation has to be multiplied by two as well.

The final failure rate is the probability that the mid bus breaks together with two cables or together with another side bus. When the mid bus breaks, every motor only has one connection left. Nevertheless, the middle bus is powered by two different cables, so the probability that it fails is lower than for other busses. In total, using Equation 5.5, 28 different combinations of two broken cables can lead to a critical fault. If one other bus should fail it would also lead to a critical fault. The equation for calculating the critical failure rate of this event is given below (Equation 5.11).

$$\lambda_{F5} = (\lambda_{Bus} + (\lambda_{Cab} + \lambda_{CB})^2) \cdot (24 \cdot (\lambda_{Cab} + \lambda_{CB})^2 + 2 \cdot (\lambda_{Bus} + \lambda_{Cab} + \lambda_{CB})) = 1.79 \cdot 10^{-24}[h^{-1}] \tag{5.11}$$

The total critical failure rate of the eight battery pack architecture (λ_{Tot}) is given in Equation 5.12.

$$\lambda_{Tot2} = \lambda_{F1} + \lambda_{F4} + \lambda_{F5} = 2.71 \cdot 10^{-15}[h^{-1}] \tag{5.12}$$

Power side

The top part of the PMAD subsytems are a little different for the two architectures. The four battery pack architecture has a connection between its left and right busbars, while the other has two separate busbars. However, both of the busbars on one side are connected to each other.

The biggest difference is that the four battery pack architecture separates the left and right side entirely

while the other architecture is bound together in the lower side again. Below, the reliability of the top side of the PMAD will be calculated for both architectures.

Four battery pack architecture
The events that can lead to a critical failure of the four battery architecture are given below.

- The failure of two busses (λ_{F6})
- The failure of the line or circuit breaker to the H-bus or the H-bus itself (λ_{F7})
- The failure of the connection (cable and/or circuit breaker) to the two generators, 4 batteries or half of the batteries and one generator (λ_{F8})

The fault tree for the subsystem with the above fault events is given in Figure 5.9.

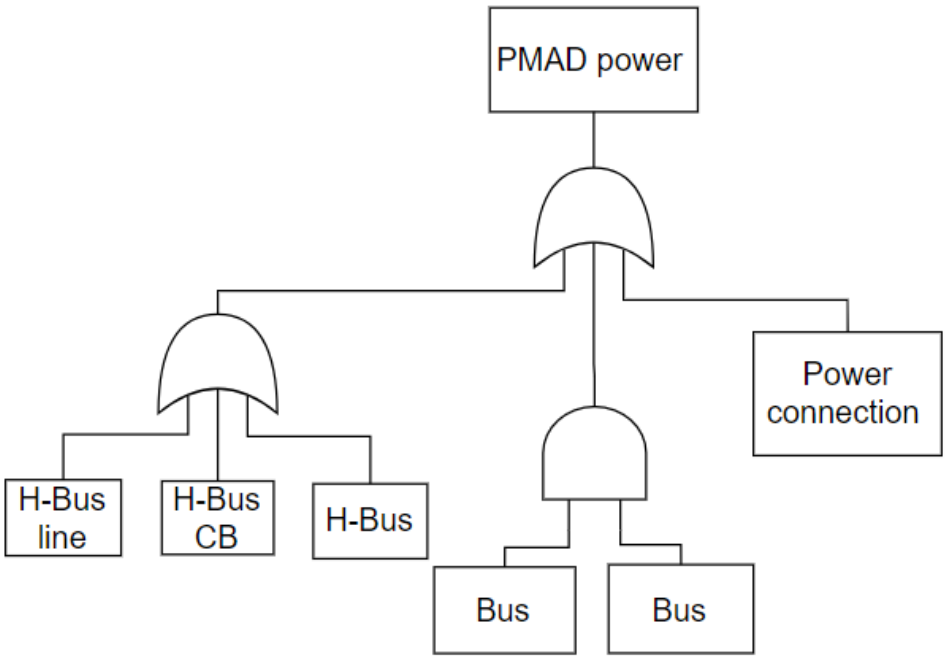

Figure 5.9: Fault tree of faults in power side of four battery architecture

Calculating the probability of failure of two busses is the simple Equation 5.13.

$$\lambda_{F6} = \lambda_{Bus}^2 = 1.57 \cdot 10^{-17}[h^{-1}] \tag{5.13}$$

The probability that the second mentioned event (the failure of the line or circuit breaker to the H-bus, or the H-bus itself) will occur is given in Equation 5.14.

$$\lambda_{F7} = \lambda_{Cab} + \lambda_{CB} + \lambda_{Bus} = 6.09 \cdot 10^{-6}[h^{-1}] \tag{5.14}$$

The final event, the failure of connection to the power subsystem, is done exactly like the power subsystem is calculated in Equation 5.3. The only difference is that the failure rate of the cables and circuit breakers has to be used instead of the failure rates of the internal power components (i.e. λ_{Cab} and λ_{CB} instead of $\lambda_{BF}, \lambda_{CF}, \lambda_{FTS}, \lambda_{PF}$ and λ_{RF}). Equation 5.15 shows the calculation for the probability of this event.

$$\lambda_{F8} = (\lambda_{Cab} + \lambda_{CB})^2 + (\lambda_{Cab} + \lambda_{CB})^4 + 2 \cdot (\lambda_{Cab} + \lambda_{CB}) \cdot 6 \cdot (\lambda_{Cab} + \lambda_{CB})^2 = 3.71 \cdot 10^{-11}[h^{-1}] \tag{5.15}$$

When adding all of the separate failure rates up, the final critical failure rate of the top side of the four battery architecture's PMAD subsystem (Equation 5.16).

$$\lambda_{Tot3} = \lambda_{F6} + \lambda_{F7} + \lambda_{F8} = 6.09 \cdot 10^{-6}[h^{-1}] \tag{5.16}$$

Eight battery pack architecture
There are multiple events in this architecture that can lead to a critical failure:

- An entire side cannot supply power together with one of these components of the other side: A generator cable, a battery cable, a line or circuit breaker to the H bus, the H bus itself or the two top busses. (λ_{F9})
- The cables from the power supply fail in the same way that was described in the power subsystem part: All batteries, all generators or four batteries with one generator. (λ_{F10})

If an entire side cannot supply power, it could have multiple reasons. The two upper busses, the H-bus or the line or circuit breaker to the H-bus could be broken. A visualtisation of this is shown in the fault tree of Figure 5.10.

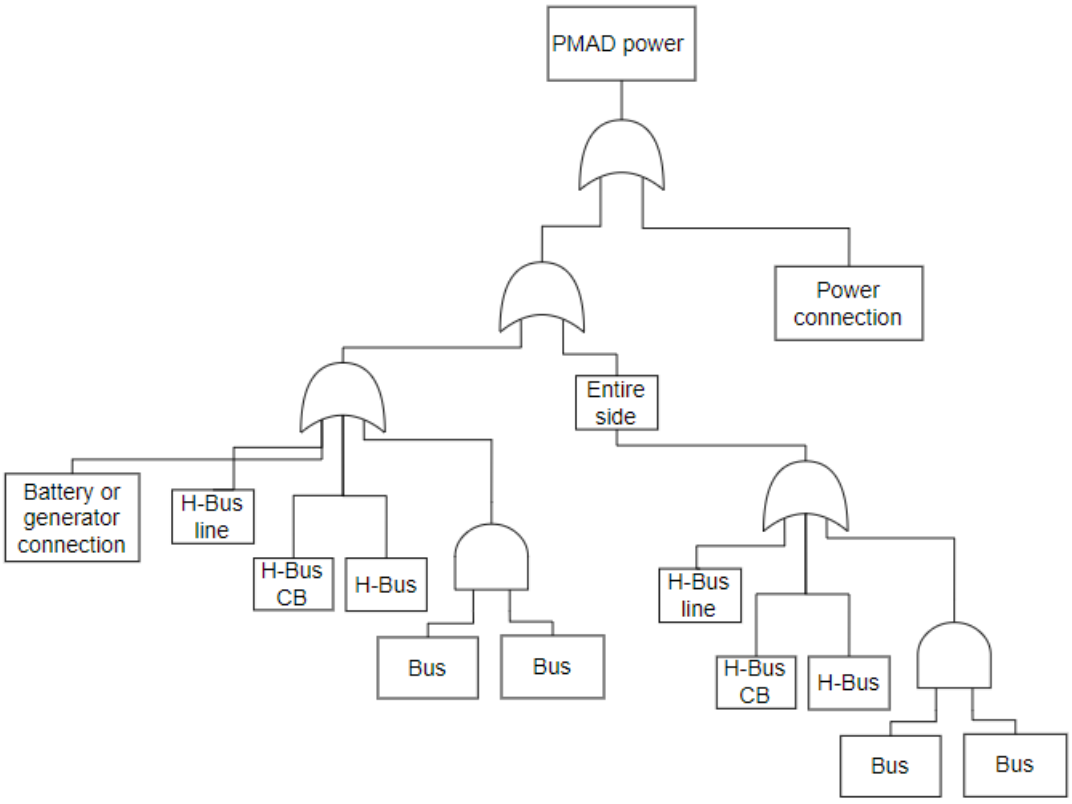

Figure 5.10: Fault tree of faults in power side of eight battery architecture

With this FTA in combination with the failure rates mentioned in Table 5.5 the critical failure rate of the upper PMAD subsystem can be determined. The probability of the failure of an entire side is given in Equation 5.17:

$$\lambda_{side} = \lambda_{Bus}^2 + \lambda_{Bus} + \lambda_{Cab} + \lambda_{CB} = 6.09 \cdot 10^{-6}[h^{-1}] \tag{5.17}$$

The probability that this failure occurs together with one of the faults mentioned in the first event is given

in Equation 5.18.

$$\lambda_{F9} = \lambda_{side} * (\lambda_{Bus}^2 + \lambda_{Cab} + \lambda_{CB} + \lambda_{Bus}) = 3.71 \cdot 10^{-11}[h^{-1}] \tag{5.18}$$

To calculate the probability of failure of the cables from the power supply, the probability has to be approached in the same way as the probability for the batteries to fail (Equation 5.4), just like with the four battery pack architecture. The equation to calculate the reliability for this power side is given in Equation 5.19.

$$\lambda_{F10} = (\lambda_{Cab} + \lambda_{CB})^2 + (\lambda_{Cab} + \lambda_{CB})^8 + 2 \cdot (\lambda_{Cab} + \lambda_{CB}) \cdot 70 \cdot (\lambda_{Cab} + \lambda_{CB})^4 = 3.71 \cdot 10^{-11}[h^{-1}] \tag{5.19}$$

Finally, the total critical failure rate of the eight battery architecture PMAD top side is given in Equation 5.20.

$$\lambda_{Tot4} = \lambda_{F9} + \lambda_{F10} = 7.42 \cdot 10^{-11} \tag{5.20}$$

Total

The total critical failure rate of the PMAD subsystem can now be calculated by adding the top and bottom failure rates. Equation 5.21 shows the failure rate of the four battery pack architecture PMAD subsystem and Equation 5.22 gives the failure rate of the eight battery pack architecture PMAD subsystem.

$$\lambda_{PMAD4} = \lambda_{Tot1} + \lambda_{Tot3} = 6.09 \cdot 10^{-6} \tag{5.21}$$

$$\lambda_{PMAD8} = \lambda_{Tot2} + \lambda_{Tot4} = 7.42 \cdot 10^{-11} \tag{5.22}$$

Listed in Table 5.6 are all of the failures and its rates are given for the entire PMAD of both architectures.

Fault	λ	**Failure rate per flight hour**
Four battery pack architecture		
Propulsion side		
Both connections of two separate motors	λ_{F1}	$2.82 \cdot 10^{-23}$
Two busses on one side	λ_{F2}	$2.02 \cdot 10^{-10}$
One bus, two lines	λ_{F3}	$5.42 \cdot 10^{-15}$
Entire propulsion side of the PMAD	λ_{Tot1}	$2.02 \cdot 10^{-10}$
Power side		
Two busses	λ_{F6}	$1.57 \cdot 10^{-17}$
Cable or CB to H-bus of H-bus	λ_{F7}	$6.09 \cdot 10^{-6}$
Generator or battery connection	λ_{F8}	$3.71 \cdot 10^{-11}$
Entire power side of the PMAD	λ_{Tot3}	$6.09 \cdot 10^{-6}$
Total	λ_{PMAD4}	$6.09 \cdot 10^{-6}$
Eight battery pack architecture		
Propulsion side		
Both connections of two separate motors	λ_{F1}	$2.82 \cdot 10^{-23}$
One side bus, two cables	λ_{F4}	$2.71 \cdot 10^{-15}$
Mid bus, two cables or side bus	λ_{F5}	$1.79 \cdot 10^{-24}$
Entire propulsion side of the PMAD	λ_{Tot3}	$2.71 \cdot 10^{-15}$
Power side		
One side and component from other side	λ_{F9}	$3.71 \cdot 10^{-11}$
Entire power side of the PMAD	λ_{F10}	$3.71 \cdot 10^{-11}$
Entire power side of the PMAD	λ_{Tot4}	$7.42 \cdot 10^{-11}$
Total	λ_{PMAD8}	$7.42 \cdot 10^{-11}$

Table 5.6: PMAD failure rates

5.3.4. Motor subsystem

The motor subsystem of both architectures is exactly the same. There are eight motors that are powered through the PMAD, and there is only one way to cause a critical failure in the motor side. This is when two or more motors fail. The fault tree of the motor subsystem is given in Figure 5.11. While there is only one way to cause a critical fault, there are a lot of motor combinations to take into account. This makes the fault tree still a lot more complex. The probability that more than two motors fail could also be put in the fault tree, but the chance of that happening is negligible compared to the probability of two failures and would make the fault tree too complex.

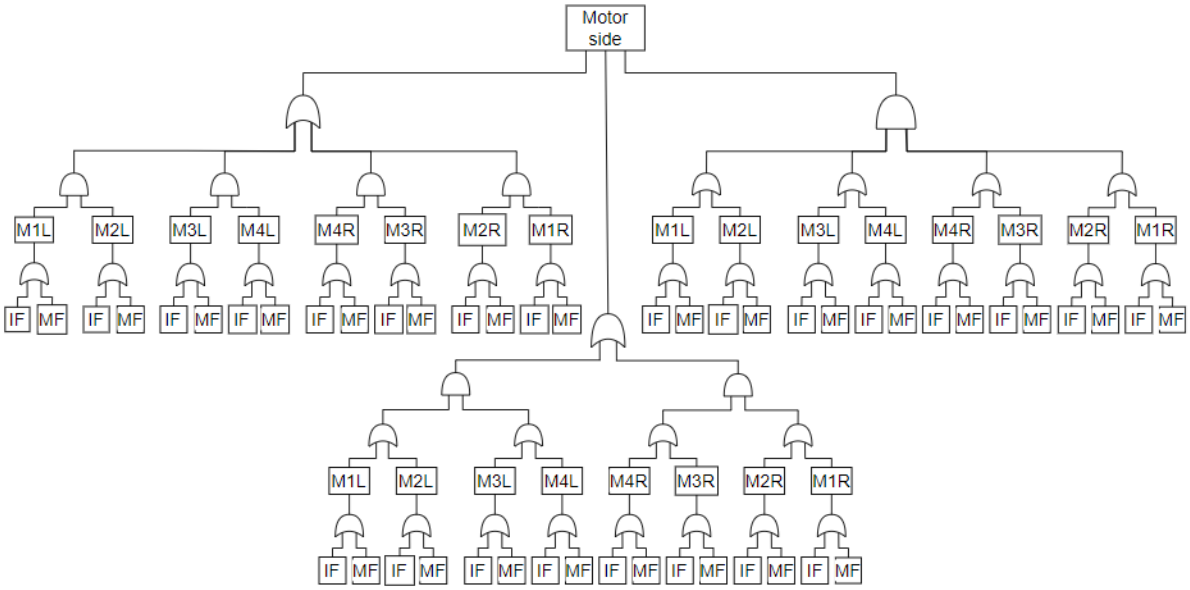

Figure 5.11: Motor side fault tree for both architectures

In the bottom are the basic events, the inverter and internal motor failure. The intermediate event is the failure of one motor. This event has a value of $\lambda_{MF} + \lambda_{IF} = 5.13 \cdot 10^{-5}[h^{-1}]$. With these values the table for motor system failures can be created.

Intermediate event	λ	Failure rate $[h^{-1}]$	Basic event	λ	Failure rate $[h^{-1}]$
Motor system failures					
Motor fault	λ_M	$5.13 \cdot 10^{-5}$	Internal fault Inverter fault	λ_{MF} λ_{IF}	$5.9 \cdot 10^{-6}$ $4.54 \cdot 10^{-5}$

Table 5.7: Failure rates motor side

With these failure rates and the fault tree, the critical failure rate of the motor system for both architectures can be calculated. The equation to calculate this is given below (5.23).

$$\text{Total failure rate of motor subsystem} = 4\lambda_M^2 + 8\lambda_M^2 + 16\lambda_M^2 = 7.37 \cdot 10^{-8}[h^{-1}] \tag{5.23}$$

5.3.5. Total failure rate

Now that the values for the different subsystems are known, they can be added together to get a final result for both of the architectures. In Table 5.8, the critical failure rates of the subsystems together with the total critical failure rate of both architectures are given.

Subsystem faults	Four battery failure rate[h^{-1}]	Eight battery failure rate[h^{-1}]
Power subsystem	$2.84 \cdot 10^{-9}$	$2.83 \cdot 10^{-9}$
PMAD subsystem	$6.09 \cdot 10^{-6}$	$7.42 \cdot 10^{-11}$
Motor subsystem	$7.37 \cdot 10^{-8}$	$7.37 \cdot 10^{-8}$
Total	$6.09 \cdot 10^{-6}$	$7.66 \cdot 10^{-8}$

Table 5.8: Failure rates

It can clearly be seen that the weakest part of the four battery pack architecture is the PMAD. The main reason is for this is the cable from the upper busses to the H-bus. If the H-bus or the cable connected between the H-bus and upper busses fail, a critical failure is already reached. The eight battery pack architecture gets much closer to the required critical failure rate of 10^{-9}, but the motor and power system are just above this number. If other batteries, generators and motors are available in the future that have a higher reliability, the results could go below the aimed failure rate. The robustness of the eight battery pack architecture PMAD subsystem proves that with more connections and redundancy, a low critical failure rate is achieved.

5.4. Grid Topologies: Reliability Assessment

A comparison of the weights of both architectures, as detailed in Table 4.1, against the critical failure rates in Table 5.8, reveals a correlation between these variables. Specifically, a lower critical failure rate is associated with a lighter system, whereas a higher critical failure rate corresponds to a heavier system. The Power Management and Distribution (PMAD) subsystem is the primary variable between the two architectures, aside from the size and number of battery packs. Further breakdown of the impact of the different components of the system for the PMAD can be seen in Table 5.6.This in itself should make for a very obvious conclusion; increasing the weight by increasing the complexity makes the grid more reliable.

The four battery pack architecture features a significantly simpler PMAD subsystem compared to the more redundant and complex subsystem of the eight battery pack architecture. This increased redundancy contributes to the greater weight of the eight battery pack system. However, this weight remains within the maximum permissible limit specified in Chapter 2. Given that the weight is still within acceptable limits and the critical failure rate is notably lower than that of the four battery pack architecture, the eight battery pack configuration is deemed more suitable for the AEA propulsion system. Nevertheless, further research is required to reduce the critical failure rate to the target value of 10^{-9} per flight hour, as discussed in Chapter 6.

The balance between weight and reliability is a crucial consideration in the design of AEA. Achieving a lower critical failure rate often necessitates increased redundancy, which in turn increases the weight of the system. This trade-off must be carefully managed to ensure both safety and performance. Further investigation into the failure rates of different sub components, control aspects (which have not been extensively covered in this thesis), and comprehensive testing or simulations can significantly enhance the depth of this analysis.

Implementing detailed studies on the steady-state and fault condition power flows can provide valuable insights into the real-life significance of the design choices. By modeling these conditions, designers can identify potential weaknesses and develop strategies to mitigate them, thereby improving the overall reliability and efficiency of the system. Advanced simulations and empirical testing can also help in refining the PMAD subsystem and optimizing the balance between weight and reliability, ultimately contributing to the development of a more robust and effective propulsion system for AEA.

6

Reflection & Discussion

6.1. Intergroup Results

As was mentioned in the introductory sections of this thesis, this project was divided into two parts; one the work presented in this thesis and the other the work done by the other subgroup; regarding the design and prototyping of a *Bidirectional Solid State Circuit Breaker for AEA*. The Circuit Breaker group successfully designed, optimised and built a design for a Bidirectional Solid State Circuit Breaker, suited for usage into the AEA propulsion grid as designed in this thesis. The specific ratings and achieved goals of the circuit breaker design are listed below:

- Peak fault current of 1500 A
- Peak fault voltage of 3.6 kV
- Mass of 28.6378 kg
- Failure rate of $1.39 \cdot 10{-}7\ [h^{-1}]$ (without fuse)
- Failure rate of $3.17 \cdot 10{-}10\ [h^{-1}]$ (with fuse)

The mass of the designed breaker is significantly higher than assumed in the structural design of this thesis. Nonetheless, the reliability of the designed breaker is also significantly improve compared to the estimated value used in the reliability assessment. All in all, the work done in that thesis successfully complements the work presented in this paper and further combining could have significant benefits on future work.

6.2. Intragroup Results

In this thesis, considerations and design choices for the transmission network of the AEA grid, different grid topology designs and their components were presented and structurally analysed. Moreover, a reliability assessment was performed on this grid topology per subcomponent using a FMEA, eventually building on to a critical failure of the complete system using a FTA. Specifically, the following results and design choices were achieved and made that adhere to the Programme of Requirements as defined in Chapter 2.

Transmission Network Results

- The cable structure and materials were determined; using aluminium for the conductor, metal sheath and PTFE (Teflon) for the insulation.
- The conductor radius was found for the different voltage levels and conductor temperatures as shown in Table 3.1.
- The system voltage level was set at 3000 V based on weight considerations.

- The thickness of the supplementary layers were determined as follows: 1 mm for the outer jacket and metal sheath, 0.6 mm for the inner and outer semiconducting layers.
- The insulation thickness of the cable was determined through the SVD method by evaluating Partial Discharge effects and high voltage considerations.
- The weights of the cable per meter length as well as the corresponding insulation thickness were calculated for the different power levels, as shown in Table 3.2.

Grid Topology Results

- Different grid structures, elements and topologies and their reliability impact were investigated.
- The AEA propulsion grid was structurally built up by exploring all its sub-components, their specifications and weights.
- The DC-DC converter weights were taken to be 43.2 kg (4 batteries) or 21.6 kg (8 batteries).
- Through consideration of both weight and reliability, two final topologies were designed for the propulsion grid as shown in Figures 4.13 and 4.15.
- Via an in-depth structural analysis of the grid in a simplification of the real-world scenario, the total weight burden of the selected grids was calculated, including the locations of the components in the plane's grid, the estimated length of the cabling system & and the mass contribution of all the sub-components.
- The total weights of both topologies were 3737.00 kg (8 battery) and 1785.79.79 kg (4 battery).

Reliability Assessment Results

- A FMEA was constructed analysing the different failure modes of the sub-components as defined in Section 4.2.
- 21 failure modes were identified and analysed on their severity in different stages of flight, causes, effects and occurrence.
- Failure rate estimates per sub-components were made based on literature and existing MEA studies and defined as shown in Table 5.3.
- A FTA was made structured top-down with critical failure mode and conditions as defined in Section 5.3.1.
- The inter-relations between the failures of sub-components and systems were explored, producing a failure rate per subsystem and an eventual critical failure rate for the two designed topologies.
- The critical failure rates were determined to be $6.09 \cdot 10^{-6}\mathrm{h}^{-1}$ and $7.66 \cdot 10^{-8}\mathrm{h}^{-1}$.
- A balanced evaluation of both topologies was made based on their mass burden and reliability (failure rate), resulting in the choice for the 8 battery topology as shown in Figure 4.13.
- A RBD was constructed for the motor subsystem to give insight into the interconnections between a subsystem and to identify points of further investigation following this thesis.

6.3. Discussion

As with all scientific research, it is important to consider the boundaries, scope and necessary assumptions made in the process of developing this thesis. In this paper, quite some subjects were either simplified or presumed in order to keep to the scope of the project that requires additional attention. This discussion will be structured per chapter of this thesis; the transmission network, the grid topology and the reliability assessment.

6.3.1. Transmission Network

For the transmission network and especially the cable structure and sizing there are several points to reflect on. First and foremost, it should be noted that although the analysis is quite complete and in-depth, a lot of assumptions were made in the design. For example, the semiconductor, shield and outer jacket layer were not discussed in detail (in order to keep to the scope of the project), but naturally could benefit from more attention in the cabling design.

Furthermore, the (operating) temperature of the conductor should be investigated in more detail in order to achieve more accurate values for the conductor sizing. To adhere to the weight constraints set in the programme of requirements this was the main focus point of the design.

Nevertheless, the efficiency of the cable and its different materials could have received some more attention, as well as the impact of voltage drop across the cables as well. Especially for the longer cables such as the generator lines, this might have a noteworthy impact on the system.

In addition, it is important to note that all cable weights and radii are designed for peak powers and boundary condition situations, which mostly occur during the short period of take-off. The majority of the time the aircraft will be operational in cruising and the system will demand (significantly) less power, meaning the cable is designed with some margin in terms of its conductor and insulating sizing.

Additionally, the consideration of the environmental impact on the temperature considerations could have been investigated more thoroughly, as well as humidity and wear-out effects in aircraft.

Lastly, in the calculations for temperature differences and heat losses values were taken to be true within an acceptable accuracy range. In order to make the analysis more meticulous this precision could be improved, making the cable design even more optimised.

All in all, although there are always points to improve on, the analysis presented was quite broad and in-depth, considering all relevant elements of cable design while adhering to the programme of requirements presented in Section 2.2.

6.3.2. Grid Topology

For the grid topology, there are several elements that could benefit from additional research and more in-depth analysis. The first and foremost part of the design that demands attention here is the omission of the control part of the grid. By assuming the control to work in a 'black-box' fashion this thesis was able to produce a grid topology that could analysed on both quantitative and qualitative levels. However, its presence and proper function is paramount, especially in AEA applications. This is mainly to ensure the reliability and maintain nominal operation, for example when to divert power across different paths or when to (temporarily) turn off parts of the system in fault conditions.

Secondly, this thesis focused its analysis purely on the 'high-voltage' part of the grid, ignoring all the secondary loads and systems of the system, such as the WIPS, avionics, ECS and perhaps more importantly, the general control systems discussed above. Naturally, these systems are also powered through the batteries and have their own grid, although their power demand (and voltage levels) are significantly lower than that of the propulsion grid. For completeness, these grids and their interconnections with the propulsion grid should also be considered. Moreover, this grid and its components also contribute to the total mass burden on the system, making efficient design a further point of focus here. Henceforth, it should be noted that faults in these systems could potentially impact the propulsion system and its reliability as well (both directly and indirectly). Additionally, the power converters to these lower voltage levels for the system are to be added to the electrical mass. The mass and size of these converters will depend on future technology and the voltage level of these systems.

Moreover, as was stated throughout Chapter 4, this thesis had its focus in the optimisation of the transmission network and grid. Sub-components of the grid were explored and incorporated in the design, but the main objective of this chapter was finding the most optimum way of the interconnection network for weight and redundancy, through minimising cable length and different grid structures to

improve reliability. Sub-components such as the battery packs, generators and motors were taken as given boundary conditions as specified by [4]. Naturally, a more sustained and in-depth analysis of the sub-components could further benefit the redundancy and quality of the grid.

In addition, due to the fact that extensive research into the sub-components was outside the scope of this thesis, this intrinsically means the structural analysis of the designed grid was also subject to a set of assumptions. Although these weight estimations were taken to be within an acceptable accuracy standard, it should be noted that these can differ in reality. Even though this might influence the results presented in Section 4.3.6, the weight calculations for the grid (and its mass budget required by Section 2.2) are already specified exclusively for the PMAD network, which excludes the sub-components that have large mass implications for the system (such as the motors or batteries).

At last, it is worth mentioning that the presented methodology of designing the grid and its proposed structure is only one of the ways of interpreting the given problem as specified by Chapter 2. There are many ways of designing the grid, that all depend on the sub-components, requirements set for all the parameters of the grid and the relevant choices made in system variables. Thus, further analysis and comparison between different topologies could enhance the quality and efficiency of the final grid design.

6.3.3. Reliability Assessment

In the reliability assessment, there are a number of features to reflect on. To start, it should be noted that the failure rate estimations are subject to a margin for error seeing as there is no empirical data available on comparable systems. By taking current studies on existing EPS in MEA applications it was assumed that their failure rates were likely to be in the same order of magnitude as for the AEA design. Clearly, a more accurate reliability analysis can be performed once the development of AEA advances. At that time, it will be very interesting to perform a similar analysis and compare it to the estimates made in this paper to either confirm or debunk the presented results.

Second, as was the case in the grid topology design, the control system of the EPS (and the general control system) was excluded from the analysis to stay within the scope of the project. Nonetheless, it is also of large significance for the reliability analysis and failure rate estimation. Control faults can be even more severe than 'regular' faults in certain subsystems, since it could mean that a fault is not handled properly and therefore could immediately form a critical failure mode while theoretically, it could be a non-critical fault due to proper grid design. As will be mentioned in Section 7.2, this should be one of the next steps in reliable grid design for AEA, building on to the work of this thesis.

The battery packs and their failure rate estimates were a very high estimate. Being the worst failure rate by a significant margin, this requires extra attention in this discussion. As was mentioned in Section 5.1.3, the current state of the battery technology would produce a relatively too high failure rate for the system to reach the critical failure rate as set by the requirement in Section 2.2. However, seeing as this estimate was made using data from today and the AEA is set to be commercially launched in 2033, it can be assumed that this rate will drastically decrease to an acceptable level by that time.

Furthermore, in order to be able to analyse the complete system for reliability, all sub-components and their failure rates had to be taken into account. However, as was mentioned in Section 5.1.1, it was decided that every subcomponent failure mode would be taken as 'general subcomponent failure' in the further reliability assessment of the grid in Section 5.3, with the aim of reducing the complexity of the analysis. Notwithstanding, it is imperative to acknowledge that the reliability analysis could be significantly improved by an in-depth study of different component failure modes and their failure rate interconnections. Especially to study the probability of cascaded failures it can be very interesting to build further on the work started in Section 5.3 of this thesis. An example of such a study could be done through frameworks such as the RBD as was briefly mentioned in 5.2, which can provide further numerical insights into cascaded failures and subcomponent relations.

7

Conclusion & Future Work

7.1. Conclusion

To conclude, the goal of this thesis was to produce a design for the propulsion drivetrain grid, optimised for weight and conducting a thorough reliability analysis on the designed grid. Through weight-optimised design of the transmission network followed by qualitative redundant grid design, the topologies were analysed on their reliability per subcomponent building on to a critical failure rate its overall reliability could be tested on. This thesis started with an in-depth study on the cabling structure, materials and parameters present in the transmission network. Heat losses due to convection and radiation were considered and through a rigorous temperature analysis the relation between the conductor temperature, surface temperature and the conductor radius was obtained. A balanced choice was made on the voltage level and edge case conductor temperature, resulting in a final conductor radius. High voltage phenomena were also considered in designing the insulation as part of Partial Discharge Mitigation. Combining these results, an optimal value for the cable weight was found. Subsequently, the grid topology was investigated using literature and the E9X case study. The design process was structured bottom-up, assessing weight and reliability concerns along the way and looking at the different sub-components of the system, producing two grid topologies within the mass budget. The chapter was concluded by a structural analysis putting the grid design in practice and producing a total weight value for the topology. Concurrently, the grid was assessed on its reliability. A Failure Mode and Effects Analysis was produced focusing on the different failure modes of the sub-components, analysing fault severity, causes, effects and their occurrence, producing failure rate estimates for every component. Next, the Fault Tree Analysis was generated in a top-down fashion to produce critical failure rates for each topology for the critical fault 'loss of propulsion', allowing for comparison and a final choice of topology. Concluding this thesis, a balanced evaluation of both topologies based on their total weight and reliability was created and a justified choice for one final topology was made. All in all, this thesis produced a effective design for the propulsion grid of an AEA, evaluating the weight of its transmission network and optimising its grid structure for both mass and reliability concerns.

7.2. Future Work

As was mentioned at the beginning and evident throughout this thesis, there are still several challenges around the successful commercial launch of AEA. There are a lot of points of investigation that still require more attention, ranging from the improvement of the battery-technology such that it can deliver the required power rating and/or is more weight efficient, improvements in motor design to deliver more peak power and enhanced protection devices to allow for reliable grid operation that stays within the grid's mass budget. Specifically for the work done in this thesis, there are numerous points additional research can be done in to improve and build on the current status of the project. First and foremost, as was already widely discussed, adding successful and efficient control systems to the grid can effectively improve the reliability of the system and will allow the topology to properly handle fault scenarios. Additionally, further research in the sub-components of the system can be done in order to provide a more in-depth and clearer sketch of the grid, as well as providing more accurate results of the reliability analysis. Moreover, considering more research into different failure modes and their probability can

significantly enhance the accuracy of the FTA and the critical failure rate it produces. Displaying the interconnections and cascaded failure, the RBD forms a good framework to complement the existing reliability assessment presented in this paper. Creating and calculating such a diagram can be done to further deepen the base of the analysis and also used as a tool to enhance overall reliability. Furthermore, investigation into a power flow analysis of fault conditions can be used to rigorously test the designed grids for real life failure modes and scenarios. This could then be used for optimising the designed grids for both weight and reliability; providing an accurate reference. Additionally, as was mentioned in 4.3.6, there are several improvements that can be done in order to enhance the quality of the structural analysis that can further optimise the weight. Improving the efficiency of this could free up space in the weight budget, allowing for more redundancy in the design.

Bibliography

[1] P. J. Ansell and K. S. Haran, "Electrified airplanes: A path to zero-emission air travel," *IEEE Electrification Magazine*, vol. 8, no. 2, pp. 18–26, 2020, Cited by: 56. DOI: 10.1109/MELE.2020.2985482. [Online]. Available: https://www.scopus.com/inward/record.uri?eid=2-s2.0-85086764625&doi=10.1109%2fMELE.2020.2985482&partnerID=40&md5=5857787b932fea3229bb60ce79e666c0.

[2] A. Barzkar and M. Ghassemi, "Components of electrical power systems in more and all-electric aircraft: A review," *IEEE Transactions on Transportation Electrification*, vol. 8, no. 4, pp. 4037–4053, 2022, Cited by: 54. DOI: 10.1109/TTE.2022.3174362. [Online]. Available: https://www.scopus.com/inward/record.uri?eid=2-s2.0-85132508781&doi=10.1109%2fTTE.2022.3174362&partnerID=40&md5=74aff1e8a7ff5e091415593323895510.

[3] A. Barzkar and M. Ghassemi, "Electric power systems in more and all electric aircraft: A review," *IEEE Access*, vol. 8, pp. 169 314–169 332, 2020, Cited by: 175; All Open Access, Gold Open Access. DOI: 10.1109/ACCESS.2020.3024168. [Online]. Available: https://www.scopus.com/inward/record.uri?eid=2-s2.0-85097152698&doi=10.1109%2fACCESS.2020.3024168&partnerID=40&md5=98c9d8e3be318de6069b707cbe5afaa9.

[4] R. de Vries, R. E. Wolleswinkel, M. F. M. Hoogreef, and R. Vos, "A new perspective on battery-electric aviation, part ii: Conceptual design of a 90-seater," Cited by: 2; All Open Access, Green Open Access, 2024. DOI: 10.2514/6.2024-1490. [Online]. Available: https://www.scopus.com/inward/record.uri?eid=2-s2.0-85192109026&doi=10.2514%2f6.2024-1490&partnerID=40&md5=11e3f7aedafea100c68487d6d470f410.

[5] R. E. Wolleswinkel, R. de Vries, M. F. M. Hoogreef, and R. Vos, "A new perspective on battery-electric aviation, part i: Reassessment of achievable range," Cited by: 2; All Open Access, Green Open Access, 2024. DOI: 10.2514/6.2024-1489. [Online]. Available: https://www.scopus.com/inward/record.uri?eid=2-s2.0-85191656297&doi=10.2514%2f6.2024-1489&partnerID=40&md5=6c9ca35d1115062d6364b8754d07d61a.

[6] M. G. Niasar, *High voltage cable systems, lecture 2 - cable components and cable manufacturing*, Lecture notes, Delft University of Technology, Accessed: 2024-02-23, 2024. [Online]. Available: https://brightspace.tudelft.nl/d2l/le/content/595680/viewContent/3620353/View.

[7] Tibtech Innovations, *Metal conductivity properties*, https://www.tibtech.com/metal-conductivity, Accessed: 2024-06-07, 2024.

[8] ELEK Software, *Sheath bonding design guide for high voltage cables*, https://elek.com/articles/sheath-bonding-design-guide-for-hv-cables/, Accessed: 2024-06-07, 2024.

[9] M. Vakilian, T. Blackburn, R. James, and et al., "Semiconducting layer as an attractive pd detection sensor of xlpe cables," *IEEE Transactions on Dielectrics and Electrical Insulation*, vol. 13, no. 4, pp. 885–891, 2006. DOI: 10.1109/TDEI.2006.1667752.

[10] T. L. Bergman, A. S. Lavine, F. P. Incropera, and D. P. DeWitt, *Fundamentals of Heat and Mass Transfer*, 7th. Hoboken, New Jersey: John Wiley & Sons, Inc., 2011.

[11] TU Delft OpenCourseWare, *6.2.4 example a: Radiator*, https://ocw.tudelft.nl/course-lectures/6-2-example-radiator/, Accessed: 2024-06-07, 2024.

[12] Khan Academy, *What is the ideal gas law?* https://www.khanacademy.org/science/physics/thermodynamics/temp-kinetic-theory-ideal-gas-law/a/what-is-the-ideal-gas-law, Accessed: 2024-06-07, 2024.

[13] M. Bhide, Y. Liang, G. R. C. Mouli, M. G. Niasar, and P. Bauer, “Hybrid reconfigurable battery pack for all-electric aircraft: Synergizing high-specific-energy and power battery types,” Submitted to IEEE Transportation Electrification Conference Expo, 2024.

[14] The Engineering ToolBox, *Plastics - thermal conductivity coefficients*, https://www.engineeringtoolbox.com/thermal-conductivity-plastics-d_1786.html, Accessed: 2024-06-07, 2024.

[15] H. Schefer, L. Fauth, T. H. Kopp, R. Mallwitz, J. Friebe, and M. Kurrat, “Discussion on electric power supply systems for all electric aircraft,” *IEEE Access*, vol. 8, pp. 84 188–84 216, 2020, Cited by: 109; All Open Access, Gold Open Access, Green Open Access. DOI: 10.1109/ACCESS.2020.2991804. [Online]. Available: https://www.scopus.com/inward/record.uri?eid=2-s2.0-85084918886&doi=10.1109%2FACCESS.2020.2991804&partnerID=40&md5=cd75eb8f061ffd3b5b58d8e36035c146.

[16] G. Bahder, S. Hvidsten, and H. Faremo, “Insulation thickness determination of polymeric power cables,” *IEEE Transactions on Dielectrics and Electrical Insulation*, vol. 1, no. 4, pp. 567–573, 1994. DOI: 10.1109/94.311705.

[17] Galaxy Wire Cable, Inc., *Polytetrafluoroetheylene (ptfe) / teflon® insulation material for wire and cable*, https://www.galaxywire.com/custom-wire-cable/jacket-insulation/ptfe-teflon-polytetrafluoroethylene/, Accessed: 2024-06-08, 2024.

[18] The Chemours Company, *Teflon™ ffr 880 fluoroplastic foam resin*, Accessed: 2024-06-08, 2020.

[19] A. Martins and M. Pinheiro, “On the propulsive force developed by asymmetric capacitors in a vacuum,” *Physics Procedia*, vol. 20, pp. 112–119, Dec. 2011. DOI: 10.1016/j.phpro.2011.08.010.

[20] J. Wilkerson, M. Jacobson, M. A, *et al.*, “Analysis of emission data from global commercial aviation: 2004 and 2006,” *ATMOSPHERIC CHEMISTRY AND PHYSICS*, vol. 2010, pp. 2945–2983, Feb. 2010. DOI: 10.5194/acpd-10-2945-2010.

[21] The Engineering ToolBox, *International standard atmosphere*, https://www.engineeringtoolbox.com/international-standard-atmosphere-d_985.html, Accessed: 2024-06-07, 2024.

[22] X. Zhao, J. M. Guerrero, and X. Wu, “Review of aircraft electric power systems and architectures,” Cited by: 86; All Open Access, Green Open Access, 2014, pp. 949–953. DOI: 10.1109/ENERGYCON.2014.6850540. [Online]. Available: https://www.scopus.com/inward/record.uri?eid=2-s2.0-84904962162&doi=10.1109%2fENERGYCON.2014.6850540&partnerID=40&md5=2b66577f0c92ab6561f3c41f95bc7d4a.

[23] European Aviation Safety Agency, *Certification specifications and acceptable means of compliance for large aeroplanes (cs-25)*, Amendment 27, European Aviation Safety Agency, Cologne, Germany, Nov. 2021.

[24] C. Emissions, A. Board, D. Sciences, and N. Medicine, *Commercial aircraft propulsion and energy systems research: Reducing global carbon emissions*. Sep. 2016, pp. 1–122. DOI: 10.17226/23490.

[25] A. K. R. Siddavatam, K. Rajashekara, R. P. Reddy, *et al.*, “Fault-tolerant architectures with enhanced bus protection for electric/hybrid aircraft systems,” *IEEE Transactions on Transportation Electrification*, vol. 9, no. 3, pp. 3564–3578, 2023, Cited by: 1. DOI: 10.1109/TTE.2022.3208798. [Online]. Available: https://www.scopus.com/inward/record.uri?eid=2-s2.0-85139436315&doi=10.1109%2fTTE.2022.3208798&partnerID=40&md5=5a082ad40e788e1321e9303d960816b0.

[26] M. Armstrong, M. Blackwelder, A. Bollman, *et al.*, “Architecture, voltage, and components for a turboelectric distributed propulsion electric grid,” Jan. 2015.

[27] A. K. R. Siddavatam, K. Rajashekara, R. P. Reddy, H. Huang, H. S. Krishnamoorthy, and F. Wang, “A h-type architecture for electric/hybrid-electric aircraft propulsion systems,” *IET Electrical Systems in Transportation*, vol. 13, no. 1, 2023, Cited by: 1; All Open Access, Gold Open Access. DOI: 10.1049/els2.12065. [Online]. Available: https://www.scopus.com/inward/record.uri?eid=2-s2.0-85150681317&doi=10.1049%2fels2.12065&partnerID=40&md5=618eb45b9437c01df7ddf32243f954de.

[28] M. Ghassemi, A. Barzkar, and M. Saghafi, “All-electric nasa n3-x aircraft electric power systems,” *IEEE Transactions on Transportation Electrification*, vol. 8, no. 4, pp. 4091–4104, 2022, Cited by: 30. DOI: 10.1109/TTE.2022.3158186. [Online]. Available: https://www.scopus.com/inward/record.uri?eid=2-s2.0-85126332193&doi=10.1109%2fTTE.2022.3158186&partnerID=40&md5=71ec1effaad4bdef425de97952a94782.

[29] N. A. U.S. Department of Energy’s (DOE) Argonne National Laboratory DOE’s Vehicle Technologies Office (VTO) and S. A. (G. R. Center, “Joint assessment of the rd needs for electric aviation,” Argonne National Laboratory, Tech. Rep., 2021.

[30] J. R. Rakoski Zientarski, J. R. Pinheiro, M. L. da Silva Martins, and H. L. Hey, “Understanding the partial power processing concept: A case-study of buck-boost dc/dc series regulator,” in *2015 IEEE 13th Brazilian Power Electronics Conference and 1st Southern Power Electronics Conference (COBEP/SPEC)*, 2015, pp. 1–6. DOI: 10.1109/COBEP.2015.7420092.

[31] D. Izquierdo, A. Barrado, C. Raga, M. Sanz, and A. Lazaro, “Protection devices for aircraft electrical power distribution systems: State of the art,” *IEEE Transactions on Aerospace and Electronic Systems*, vol. 47, no. 3, pp. 1538–1550, 2011. DOI: 10.1109/TAES.2011.5937248.

[32] RTX, “Rtx developing innovative solid-state circuit breaker for hybrid-electric aircraft under nasa contract,” *RTX News Center*, 2023, Accessed: 2024-06-13. [Online]. Available: https://www.rtx.com/news/news-center/2023/10/04/rtx-developing-innovative-solid-state-circuit-breaker-for-hybrid-electric-aircraf.

[33] K. Sharma and S. Srivastava, “Failure mode and effect analysis (fmea) implementation: A literature review,” Apr. 2018.

[34] T. A. ter Horst, F. Walterbos, and M. Hoogreef, *Effect of different failure modes in aircraft and their severity on different stages of flight*, May 2024.

[35] S. Ong, *The slog continues for lithium-air batteries*, Jun. 2021. [Online]. Available: https://spectrum.ieee.org/lithium-air-batteries-battery-news.

[36] V. Viswanathan, A. H. Epstein, Y.-M. Chiang, *et al.*, “The challenges and opportunities of battery-powered flight,” *Nature*, vol. 601, no. 7894, pp. 519–525, 2022, Cited by: 140; All Open Access, Green Open Access. DOI: 10.1038/s41586-021-04139-1. [Online]. Available: https://www.scopus.com/inward/record.uri?eid=2-s2.0-85123757805&doi=10.1038%2fs41586-021-04139-1&partnerID=40&md5=5ad91a68eff36c2868db87145d866eda.

[37] J. B. Fritzke, J. H. J. Ellison, L. Brazel, G. Horwitz, S. Menkin, and C. P. Grey, “Spiers memorial lecture: Lithium air batteries – tracking function and failure,” *Faraday Discuss.*, vol. 248, pp. 9–28, 0 2024. DOI: 10.1039/D3FD00154G. [Online]. Available: http://dx.doi.org/10.1039/D3FD00154G.

[38] N. Imanishi and O. Yamamoto, “Perspectives and challenges of rechargeable lithium–air batteries,” *Materials Today Advances*, vol. 4, p. 100 031, 2019, ISSN: 2590-0498. DOI: https://doi.org/10.1016/j.mtadv.2019.100031. [Online]. Available: https://www.sciencedirect.com/science/article/pii/S2590049819301055.

[39] [Online]. Available: https://www.aircraftsystemstech.com/p/electric-and-starter-generator-starting.html.

[40] A. Babin, R. Polyakov, L. Savin, and V. Tyurin, “Statistical analysis of turbo generator sets failure causes,” *Vibroengineering PROCEDIA*, vol. 31, pp. 129–133, May 2020. DOI: 10.21595/vp.2020.21331.

[41] C. Emissions, A. Board, D. Sciences, and N. Medicine, *Commercial aircraft propulsion and energy systems research: Reducing global carbon emissions*. Sep. 2016, ch. 2: Aircraft Propulsion Integration, pp. 1–122. DOI: 10.17226/23490.

[42] *Reliability Prediction of Electronic Equipment: Military Handbook*$_1$991. U.S. Dept. of Defense, 1991, vol. MIL-HDBK-217F.

[43] *Nonelectronic Parts Reliability Data 2016*$_2$015. Quanterion Solutions Incorporated, 2015.

[44] Z. Jia, Z. Liu, C.-M. Vong, and X. Liu, “Real-time response-based fault analysis and prognostics techniques of nonisolated dc–dc converters,” *IEEE Access*, vol. 7, pp. 67 996–68 009, 2019. DOI: 10.1109/ACCESS.2019.2901390.

[45] K. Millar, K. Fong, R. P. Alzola, P. J. Norman, and G. M. Burt, “System wide reliability impact of power converters in more-electric aircraft applications,” Cited by: 0; All Open Access, Green Open Access, 2023. DOI: 10.4271/2023-01-0991. [Online]. Available: https://www.scopus.com/inward/record.uri?eid=2-s2.0-85151387998&doi=10.4271%2f2023-01-0991&partnerID=40&md5=048ad97a9fde33bb1c717c620788d6c5.

[46] K. Xu, N. Xie, C. Wang, and X. Shi, “Modeling and simulation of variable speed variable frequency electrical power system in more electric aircraft,” *The Open Electrical Electronic Engineering Journal*, vol. 11, pp. 87–98, Apr. 2017. DOI: 10.2174/1874129001711010087.

[47] M. Z. Khaneghah, M. Alzayed, and H. Chaoui, “Fault detection and diagnosis of the electric motor drive and battery system of electric vehicles,” *Machines*, vol. 11, no. 7, 2023, ISSN: 2075-1702. DOI: 10.3390/machines11070713. [Online]. Available: https://www.mdpi.com/2075-1702/11/7/713.

[48] S. Lin, Y. Lei, J. Liu, and L. Liu, “Analysis and prevention of commutation failure caused by hvdc rectifier ac faults,” *IET Generation, Transmission & Distribution*, vol. 16, no. 7, pp. 1416–1424, 2022. DOI: https://doi.org/10.1049/gtd2.12377. eprint: https://ietresearch.onlinelibrary.wiley.com/doi/pdf/10.1049/gtd2.12377. [Online]. Available: https://ietresearch.onlinelibrary.wiley.com/doi/abs/10.1049/gtd2.12377.

[49] Y. J. Bao, K. W. E. Cheng, K. Ding, and D. H. Wang, “The study on the busbar system and its fault analysis,” in *2013 5th International Conference on Power Electronics Systems and Applications(PESA)*, 2013, pp. 1–7. DOI: 10.1109/PESA.2013.6828246.

[50] G. Gautam, M. Zhang, W. Yuan, G. Burt, and D. Malkin, “Fault tolerant superconducting busbar with reduced self-field effect on critical current design for all electric aircraft,” *IEEE Transactions on Applied Superconductivity*, vol. 34, no. 3, pp. 1–5, 2024, Cited by: 1. DOI: 10.1109/TASC.2024.3351610. [Online]. Available: https://www.scopus.com/inward/record.uri?eid=2-s2.0-85182347478&doi=10.1109%2fTASC.2024.3351610&partnerID=40&md5=246fccd258912c9082b1a32bf2e07604.

[51] J. Brombach, A. Lucken, B. Nya, M. Johannsen, and D. Schulz, “Comparison of different electrical hvdc-architectures for aircraft application,” Cited by: 70, 2012. DOI: 10.1109/ESARS.2012.6387380. [Online]. Available: https://www.scopus.com/inward/record.uri?eid=2-s2.0-84873428223&doi=10.1109%2fESARS.2012.6387380&partnerID=40&md5=97d0d57416669b91834e6b657b930a2a.

[52] S. D. et al., “Module development of a high-power-density high-efficiency cryogenic solid-state circuit breaker for electrified aircraft propulsion,” *University of Tennessee*, 2023. [Online]. Available: https://curent.utk.edu/Module_Development_of_a_High-Power-Density_High-Efficiency_Cryogenic_Solid-State_Circuit_Breaker.

[53] J. M. Cardó, “Design and simulation of a microgrid used in more electric aircraft,” Ph.D. dissertation, Universitat Politècnica de Catalunya, 2023. [Online]. Available: https://upcommons.upc.edu/Design_and_Simulation_of_a_Microgrid_used_in_a_More_Electric_Aircraft.

[54] B. Kasztenny and M. J. Thompson, “Breaker failure protection — standalone or integrated with zone protection relays?” In *2011 64th Annual Conference for Protective Relay Engineers*, 2011, pp. 385–395. DOI: 10.1109/CPRE.2011.6035639.

[55] Y. Wang, C. Zhang, C. Zhang, and L. Li, “Review of high-power-density and fault-tolerant design of propulsion motors for electric aircraft,” *Energies*, vol. 16, no. 19, 2023, ISSN: 1996-1073. DOI: 10.3390/en16197015. [Online]. Available: https://www.mdpi.com/1996-1073/16/19/7015.

[56] Q. Tang, X. Shu, G. Zhu, J. Wang, and H. Yang, “Reliability study of bev powertrain system and its components—a case study,” *Processes*, vol. 9, p. 762, Apr. 2021. DOI: 10.3390/pr9050762.

[57] W. Wang, J. Loman, R. Arno, P. Vassiliou, E. Furlong, and D. Ogden, “Reliability block diagram simulation techniques applied to the ieee std. 493 standard network,” *Industry Applications, IEEE Transactions on*, vol. 40, pp. 887–895, Jun. 2004. DOI: 10.1109/TIA.2004.827805.

[58] R. D. Telford, S. J. Galloway, and G. M. Burt, “Evaluating the reliability availability of more-electric aircraft power systems,” in *2012 47th International Universities Power Engineering Conference (UPEC)*, 2012, pp. 1–6. DOI: 10.1109/UPEC.2012.6398542.

[59] M. S. Saglimbene, “Reliability analysis techniques: How they relate to aircraft certification,” in *2009 Annual Reliability and Maintainability Symposium*, 2009, pp. 218–222. DOI: 10.1109/RAMS.2009.4914678.

A

Graphs

A.1. Temperature comparison

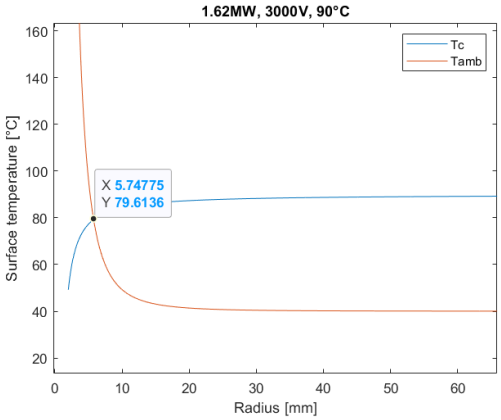

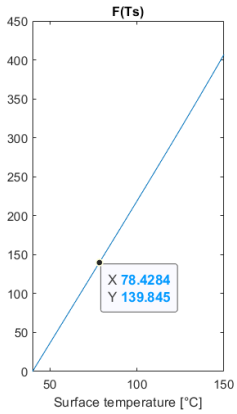

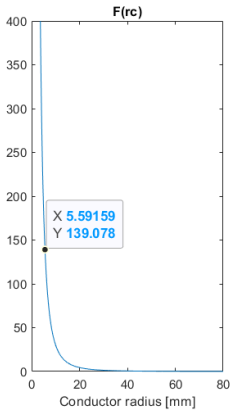

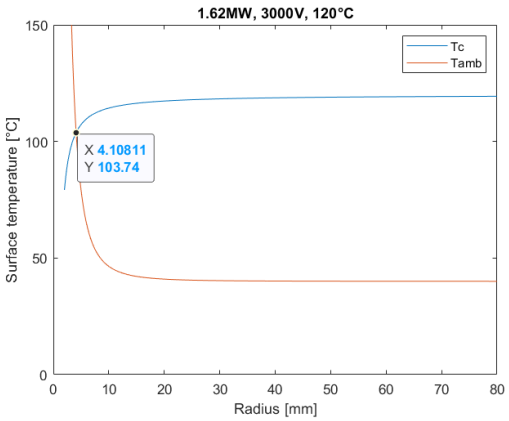

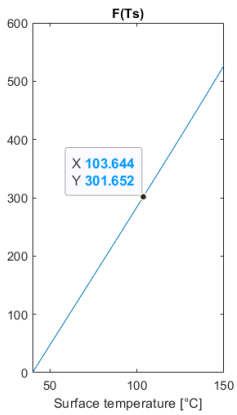

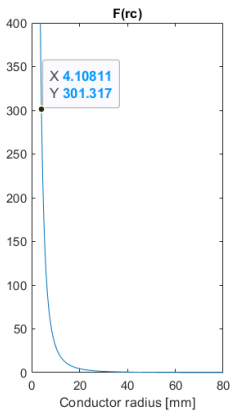

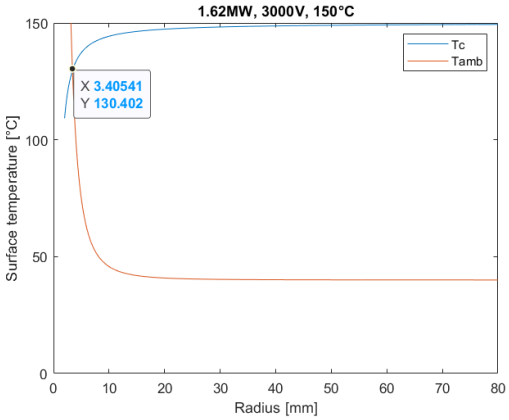

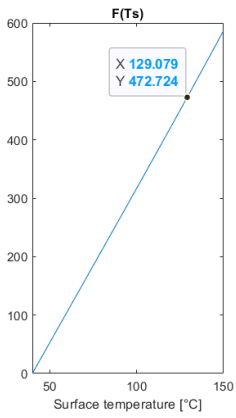

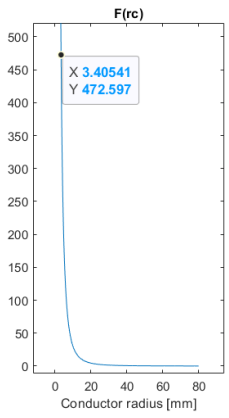

A.2. Power comparison

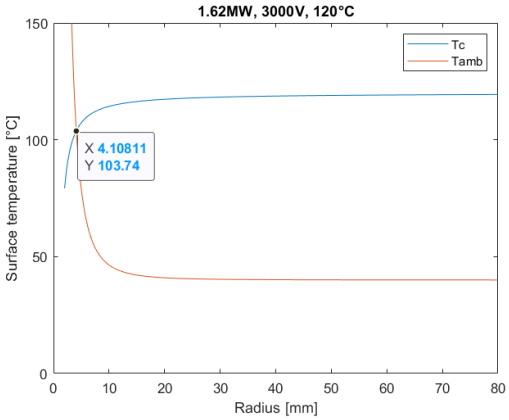

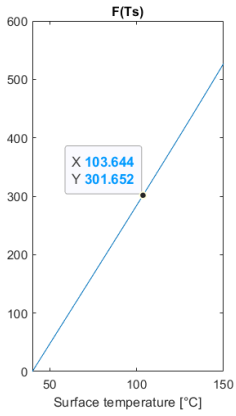

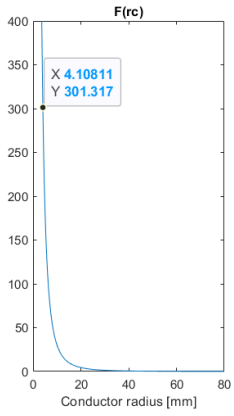

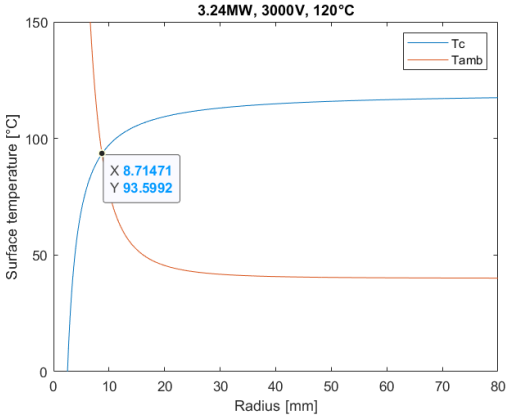

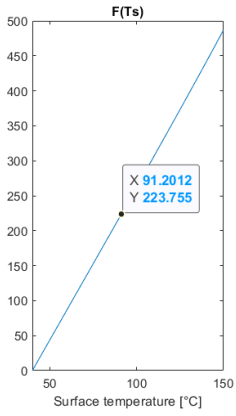

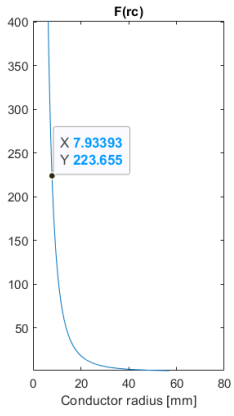

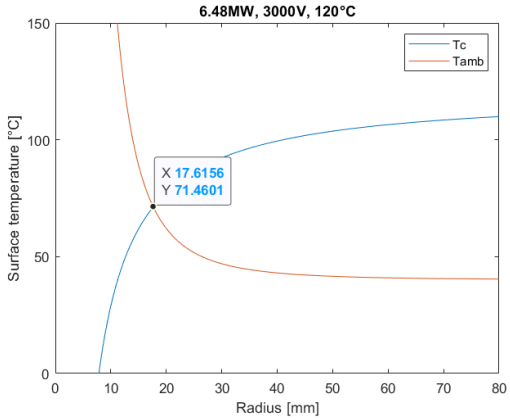
6.48MW, 3000V, 120°C
Tc
Tamb
X 17.6156
Y 71.4601
Surface temperature [°C]
Radius [mm]

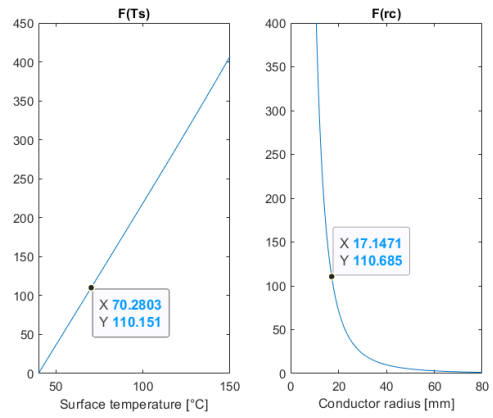
F(Ts)
X 70.2803
Y 110.151
Surface temperature [°C]
F(rc)
X 17.1471
Y 110.685
Conductor radius [mm]

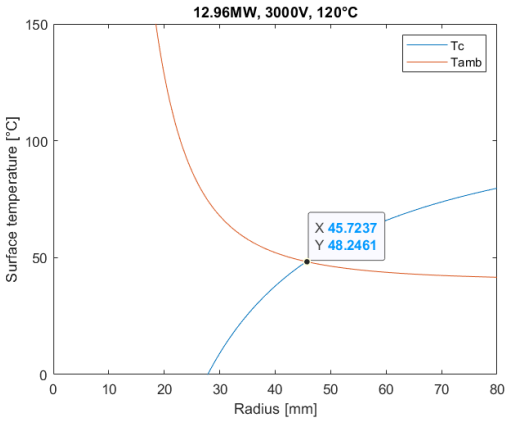
12.96MW, 3000V, 120°C
Tc
Tamb
X 45.7237
Y 48.2461
Surface temperature [°C]
Radius [mm]

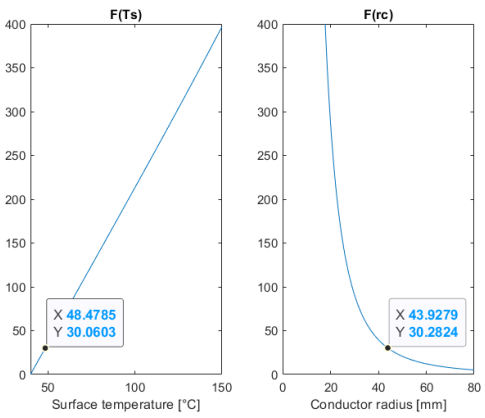
F(Ts)
X 48.4785
Y 30.0603
Surface temperature [°C]
F(rc)
X 43.9279
Y 30.2824
Conductor radius [mm]

A.3. Voltage comparison

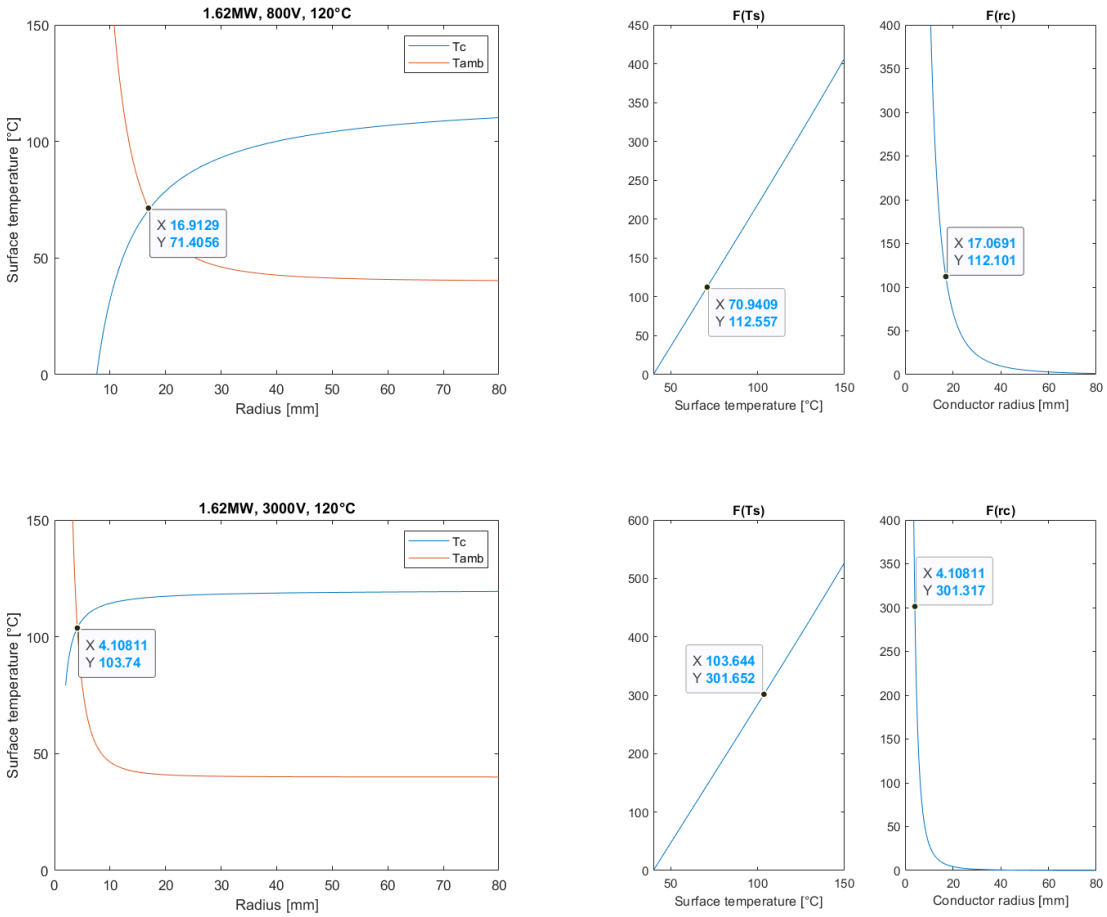

A.4. h-Ts comparison

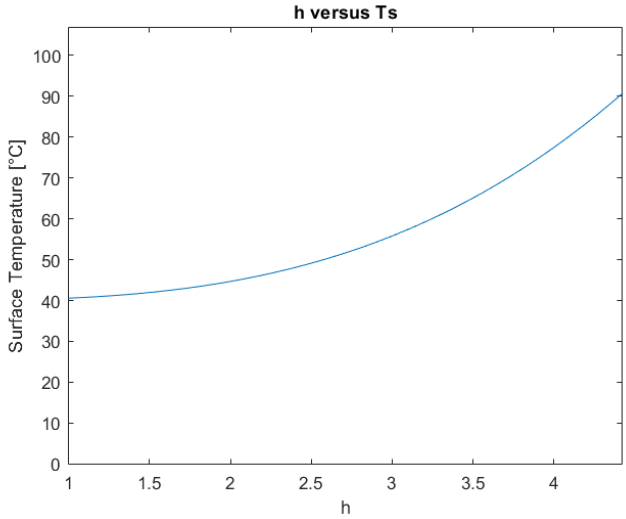

Figure A.1: h/Ts comparison

B

FMEA

B.1. Interview with Dr. Ir. Maurice Hoogreef

Effect of different failure modes in aircraft and their severity on different stages of flight
Date: 14th of May, 2024
Conducted by: Floor Walterbos & Tim ter Horst

1. **For motor failure, if one engine fails, how severe is this and how differs this in the different stages of flight (take-off, cruising & landing)?**

   In general, motor failure is most critical during the take-off phase. This is where you need the most power, especially after reaching decision speed ("V1"). According to regulations, aircraft motors are designed to be able to take-off even if one engine fails (in 2-motor aircraft) after reaching 'take-off safety speed' ("V2"), under a specific minimum 'climb angle'. Therefore, although motor failure in take-off phase is very critical, the aircraft should be able to take off to a certain extent and be brought back to the ground safely. For an 8-motor aircraft it is less critical if 1 engine fails since the power is distributed and therefore it is relatively easier for the other motors to take over. In the cruising phase engine failure is not at all very critical. Aircraft are designed to be able to at least safely glide to a landing in case of complete propulsive failure. Most aircraft are designed to be able to glide for about 20-30 minutes without direct propulsive drive. However, a cascaded motor failure can mean that you have to make an emergency landing and therefore can have influence on the mission but in itself a single engine failure will not have a severe impact on cruising. During landing it is more important, since you have to be able to correct for external conditions and there is less margin for error. It is less vital than during take-off but more critical than cruising. In your case, since the propeller is directly attached to the wing you inherently generate more lift so the other motors are able to reach the required lift more easily anyways. However, this also generates more resistance on the wing which could make take-off more difficult as well, but on the other hand be more beneficial for landing.

2. **What do you think is the most critical failure in our aircraft and why?**

   In the case of the battery-electric aircraft you are working with, I would argue the batteries (and failure in these) are more important. This is because there is less back-up for these and not easily recovered. I would say that the supply of power in that sense is more important for the system than the drive. Furthermore, the batteries power the secondary systems in the aircraft as well, such as avionics and control systems, and failures in those mean that you also lose your steering. Again, this is most critical in the take-off phase for the same reason as mentioned above.

3. **In normal aircraft, how is engine failure managed?**

   It depends on the phase of the flight, but normally an aircraft is designed to be able to handle a single engine failure due to oversizing of the motors. In the take-off it depends whether decision speed was already reached, but the aircraft is designed to be able to take-off after V1 anyways. During cruising it again depends on the severity of the engine failure and its nature. If it is a

temporary failure it is not really a problem except when it is in take-off phase of flight, where naturally you need all the power and a small change in propulsive drive can make a large difference. During cruising it is no problem to lose motor drive temporarily, and permanent engine failure is handled like I described before; depending on the severity an aircraft is able to safely cruise to an emergency landing. Only when there is cascaded failure the safety of the emergency landing itself will fall subject to more danger.

4. **How are temporary faults in the propulsion system managed, and how long does it take before such a fault becomes critical?**

   Like I mentioned before, temporary faults in the propulsive drivetrain of the aircraft are very critical during the take-off phase. If an engine fails it immediately results in less drive where it is very much needed during the take-off, especially before reaching decision speed. Therefore a temporary fault resulting in a loss of propulsion in the take-off phase is as severe as a permanent fault. During cruising, temporary faults (especially where the fault can be resolved through re-routing of power or temporarily shutting off parts of a system and turning it on again) are not at all critical. During landing this is more severe, especially in your case since your aircraft will be far heavier during this stage of flight as the battery packs will not lose weight and your aircraft's propulsive system will demand more power.

5. **In what stages of flight do you think faults are the most critical?**

   In general, failures are the most critical during take-off since there is a small time window where the demand on the propulsive system is heaviest and there is little-to no room for error. Furthermore, the decision speed plays an important role; after reaching this speed the pilot must make a decision whether to take-off or to abort the take-off. Therefore, if a fault occurs after decision 'take-off' is made, it inherently poses a far higher safety risk. Like I mentioned earlier, during cruising faults are in general less critical since by design an aircraft has better safety and ability to descend and safely make an emergency landing. Naturally, this also depends on the specific location of the aircraft; if it is above sea/water or in the mountains the severity of the fault clearly increases. During the landing-phase, depending on the location of the fault, the severity should be considered higher due to the lower speed and heavier weight of the batteries, but still quite a bit more manageable than for take-off.

6. **How severe do you think a fault in a reserve generator can be?**

   Everything in an aircraft has either double or triple layers of back-up systems to make sure nominal operation can continue under fault conditions. Therefore, a fault in a back-up system, although it does not directly impact the flight status, could have a severe impact in case of failures in your primary system. Specifically for your case it could be catastrophic in some ways because if there are other faults following after the generator fails there is no back-up anymore and the aircraft loses all drive. In your case, since the generator has no back-up itself it could be a serious issue. Furthermore, in normal aircraft the back-up system also has an Auxiliary Power Unit (APU) that supplies power to all secondary systems. However, in your case the back-up for all power systems are the reserve generators; meaning that if power is lost in your aircraft and you do not have a working generator not only can you not provide propulsive power but you also lose all your steering, navigation and communication tools.

7. **How strict are the laws and regulations regarding faults/safety in an aircraft?**

   There are a set of rules, called the CS-25, which specify certain properties an aircraft needs to have in order for it to be considered 'safe'. An example is the specified climb angle an aircraft needs to be able to attain after 1 engine failure I talked about before. Furthermore, it specifies a benchmark set of requirements for the aircraft. However, these are actually quite general and subject to 'safe' in general. If you can demonstrate, based on valid parameters, that your aircraft is safe and reliable enough it should pass the CS-25 requirements.

8. **How important is propulsion during the landing phase and how significant is the difference in our battery-electric AEA compared to a regular aircraft?**

   Normally, like I mentioned earlier, the propulsion system plays quite an important part during the landing phase. In order to keep a constant speed and steady, properly controlled, descent the

propulsion system is very important. Moreover, there is little room and margin for error in this phase once the final part of the descent has been started (starting from about 1500m altitude). If you suddenly lose propulsion in this part it is very hard for the pilot to correct for this failure due to the significantly lower speed and low altitude. This, in combination with the fact that your aircraft is heavier in this stage of the flight anyways due to the batteries, makes that a failure in the propulsion system in this part of the flight is quite significant.

9. **In the case of a go-around (=doorstart), how important are the engines/backup generators and how often does this occur?**

   In case of a go-around the aircraft needs to immediately switch back to full power in order for it to successfully make a climb again. The engines need to be able to do this as fast as possible, since the aircraft needs to generate enough lift/get back in the air before the runway ends. In the case of your aircraft this should not be a problem since power is transferred immediately in an electric drivetrain, while for gas-powered engines this normally takes about 1-2 seconds. However, a failure in the motors in this case would be very severe since it could mean the go-around is unsuccessful and the plane is not able to successfully re-enter into climb. Furthermore, the back-up system is quite important here for the same reason I mentioned already. And once again, since your aircraft did not lose any weight during flight (it is battery-powered), it will require the same power as it did for regular take-off. I am not really sure how often it precisely occurs, for this you should research a bit.

B.2. FMEA complete table

	Process Step/Input	Potential Failure Mode	Potential Failure Effects	SEVERITY - TAKE OFF (1 - 10)	SEVERITY - CRUISING (1 - 10)	SEVERITY - LANDING (1 - 10)	SEVERITY - AVERAGE (1 - 10)	Potential Causes	OCCURRENCE (1 - 10)	Current Controls	DETECTION (1 - 10)	SEVERITY (1 - 10)	OCCURRENCE (1 - 10)	DETECTION (1 - 10)	RPN
	What is the process step, change or feature under investigation?	In what ways could the step, change or feature go wrong?	What is the impact on the customer if this failure is not prevented or corrected?					What causes the step, change or feature to go wrong? (how could it occur?)		What controls exist that either prevent or detect the failure?					
1	Batteries/EEU's	Battery failure: degradation of performance/'wearout'	Less energy available for system, deg > 10%.	2	2	2	2,0	Overusage, usage of time.	3	Battery sensor to check performance, output power sensor	n.a.	2,0	3	n.a.	6,0
2	Batteries/EEU's	Battery failure: temporary loss of supply	Loss of power source, possibility of significant loss of propulsion	9	5	6	6,7	Environmental or operation conditions, such as temperature fluctuations or partial blockages of the air cathode or partial discharge	3	Measure power, voltage or current values on the grid or at the converter.	n.a.	6,7	3	n.a.	20,0
3	Batteries/EEU's	Battery failure: permanent loss of battery	Loss of power source, possibility of significant loss of propulsion	9	7	8	8,0	Thermal runaway, caused by internal/external short, overcharging	5	Measure power, voltage or current values on the grid or at the converter.	n.a.	8,0	5	n.a.	40,0
4	Generator	Failure to start (FTS) generator in case of motor failure (temporary generator failure)	No backup for motors, potential of critical failure	8	3	6	5,7	Ignition/start failure, failure in fuel supply resulting in no fuel to generator, failure in control system operating the generator	3	Rigorous testing of (sub)systems surrounding generator	n.a.	5,7	3	n.a.	17,0
5	Generator	Generator broken (permanent generator failure)	No backup for motors, potential critical failure in case of cascaded motor failure	9	5	6	6,7	Short circuit in stator core, fault in windings, insulation faults of windigs	3	Measure output power of generator	n.a.	6,7	3	n.a.	20,0
7	Power Converter - Battery (DC-DC/Converter)	Converter permanent fault	Battery permanent disconnected from grid, loss of power source	9	7	8	8,0	Transistor short circuit	4	Measure output power of converter	n.a.	8,0	4	n.a.	32,0
9	Power Converter - Motor (DC-AC/Inverter)	Inverter permanent fault	Loss of engine/part of propulsion	9	5	7	7,0	Short/open circuit in the switches	4	Measure input power to motor	n.a.	7,0	4	n.a.	28,0
11	Power Converter - Generator (AC-DC/Rectifier)	Rectifier permanent fault	No backup for motors, potential critical failure in case of cascaded motor failure	9	5	6	6,7	Commutation failure	4	Use thyristor or IGBT to measure power	n.a.	6,7	4	n.a.	26,7
13	Grid/Busbar (Motors)	Busbar permanent disconnect	Partial loss of power to motors	9	5	6	6,7	Environmental issues such as humidity, construction assembly issues, sealing issues	2	Humidity/water sensors, maintenance	n.a.	6,7	2	n.a.	13,3
15	Grid/Generator Line	Generator line failure/disconnect	No backup for motors, potential critical failure in case of cascaded motor	9	5	6	6,7	Short circuit, failure due to humidity, wearout, additional factors	3	Proper maintananance, sensors on the line or after the line	n.a.	6,7	3	n.a.	20,0
17	Grid/Cables (Battery connections)	Line failure: permanent disconnect	Loss of power source, possibility of significant loss of propulsion	9	7	8	8,0	Short circuit, failure due to humidity, wearout, additional factors	3	Proper maintananance, sensors on the line or after the line	n.a.	8,0	3	n.a.	24,0
18	Grid/Cables (Motor connections)	Line failure: permanent disconnect	Loss of engine/part of propulsion	9	5	7	7,0	Short circuit, failure due to humidity, wearout, additional factors	3	Proper maintananance, sensors on the line or after the line	n.a.	7,0	3	n.a.	21,0
19	Circuit Breaker	Failure to open in case of fault	Possibility of short circuit in plane, significant risk of overdischarging of batteries	9	9	9	9,0	Incorrect detection of fault current/voltage, incorrect function of subcomponents	3	Proper testing of sensing part of CB at overrated values	n.a.	9,0	3	n.a.	27,0
20	Circuit Breaker	Circuit breaker breaks while trying to disconnect	Permanent line failure	8	5	6	6,3	Fault has higher ratings than breaker's limitations	3	In-depth study of potential failures in system CB is placed in to properly define	n.a.	6,3	3	n.a.	19,0
21	Circuit Breaker	Circuit breaker does not close again after opening	Fault resolved but still temporary line disconnect, thus temporary loss of	8	4	6	6,0	Component failure, fault not handled properly, control system failure	3	Control system testing and backup, improved sensing	n.a.	6,0	3	n.a.	18,0
22	Motor	Temporary engine failure	Loss of thrust and propulsion, and therefore flight abilities	9	2	6	5,7	Overheating	3	Measure output RPM of propellor, visual inspection, proper testing pre-flight	n.a.	5,7	3	n.a.	17,0
23	Motor	Permanent engine failure	(partial) loss of propulsive power of aircraft	9	5	7	7,0	Electrical faults such as: inter-turn short, open/short phase faults, demagnitisation	3	Measure output RPM of propellor, visual inspection, proper testing pre-flight	n.a.	7,0	3	n.a.	21,0
24	Motor	Partial loss of propoulsion	Less output thrust produced by motor than needed	7	3	6	5,3	Worn bearings/poor contact of motor connections, reduced winding isolation	3	Timely replacement of subcomponents of motor	n.a.	5,3	3	n.a.	16,0
			Sum of values	200	113	151	154,7		65		n.a.	154,7	65	n.a.	426,3

C

Python codes

C.1. Pareto Chart Generation Script

```python
import pandas as pd
import matplotlib.pyplot as plt

# Manually creating the data based on the provided image
data = {
    'Failure Mode': [
        "Batteries/EEU's (1)", "Batteries/EEU's (2)", "Batteries/EEU's (3)",
        "Generator (4)", "Generator (5)", "Power Converter - DC-DC/Converter (6)",
        "Power Converter - DC-AC/Inverter (7)", "Power Converter - AC-DC/Rectifier (8)",
        "Busbar (Batteries) (9)", "Busbar (Motors) (10)", "Busbar (Generator) (11)",
        "Transmission line (Generator) (12)", "Transmission line (Interconnection) (13)",
        "Transmission line (Battery) (14)", "Transmission line (Motor) (15)",
        "Circuit Breaker (16)", "Circuit Breaker (17)", "Circuit Breaker (18)",
        "Motor (19)", "Motor (20)", "Motor (21)"
    ],
    'RPN': [
        6.0, 20.0, 40.0, 17.0, 20.0, 32.0, 28.0, 26.7, 16.0, 13.3, 13.3,
        20.0, 11.0, 24.0, 21.0, 27.0, 19.0, 18.0, 17.0, 21.0, 16.0
    ]
}

# Creating the DataFrame
pareto_data = pd.DataFrame(data)

# Calculate cumulative RPN and percentage
pareto_data = pareto_data.sort_values(by='RPN', ascending=False).reset_index(drop=True)
pareto_data['Cumulative RPN'] = pareto_data['RPN'].cumsum()
total_rpn = pareto_data['RPN'].sum()
pareto_data['Cumulative Percentage'] = pareto_data['Cumulative RPN'] / total_rpn * 100

# Creating the Pareto chart with both bar and cumulative line
fig, ax1 = plt.subplots(figsize=(14, 8))

# Bar chart for RPN values
bars = ax1.bar(pareto_data['Failure Mode'], pareto_data['RPN'], color='blue')
ax1.set_xlabel('Failure Mode')
ax1.set_ylabel('RPN', color='b')
ax1.tick_params(axis='y', labelcolor='b')
plt.xticks(rotation=90, ha='right')

# Line chart for cumulative percentage
ax2 = ax1.twinx()
ax2.plot(pareto_data['Failure Mode'], pareto_data['Cumulative Percentage'], color='r', marker
    ='o')
ax2.set_ylabel('Cumulative Percentage', color='r')
ax2.tick_params(axis='y', labelcolor='r')

plt.title('Pareto Chart of Failure Modes by RPN with Cumulative Percentage')
```

```
plt.tight_layout()

# Display the chart
plt.show()
```

Listing C.1: Python script to generate Pareto Chart

C.2. Python structural code 8 batteries

```
# -*- coding: utf-8 -*-

import math
import numpy as np
import matplotlib.pyplot as plt
import csv

#%% Functions
def masscalculation(mass, bussesinfo, cablesinfo):
    summation = list(cablesinfo[:,2])
    sumcables = [float(ele) for ele in summation]
    lengthGencab = 2 * math.dist(bussesinfo['busbatLeft'][3], Generators['Gen1'])*1.2
    lencables = sum(sumcables)*Polar + lengthGencab*Polar
    summation = list(cablesinfo[:,3])
    sumcables = [float(ele) for ele in summation]
    weightcables = sum(sumcables)*Polar + lengthGencab*CableWeight['6.48MW']*Polar
    i = 0
    summation = list(businfo.values())
    sumbusses = []
    for i in range(0,len(bussesinfo)):
        sumbusses.append(summation[i][4])
    NumberCB = 46
    massPMAD = {'Cables': weightcables, 'Busses': sum(sumbusses), 'Circuit Breakers': (
    NumberCB*mass['CircuitBreaker'])}
    # Calculate the total CB weight
    return massPMAD, lencables/Polar

# This function returns a matrix of all cables going from its items to the busses it is
    connected to
def cablesitem(itembusses,items,allbusses,redundancy):
    cablesarray = np.chararray([len(items)*redundancy,4],itemsize=30)
    itemkeys = list(items)
    itembuskeys = list(itembusses)
    i=j=index =0
    density = CableWeight['1.62MW']
    for i in range(0,len(items)):
        for j in range(0,len(itembusses)):
            if itemkeys[i] in itembusses[itembuskeys[j]]:
                cable = itemkeys[i] + ' to ' + itembuskeys[j]
                distance = math.dist(items[itemkeys[i]],allbusses[itembuskeys[j]])
                length = abs(items[itemkeys[i]][0]-allbusses[itembuskeys[j]][0]) + abs(items[
    itemkeys[i]][1]-allbusses[itembuskeys[j]][1])
                cablesarray[index][0] = cable
                cablesarray[index][1] = distance
                cablesarray[index][2] = length*1.2
                cablesarray[index][3] = length*1.2*density
                index+=1
    return cablesarray

# This function produces the list of cables from the main bus with its distances and lengths
def cablesmainbus(busmain,busses):
    total = len(busmain)
    items = list(busmain.values())
    lengthtotal = 0
    for x in range(0,total):
        lengthtotal += len(items[x])
    maincables = np.chararray([lengthtotal,4],itemsize=30)
    mainbuskeys = list(busmain)
    i=j=index=0
    for i in range(0,len(busmain)):
```

```
        connections = busmain[mainbuskeys[i]]
        for j in range(0,len(connections)):
            if ('motRight' in connections[j]) or ('motLeft' in connections[j]):
                density = CableWeight['6.48MW']
            else:
                density = CableWeight['12.96MW']
            cable = mainbuskeys[i] + ' to ' + connections[j]
            distance = math.dist(busses[mainbuskeys[i]],busses[connections[j]])
            maincables[index][0] = cable
            maincables[index][1] = distance
            length = abs(busses[mainbuskeys[i]][0]-busses[connections[j]][0]) + abs(busses[
    mainbuskeys[i]][1]-busses[connections[j]][1])
            maincables[index][2] = length*1.2
            maincables[index][3] = length*1.2*density
            index+=1
        j=0
    return maincables

def getXY(array):
    X = []
    Y = []
    length=len(array)
    i = 0
    for i in range(0,length):
        X.append(array[i][0])
        Y.append(array[i][1])
    return X,Y

# This function calculates the necessary weight and length of the bus
def businfo(busses, cable):
    busseskeys = list(busses)
    buscalc = {}
    space = 0.150
    CBsize = 0.2
    i=0
    for i in range(0,len(busses)):
        countout = np.char.count(cable,busseskeys[i])
        total = sum(countout)[0]
        Xcor = busses[busseskeys[i]][0]
        if ('motLeft' in busseskeys[i]) or ('motLeft' in busseskeys[i]):
            radius = Cableradius['6.48MW']
            density = CableWeight['6.48MW']
            buslines = 1
        elif 'bat' in busseskeys[i]:
            total += 2
            density = CableWeight['12.96MW']
            buslines = 2
        else:
            radius = Cableradius['12.96MW']
            density = CableWeight['12.96MW']
            buslines = 1
        length = total*CBsize + space*(total+1)
        weight = length*density*2.5*buslines
        location = [(Xcor - length/2), (Xcor+length/2)]
        buscalc[busseskeys[i]] = [total, length, location, busses[busseskeys[i]],weight]
    return buscalc

def systeminput(batteriesnum):
    #batbusnum = 2 #input("How many buss for the Batteries?")
    #MotorBusNumber = 4 #input("How many busses for the Motors?")
    if batteriesnum == 4:
        batteries = {'B1L': [-2.5,-2], 'B2L': [-1.5,-2], 'B2R': [1.5,-2], 'B1R': [2.5, -2]}
    else:
        batteries = {'B1L': [-6.5,-2], 'B2L': [-5.5,-2], 'B3L': [-2.5,-1.5], 'B4L':
    [-1.5,-1.5], 'B4R': [1.5,-1.5], 'B3R': [2.5,-1.5], 'B2R': [5.5,-2], 'B1R': [6.5,-2]}
    generators = {'Gen1': [1, -12], 'Gen2' : [-1, -12]}
    motors = {'M1L': [-16,-1], 'M2L': [-12,-0.5], 'M3L': [-8,0], 'M4L': [-4,0.5], 'M4R':
    [4,0.5], 'M3R': [8,0], 'M2R': [12,-0.5], 'M1R': [16,-1]}
    busses = {'busbatLeft': [-4,-1.5], 'busbatRight': [4,-1.5],
              'busmotLeft': [-14,-1.25], 'busmotMid': [0,-0.5], 'busmotRight': [14,-1.25],
              'Hleft': [-10, -0.75], 'Hright': [10,-0.75]}
```

```
    batterybusses = {'busbatLeft': ['B1L', 'B2L', 'B3L', 'B4L'], 'busbatRight': ['B2R', 'B1R', 'B3R', 'B4R']}
    motorbusses = {'busmotLeft': ['M1L', 'M4R', 'M3R', 'M2L'], 'busmotMid': ['M1L', 'M4R', 'M3R', 'M2L', 'M4L', 'M1R', 'M3L', 'M2R'], 'busmotRight': ['M4L', 'M1R', 'M3L', 'M2R']}
    mainbus = {'Hleft': ['busmotLeft', 'busmotMid', 'busbatLeft'], 'Hright': ['busmotMid', 'busmotRight', 'busbatRight']}
    return batteries, generators, motors, busses, batterybusses, motorbusses, mainbus

def exportList(variable,name, fields):
    # Example.csv gets created in the current working directory
    filename = name+'.csv'
    with open(filename, 'w', newline = '') as csvfile:
        # creating a csv dict writer object
        writer = csv.writer(csvfile)
        # writing headers (field names)
        writer.writerow(fields)
        # writing data rows
        writer.writerows(variable)
    return

def exportDict(variable,name, fields):
    # Example.csv gets created in the current working directory
    filename = name+'.csv'
    with open(filename, 'w', newline = '') as f:
        # creating a csv dict writer object
        writer = csv.DictWriter(f, fieldnames=fields)
        # writing headers (field names)
        writer.writeheader()
        # writing data rows
        writer.writerow(variable)
    return
#%% Global variables and locations
masses = {'TotalBudget': 5408.6, 'Generator': 563.3, 'CircuitBreaker': 15, 'TMS': 1547.9, 'MotorandInverter': 326.6, 'Converter': 43.2}
CableWeight = {'1.62MW': 0.56, '3.24MW': 1.17, '6.48MW': 3.67, '12.96MW': 20.06}
       #kg/m
Cableradius = {'1.62MW': 5.53e-3, '3.24MW': 11.94e-3, '6.48MW': 21.07e-3, '12.96MW': 48.94e-3} # [m]
Polar = 2

NumBatteries = 8 #input("How many batteries?")
Batteries, Generators, Motors, Busses, Batterybusses, Motorbusses, mainbusses = systeminput(NumBatteries)

busBatLocX,busBatLocY = getXY([Busses['busbatLeft'],Busses['busbatRight']])
busMotLocX,busMotLocY = getXY([Busses['busmotLeft'],Busses['busmotMid'],Busses['busmotRight']])

#%% Cable, bus info

cablesmain = cablesmainbus(mainbusses, Busses)

cablesBat = cablesitem(Batterybusses,Batteries,Busses,1)
cablesMot = cablesitem(Motorbusses, Motors, Busses,2)
mdim = len(cablesBat) + len(cablesMot) + len(cablesmain)
cables = np.chararray([mdim,4],itemsize=30)
cables[0:(len(cablesmain))][:] = cablesmain
cables[(len(cablesmain)):(len(cablesBat)+len(cablesmain))][:] = cablesBat
cables[(len(cablesmain)+len(cablesBat)):(mdim)][:] = cablesMot
cables = cables.decode()

BatteryLocations = list(Batteries.values())
MotorLocations = list(Motors.values())
GeneratorLocations = list(Generators.values())

businfo = businfo(Busses, cables)

#%% Mass calculations
MassPMAD,lengthcables = masscalculation(masses, businfo, cables)
MassElectrical = sum(MassPMAD.values())
MassTotal = sum(MassPMAD.values()) + masses['TMS']
```

```

#%% Export variables
exportList(list(cables), 'cables', ['Cable name', 'Distance', 'Length', 'Weight'])
exportList(list(businfo.values()), 'businfo', ['Cables', 'Length', 'Begin and End', 'Midpoint', 'Weight'])
exportDict(masses, 'masses', masses.keys())
exportDict(MassPMAD, 'PMAD', MassPMAD.keys())

#%% Plotting

plt.rcParams["figure.figsize"] = [7.00, 4]
plt.rcParams["figure.autolayout"] = True
im = plt.imread("Aircraft.png")
fig, System = plt.subplots()
im = System.imshow(im, extent=[-28.25, 27, -25, 17], alpha=0.7)
System = plt.scatter(getXY(BatteryLocations)[0],getXY(BatteryLocations)[1],marker='D',c='b')
System = plt.scatter(getXY(MotorLocations)[0],getXY(MotorLocations)[1],marker="2", c='k')
System = plt.scatter(busBatLocX,busBatLocY, marker='_', linewidth=3, c='b')
System = plt.scatter(busMotLocX, busMotLocY, marker='_', linewidth=3, c='k')
System = plt.scatter(getXY(GeneratorLocations)[0], getXY(GeneratorLocations)[1],marker='P', c='g')
System = plt.grid()
System = plt.xlabel("Lateral axis (Pitch) [m]")
System = plt.ylabel("Longitudinal axis (Roll) [m]")
System = plt.title("8 Battery Architecture")
```

Listing C.2: Python script calculate the mass of 8 batteries topology

C.3. Python structural code 4 batteries

```
# -*- coding: utf-8 -*-

import math
import numpy as np
import matplotlib.pyplot as plt
import csv

#%% Functions
def masscalculation(mass, bussesinfo, cablesinfo):
    summation = list(cablesinfo[:,2])
    sumcables = [float(ele) for ele in summation]
    lengthGencab = 2 * math.dist(bussesinfo['mainbus'][3], Generators['Gen1'])*1.2
    lencables = sum(sumcables)*Polar + lengthGencab*Polar
    summation = list(cablesinfo[:,3])
    sumcables = [float(ele) for ele in summation]
    weightcables = sum(sumcables)*Polar + lengthGencab*CableWeight['6.48MW']*Polar
    i = 0
    summation = list(businfo.values())
    sumbusses = []
    for i in range(0,len(bussesinfo)):
        sumbusses.append(summation[i][4])
    NumberCB = 41
    massPMAD = {'Cables': weightcables, 'Busses': sum(sumbusses), 'Circuit Breakers': (NumberCB*mass['CircuitBreaker'])}
    # Calculate the total CB weight
    return massPMAD, lencables/Polar

# This function returns a matrix of all cables going from its items to the busses it is connected to
def cablesitem(itembusses,items,allbusses,redundancy):
    cablesarray = np.chararray([len(items)*redundancy,4],itemsize=30)
    itemkeys = list(items)
    itembuskeys = list(itembusses)
    i=j=index =0
    if redundancy == 1:
        density = CableWeight['3.24MW']
    elif redundancy == 2:
        density = CableWeight['1.62MW']
    for i in range(0,len(items)):
```

```
        for j in range(0,len(itembusses)):
            if itemkeys[i] in itembusses[itembuskeys[j]]:
                cable = itemkeys[i] + ' to ' + itembuskeys[j]
                distance = math.dist(items[itemkeys[i]],allbusses[itembuskeys[j]])
                length = abs(items[itemkeys[i]][0]-allbusses[itembuskeys[j]][0]) + abs(items[
    itemkeys[i]][1]-allbusses[itembuskeys[j]][1])
                cablesarray[index][0] = cable
                cablesarray[index][1] = distance
                cablesarray[index][2] = length*1.2
                cablesarray[index][3] = length*1.2*density
                index+=1
    return cablesarray

# This function produces the list of cables from the main bus with its distances and lengths
def cablesmainbus(busmain,busses):
    total = len(busmain)
    items = list(busmain.values())
    lengthtotal = -4
    for x in range(0,total):
        lengthtotal += len(items[x])
    maincables = np.chararray([lengthtotal,4],itemsize=30)
    mainbuskeys = list(busmain)
    i=j=index=0
    for i in range(0,len(busmain)):
        connections = busmain[mainbuskeys[i]]
        for j in range(0,len(connections)):
            if ('B1' in connections[j]) or ('B2' in connections[j]):
                density = CableWeight['3.24MW']
            else:
                density = CableWeight['6.48MW']
                cable = mainbuskeys[i] + ' to ' + connections[j]
                distance = math.dist(busses[mainbuskeys[i]],busses[connections[j]])
                maincables[index][0] = cable
                maincables[index][1] = distance
                length = abs(busses[mainbuskeys[i]][0]-busses[connections[j]][0]) + abs(
    busses[mainbuskeys[i]][1]-busses[connections[j]][1])
                maincables[index][2] = length*1.2
                maincables[index][3] = length*1.2*density
                index+=1
        j=0
    return maincables

def getXY(array):
    X = []
    Y = []
    length=len(array)
    i = 0
    for i in range(0,length):
        X.append(array[i][0])
        Y.append(array[i][1])
    return X,Y

# This function calculates the necessary weight and length of the bus
def businfo(busses, cable):
    busseskeys = list(busses)
    buscalc = {}
    space = 0.150
    CBsize = 0.2
    i=0
    for i in range(0,len(busses)):
        countout = np.char.count(cable,busseskeys[i])
        total = sum(countout)[0]
        Xcor = busses[busseskeys[i]][0]
        if 'main' in busseskeys[i]:
            radius = Cableradius['12.96MW']
            density = CableWeight['12.96MW']
        else:
            radius = Cableradius['6.48MW']
            density = CableWeight['6.48MW']
        length = total*CBsize + space*(total+1)
        weight = length*density*2.5
```

```
        location = [(Xcor - length/2), (Xcor+length/2)]
        buscalc[busseskeys[i]] = [total, length, location, busses[busseskeys[i]],weight]
    return buscalc

def systeminput(batteriesnum):
    #batbusnum = 2 #input("How many buss for the Batteries?")
    #MotorBusNumber = 4 #input("How many busses for the Motors?")
    if batteriesnum == 4:
        batteries = {'B1L': [-2.5,-2], 'B2L': [-1.5,-2], 'B2R': [1.5,-2], 'B1R': [2.5, -2]}
    else:
        batteries = {'B1L': [-6.5,-2], 'B2L': [-5.5,-2], 'B3L': [-2.5,-1.5], 'B4L': [-1.5,-1.5], 'B4R': [1.5,-1.5], 'B3R': [2.5,-1.5], 'B2R': [5.5,-2], 'B1R': [6.5,-2]}
    generators = {'Gen1': [1, -12], 'Gen2' : [-1, -12]}
    motors = {'M1L': [-16,-1], 'M2L': [-12,-0.5], 'M3L': [-8,0], 'M4L': [-4,0.5], 'M4R': [4,0.5], 'M3R': [8,0], 'M2R': [12,-0.5], 'M1R': [16,-1]}
    busses = {'busmot1': [-14,-1], 'busmot2': [-6,-0.5], 'busmot3': [6,-0.5], 'busmot4': [14,-1],
              'mainbus': [0, -1], 'Hleft': [-10, -1], 'Hright': [10, -1]}
    #batterybusses = {'busbat1': ['B1L', 'B2L'], 'busbat2': ['B2R', 'B1R']}
    motorbusses = {'busmot1': ['M1L', 'M4R', 'M3R', 'M2L'], 'busmot2': ['M1L', 'M4R', 'M3R', 'M2L'], 'busmot3': ['M4L', 'M1R', 'M3L', 'M2R'], 'busmot4':['M4L', 'M1R', 'M3L', 'M2R']}
    mainbus = {'mainbus': ['B1L', 'B2L', 'B2R', 'B1R', 'Hleft', 'Hright'], 'Hleft': ['busmot1', 'busmot2'], 'Hright': ['busmot3', 'busmot4']}
    return batteries, generators, motors, busses, motorbusses, mainbus

def exportList(variable,name, fields):
    # Example.csv gets created in the current working directory
    filename = name+'.csv'
    with open(filename, 'w', newline = '') as csvfile:
        # creating a csv dict writer object
        writer = csv.writer(csvfile)
        # writing headers (field names)
        writer.writerow(fields)
        # writing data rows
        writer.writerows(variable)
    return

def exportDict(variable,name, fields):
    # Example.csv gets created in the current working directory
    filename = name+'.csv'
    with open(filename, 'w', newline = '') as f:
        # creating a csv dict writer object
        writer = csv.DictWriter(f, fieldnames=fields)
        # writing headers (field names)
        writer.writeheader()
        # writing data rows
        writer.writerow(variable)
    return
#%% Global variables and locations
masses = {'TotalBudget': 5408.6, 'Generator': 563.3, 'CircuitBreaker': 15, 'TMS': 1547.9, 'MotorandInverter': 326.6, 'Converter': 43.2}
CableWeight = {'1.62MW': 0.56, '3.24MW': 1.17, '6.48MW': 3.67, '12.96MW': 20.06}
        #kg/m
Cableradius = {'1.62MW': 5.53e-3, '3.24MW': 11.94e-3, '6.48MW': 21.07e-3, '12.96MW': 48.94e-3} # [m]
Polar = 2

NumBatteries = 4 #input("How many batteries?")
Batteries, Generators, Motors, Busses, Motorbusses, mainbusses = systeminput(NumBatteries)

#busBatLocX,busBatLocY = getXY([Busses['busbat1'],Busses['busbat2']])
busMotLocX,busMotLocY = getXY([Busses['busmot1'],Busses['busmot2'],Busses['busmot3'], Busses['busmot4']])

#%% Cable, bus info

cablesmain = cablesmainbus(mainbusses, Busses)

cablesBat = cablesitem(mainbusses,Batteries,Busses,1)
cablesMot = cablesitem(Motorbusses, Motors, Busses,2)
mdim = len(cablesBat) + len(cablesMot) + len(cablesmain)
```

```
cables = np.chararray([mdim,4],itemsize=30)
cables[0:(len(cablesmain))][:] = cablesmain
cables[(len(cablesmain)):(len(cablesBat)+len(cablesmain))][:] = cablesBat
cables[(len(cablesmain)+len(cablesBat)):(mdim)][:] = cablesMot
cables = cables.decode()

BatteryLocations = list(Batteries.values())
MotorLocations = list(Motors.values())
GeneratorLocations = list(Generators.values())

businfo = businfo(Busses, cables)

#%% Mass calculations
MassPMAD,lengthcables = masscalculation(masses, businfo, cables)
MassElectrical = sum(MassPMAD.values()) + NumBatteries * masses['Converter']
MassTotal = sum(MassPMAD.values()) + NumBatteries * masses['Converter'] + masses['TMS']

#%% Export variables
exportList(list(cables), 'cables', ['Cable name', 'Distance', 'Length', 'Weight'])
exportList(list(businfo.values()), 'businfo', ['Cables', 'Length', 'Begin and End', 'Midpoint
    ', 'Weight'])
exportDict(masses, 'masses', masses.keys())
exportDict(MassPMAD, 'PMAD', MassPMAD.keys())

#%% Plotting

plt.rcParams["figure.figsize"] = [7.00, 4]
plt.rcParams["figure.autolayout"] = True
im = plt.imread("Aircraft.png")
fig, System = plt.subplots()
im = System.imshow(im, extent=[-28.25, 27, -25, 17], alpha=0.7)
System = plt.scatter(getXY(BatteryLocations)[0],getXY(BatteryLocations)[1],marker='D',c='b')
System = plt.scatter(getXY(MotorLocations)[0],getXY(MotorLocations)[1],marker="2", c='k')
#System = plt.scatter(busBatLocX,busBatLocY, marker='_', linewidth=3, c='b')
System = plt.scatter(busMotLocX, busMotLocY, marker='_', linewidth=3, c='k')
System = plt.scatter(getXY(GeneratorLocations)[0], getXY(GeneratorLocations)[1],marker='P', c
    ='g')
System = plt.grid()
System = plt.scatter(0,-1,marker='o', c = 'r')
System = plt.xlabel("Lateral axis (Pitch) [m]")
System = plt.ylabel("Longitudinal axis (Roll) [m]")
System = plt.title("4 Battery Architecture")
```

Listing C.3: Python script to calculate mass of 4 batteries topology

D

Matlab code

```
    %% Fixed variables
rhoCopper = 8.88e3; %kg/m3
rhoAlum = 2.70e3; %kg/m3
rhoInsul = 2.2e3; %kg/m3
rhoPVC = 1.38e3; %kg/m3
rCopper = 1.72e-8; %Ohm-m
rAlum = 2.82e-8; %Ohm-m
sigmaCopper = 1/rCopper;
sigmaAlum = 33.3e7;
StefBoltz = 5.67e-8; %W m^-2 K^-4
length = 1; %m
TemperaturesCon = [150+273.15 120+273.15 90+273.15]; %Kelvin
TempAmb = 40+273.15; %Kelvin
ktef = 0.3; %W m^-1 K^-1, teflon
kpla = 0.12;  %W m^-1 K^-1, PVC

tisc = 0.6e-3; %m
tosc = 0.6e-3; %m
ts = 1e-3; %m
toj = 1e-3; %m
V = 3000;%linspace(100, 4000, 1000);
eps = 2; %Teflon permittivity
emi = 0.85; %Teflon emittivity
P = 1.62e6; %W
I = P./(V); %A
dv = 33e-6; %Not sure if correct
alpha = 300; %V, not sure if correct
radius = linspace(2e-3, 80e-3, 1000); %m

%% Calculations mass
MassConCop = rhoCopper .* length .* 3.14 .* radius.^2;
MassConAlu = rhoAlum .* length .* 3.14 .* radius.^2;

MassInsul = rhoInsul .* length .* 3.14 .* ((radius + tisc + ti + tosc).^2
    - (radius).^2);
MassSheet = rhoAlum .* length .* 3.14 .* ((radius + tisc + ti + tosc + ts)
    .^2 - (radius + tisc + ti + tosc).^2);
MassJacket = rhoPVC .* length .* 3.14 .* ((radius + tisc + ti + tosc + ts
    + toj).^2 - (radius + tisc + ti + tosc + ts).^2);
```

```
NoCond = MassInsul + MassSheet + MassJacket;
MassTotal = MassConAlu + MassInsul + MassSheet + MassJacket;

%% Insulator thickness
epsamplification = (3*eps)/(1+2*eps);
%ti = 0.009; %[m], radius.*exp(((3*eps)/(1+2*eps)*1e-12.*V)./radius - 1)
    +0.001;
ti = radius.*(exp((epsamplification.*V*dv)./(alpha.*radius))-1)+0.001; %m

%% h and Ts
%h = 4.18; %Not sure if correct
htest = linspace(1, 10, 100);
Tstest = TempAmb + 273.15*(htest.^3)
    ./(3.407424*10.^-8.*(9.81./(2.65*10^-5)^2)*0.98); %Beta = 1/273.15
%TsTest = TempAmb./(1-(htest.^3)./(3.407424*10.^-8.*(9.81./(2.65*10^-5)^2)
    *0.98)) - 273.15; %Beta = 1/Ts

Tsindex = find((Tstest>((60+273.15)-1))&(Tstest<((60+273.15)+1)));
Ts = Tstest(Tsindex);
h = htest(Tsindex);

%% Temperature
% calculation simplifications
Sub1 = Ts.*(h+emi.*StefBoltz.*Ts.^3);
Sub2 = TempAmb*(h+emi*StefBoltz*TempAmb^3);
radii_all = tosc + tisc + ts + ti + toj;
%radii_allcalc = tosc + tisc + ts + ticalc + toj;
lntef = log((radius+tisc+ti+tosc)./radius);
lnpla = log((radii_all+radius)./(radius+ti+tisc+tosc+ts));

% Calculations Temp
TsC = TemperaturesCon(2) - (I.^2)./((sigmaAlum*pi.*radius.^2).*(((2*pi*
    ktef)).*lntef + ((2*pi*kpla)).*lnpla));
%TsC2 = TempCon2 - (I.^2)./((sigmaAlum*pi.*radius.^2).*(((2*pi*ktef)).*
    lntef + ((2*pi*kpla)).*lnpla));
%TsC3 = TempCon3 - (I.^2)./((sigmaAlum*pi.*radius.^2).*(((2*pi*ktef)).*
    lntef + ((2*pi*kpla)).*lnpla));
TsA = (I.^2)./(sigmaAlum.*pi^2.*radius.^2.*h.*(radius+radii_all).*2)+
    TempAmb;
%TsA1 = (I.^2)./(StefBoltz.*radius.^2) + TempAmb.*h.*2.*(radius+radii_all)
     + emi*StefBoltz*TempAmb^4*2.*(radius+radii_all);
%TsA2 =
%((I.^2)./(sigmaAlum.*radius.^2.*emi.*StefBoltz.*2.*(radius+radii_all)) +
    (h*TempAmb-h)/(emi*StefBoltz) + TempAmb^4).^(1/4) ;

%% Loop
dif = 10;
i = 0;

while (dif>5)
    index = find(((TsC+8)>TsA)&((TsC-8)<TsA));
    index = floor(mean(index));
    rc = radius(index);
    Tscros = TsC(index);
    dif = abs(Ts-Tscros);
    Tsindex = find((Tstest>((dif./2)+Ts-2))&(Tstest<((dif./2)+Ts+2)));
```

```
    h = htest(Tsindex);
    TsA = (I.^2)./(sigmaAlum.*pi^2.*radius.^2.*h.*(radius+radii_all).*2)+
   TempAmb;
    Ts = Tstest(Tsindex);
    i =+1;
end


%% Check functions
Tsarray = linspace((40+273.15), (150+273.15), 1000);
FTs = h.*(Tsarray-TempAmb) + emi.*StefBoltz.*(Tsarray - TempAmb).^4;
Frc = (I.^2)./(2*sigmaAlum.*pi^2.*(radius+radii_all).*radius.^2);

%% Plotting

figure
plot(htest, Tstest-273.15)
title('h versus Ts')
ylim([0 50])
xlabel('h')
ylabel('Surface Temperature [°C]')

figure
plot(radius*1000, ti*1000)
title('3000V');
xlabel('Conductor radius [mm]');
ylabel('Thickness insulator [mm]');
%ylim([0 .1])

figure
%subplot(1,3,1);
plot(radius*1000, TsC-273.15);
title('1.62MW, 3000V, 120°C') %Compared to conductor
xlim([0 80]);
ylim([0 150]);
xlabel('Radius [mm]')
ylabel('Surface temperature [°C]')
hold on
plot(radius * 1000, TsA-273.15);
hold off
legend('Tc', 'Tamb')

%subplot(1,3,2);
%plot(radius*1000, TsC2-273.15);
%title('Radius vs Surface temperature') %Compared to conductor
%xlim([0 20]);
%xlabel('Radius [mm]')
%ylabel('Surface temperature [C]')
%hold on
%plot(radius * 1000, TsA-273.15);
%hold off

%subplot(1,3,3);
%plot(radius*1000, TsC3-273.15);
%title('Radius vs Surface temperature') %Compared to conductor
%xlim([0 20]);
```

```
%xlabel('Radius [mm]')
%ylabel('Surface temperature [C]')
%hold on
%plot(radius * 1000, TsA-273.15);
%hold off

%ylim([-50 200]);
%subplot(1,3,2);
%plot(radius * 1000, TsA-273.15);
%xlim([0 20]);
%ylim([-50 200]);
%title('Radius vs TsA');
%xlabel('Radius [mm]')
%ylabel('Surface temperature [C]')
%subplot(1,3,3);
%plot(radius*1000, TsA2-273.15);
%ylim([-50 200]);
%title('Radius vs TsA2');
%xlabel('Radius [mm]')
%ylabel('Surface temperature [C]')

figure

subplot(1,2,1);
plot(Tsarray - 273.15, FTs);
title('F(Ts)');
xlabel('Surface temperature [°C]')
subplot(1,2,2);
plot(radius*1000, Frc);
xlim([0 80]);
ylim([0 400]);
title('F(rc)');
xlabel('Conductor radius [mm]')

%% Plot mass
figure
plot(radius*1000, MassTotal)
title('Weight of cable for different radii')
ylim([0 50])
xlabel('Conductor radius [mm]')
ylabel('Weight [kg]')
hold on
plot(radius*1000, MassConAlu)
plot(radius*1000, NoCond)
hold off
legend('Total', 'Conductor', 'Rest')
```

E

Mass code results

E.1. 8 batteries

Cable name	Distance [m]	Length [m]	Weight [kg]
Hleft to busmotLeft	4.031129	5.4	19.818
Hleft to busmotMid	10.00312	12.3	246.738
Hleft to busbatLeft	6.046693	8.1	162.486
Hright to busmotMid	10.00312	12.3	246.738
Hright to busmotRight	4.031129	5.4	19.818
Hright to busbatRight	6.046693	8.1	162.486
B1L to busbatLeft	2.54951	3.6	2.016
B2L to busbatLeft	1.581139	2.4	1.344
B3L to busbatLeft	1.5	1.8	1.008
B4L to busbatLeft	2.5	3	1.68
B4R to busbatRight	2.5	3	1.68
B3R to busbatRight	1.5	1.8	1.008
B2R to busbatRight	1.581139	2.4	1.344
B1R to busbatRight	2.54951	3.6	2.016
M1L to busmotLeft	2.015564	2.7	1.512
M1L to busmotMid	16.00781	19.8	11.088
M2L to busmotLeft	2.136001	3.3	1.848
M2L to busmotMid	12	14.4	8.064
M3L to busmotMid	8.01561	10.2	5.712
M3L to busmotRight	22.03548	27.9	15.624
M4L to busmotMid	4.123106	6	3.36
M4L to busmotRight	18.08487	23.7	13.272
M4R to busmotLeft	18.08487	23.7	13.272
M4R to busmotMid	4.123106	6	3.36
M3R to busmotLeft	22.03548	27.9	15.624
M3R to busmotMid	8.01561	10.2	5.712
M2R to busmotMid	12	14.4	8.064
M2R to busmotRight	2.136001	3.3	1.848
M1R to busmotMid	16.00781	19.8	11.088
M1R to busmotRight	2.015564	2.7	1.512

Table E.1: 8 batteries cable information.

E.2. 4 batteries

Bus	Cables	Length [m]	Begin and End	Midpoint	Weight [kg]
Left battery bus	7	2.6	[-5.3, -2.7]	[-4, -1.5]	260.78
Right battery bus	7	2.6	[2.7, 5.3]	[4, -1.5]	260.78
Left motor bus	5	1.9	[-14.95, -13.05]	[-14, -1.25]	17.4325
Middle motor bus	10	3.65	[-1.825, 1.825]	[0, -0.5]	183.0475
Right motor bus	5	1.9	[13.05, 14.95]	[14, -1.25]	17.4325
Left H-bus	3	1.2	[-10.6, -9.4]	[-10, -0.75]	60.18
Right H-bus	3	1.2	[9.4, 10.6]	[10, -0.75]	60.18

Table E.2: 8 batteries bus information.

Cables	Circuit Breakers	Busses	Motor and Inverter	Total PMAD
2187.15 kg	690 kg	859.83 kg	326.6 kg	3736.98 kg

Table E.3: 8 batteries masses

Cable name	Distance [m]	Length [m]	Weight [kg]
mainbus to Hleft	10	12	44.04
mainbus to Hright	10	12	44.04
Hleft to busmot1	4	4.8	17.616
Hleft to busmot2	4.031129	5.4	19.818
Hright to busmot3	4.031129	5.4	19.818
Hright to busmot4	4	4.8	17.616
B1L to mainbus	2.692582	4.2	4.914
B2L to mainbus	1.802776	3	3.51
B2R to mainbus	1.802776	3	3.51
B1R to mainbus	2.692582	4.2	4.914
M1L to busmot1	2	2.4	1.344
M1L to busmot2	10.01249	12.6	7.056
M2L to busmot1	2.061553	3	1.68
M2L to busmot2	6	7.2	4.032
M3L to busmot3	14.00893	17.4	9.744
M3L to busmot4	22.02272	27.6	15.456
M4L to busmot3	10.04988	13.2	7.392
M4L to busmot4	18.06239	23.4	13.104
M4R to busmot1	18.06239	23.4	13.104
M4R to busmot2	10.04988	13.2	7.392
M3R to busmot1	22.02272	27.6	15.456
M3R to busmot2	14.00893	17.4	9.744
M2R to busmot3	6	7.2	4.032
M2R to busmot4	2.061553	3	1.68
M1R to busmot3	10.01249	12.6	7.056
M1R to busmot4	2	2.4	1.344

Table E.4: 4 batteries cables information.

Bus	Cables	Length [m]	Begin and End	Midpoint	Weight [kg]
Motor bus 1	5	1.9	[-14.95, -13.05]	[-14, -1]	17.4325
Motor bus 2	5	1.9	[-6.95, -5.05]	[-6, -0.5]	17.4325
Motor bus 3	5	1.9	[5.05, 6.95]	[6, -0.5]	17.4325
Motor bus 4	5	1.9	[13.05, 14.95]	[14, -1]	17.4325
Mainbus	6	2.25	[-1.125, 1.125]	[0, -1]	112.8375
Left H-bus	3	1.2	[-10.6, -9.4]	[-10, -1]	11.01
Right H-bus	3	1.2	[9.4, 10.6]	[10, -1]	11.01

Table E.5: 4 batteries bus information.

Cables	Converters	Circuit Breakers	Busses	Motor and Inverter	Total PMAD
793.40 kg	172.8 kg	615 kg	204.59 kg	326.6 kg	1785.79 kg

Table E.6: 4 battery masses.

F

Fault analysis

F.1. Fault analysis 8 batteries topology

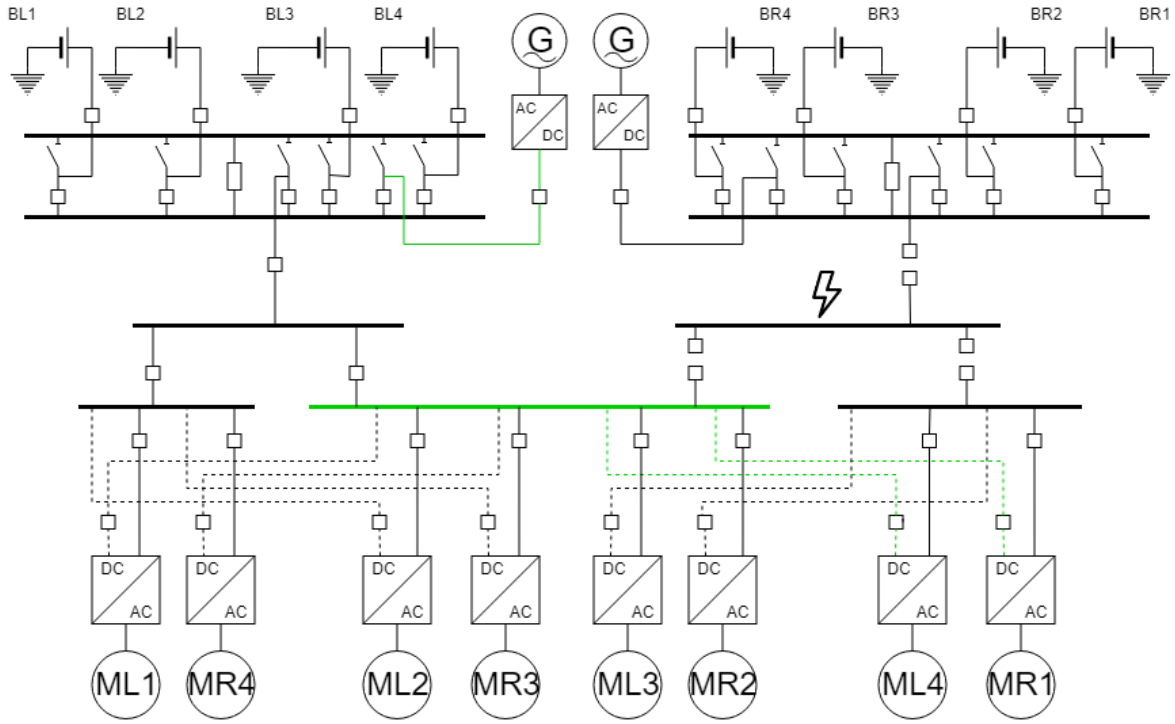

Figure F.1: Fault in the 8 battery topology at the H bus.

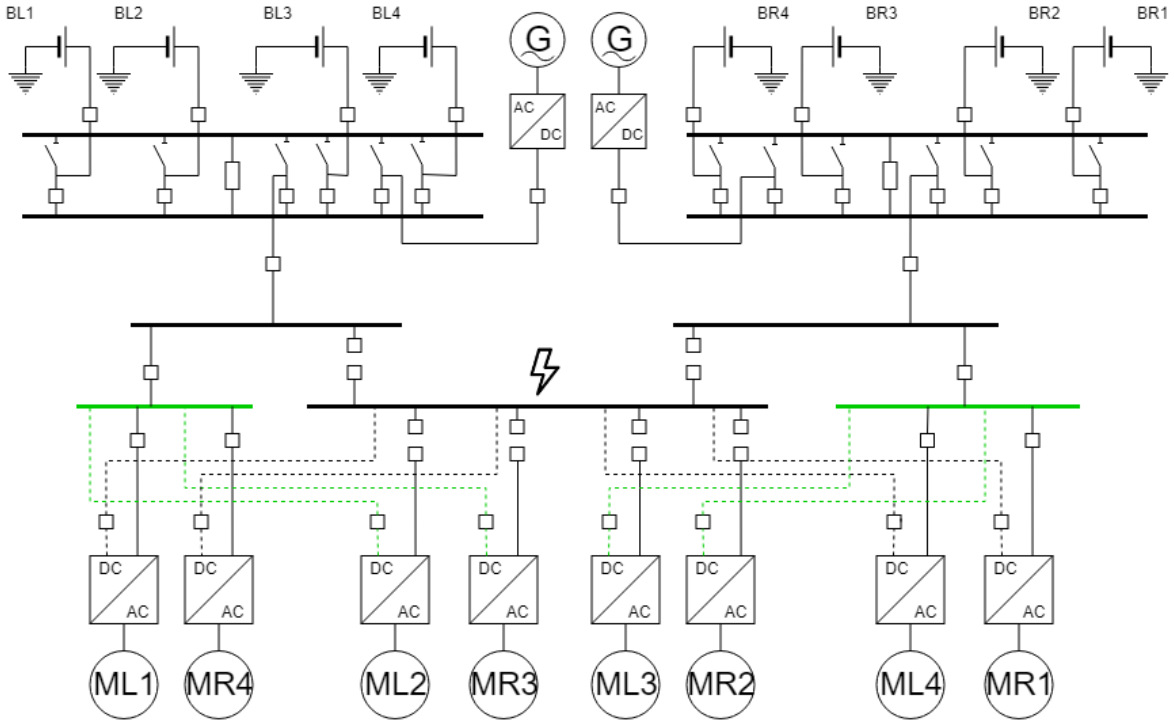

Figure F.2: Fault in the 8 battery topology at the middle motor bus.

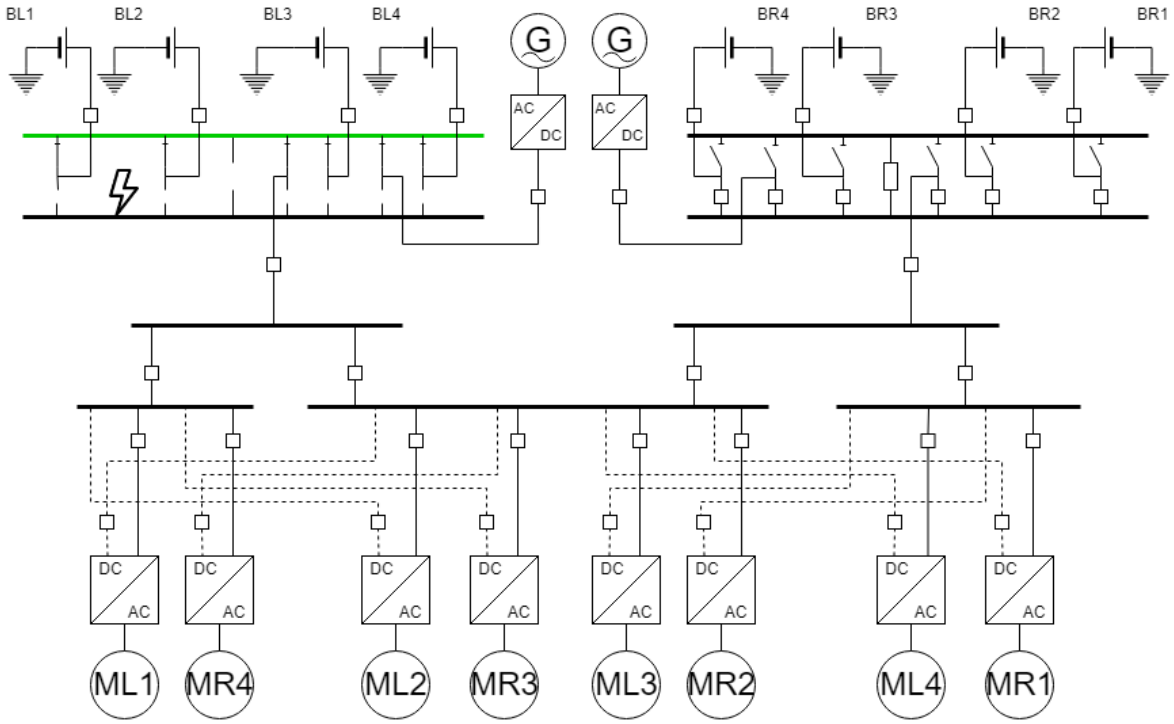

Figure F.3: Fault in the 8 battery topology at the battery bus.

F.2. Fault analysis 4 batteries topology

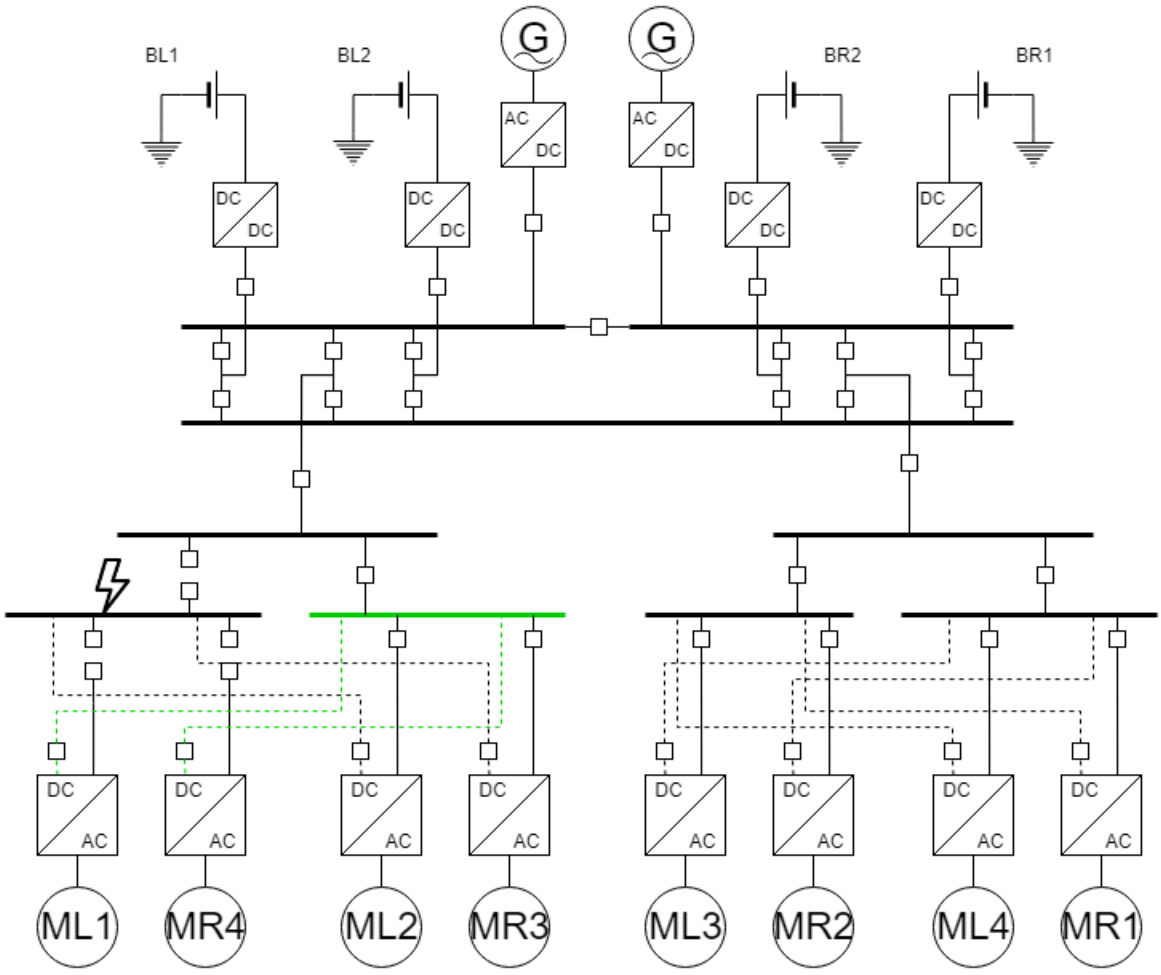

Figure F.4: Fault in the 4 battery topology at a motor bus.

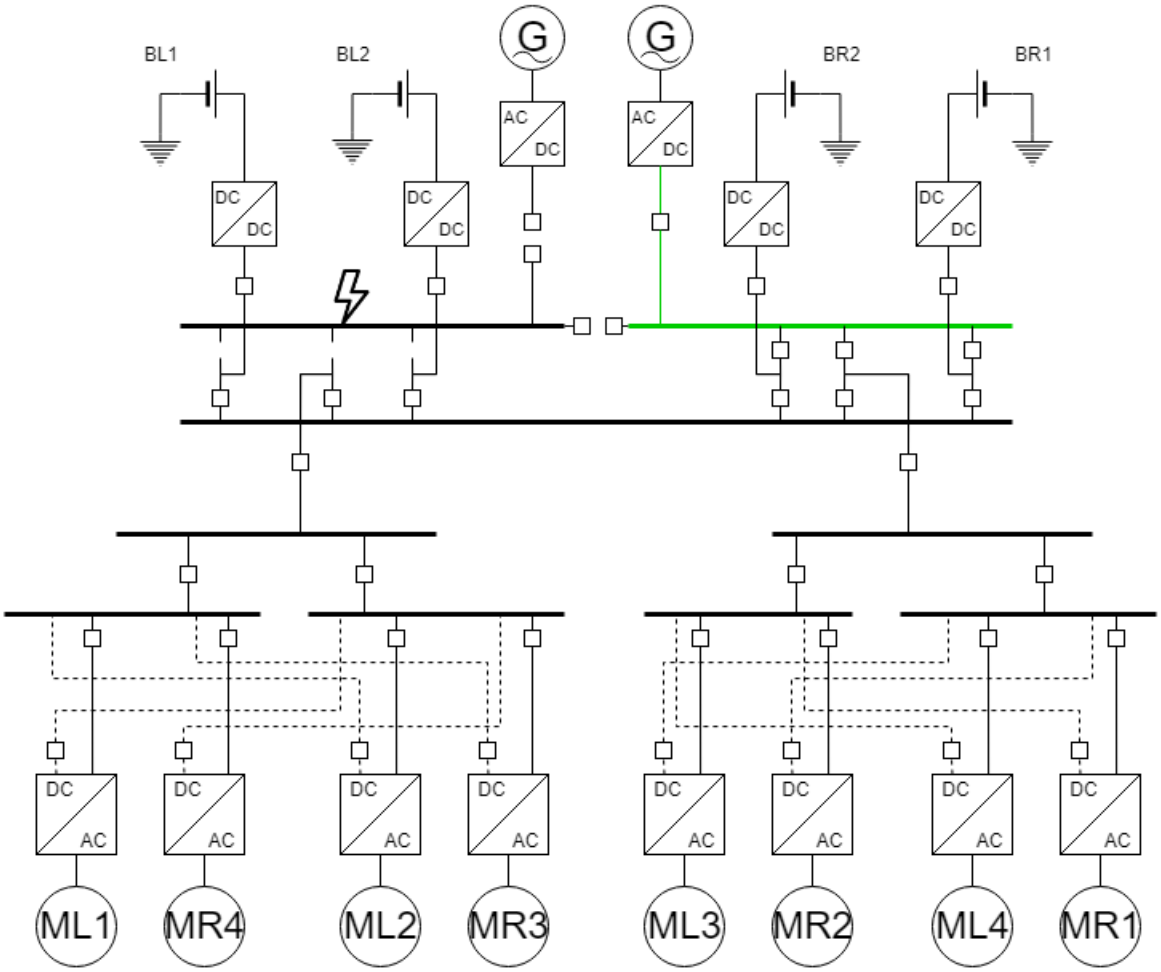

Figure F.5: Fault in the 4 battery topology at an upper battery bus.

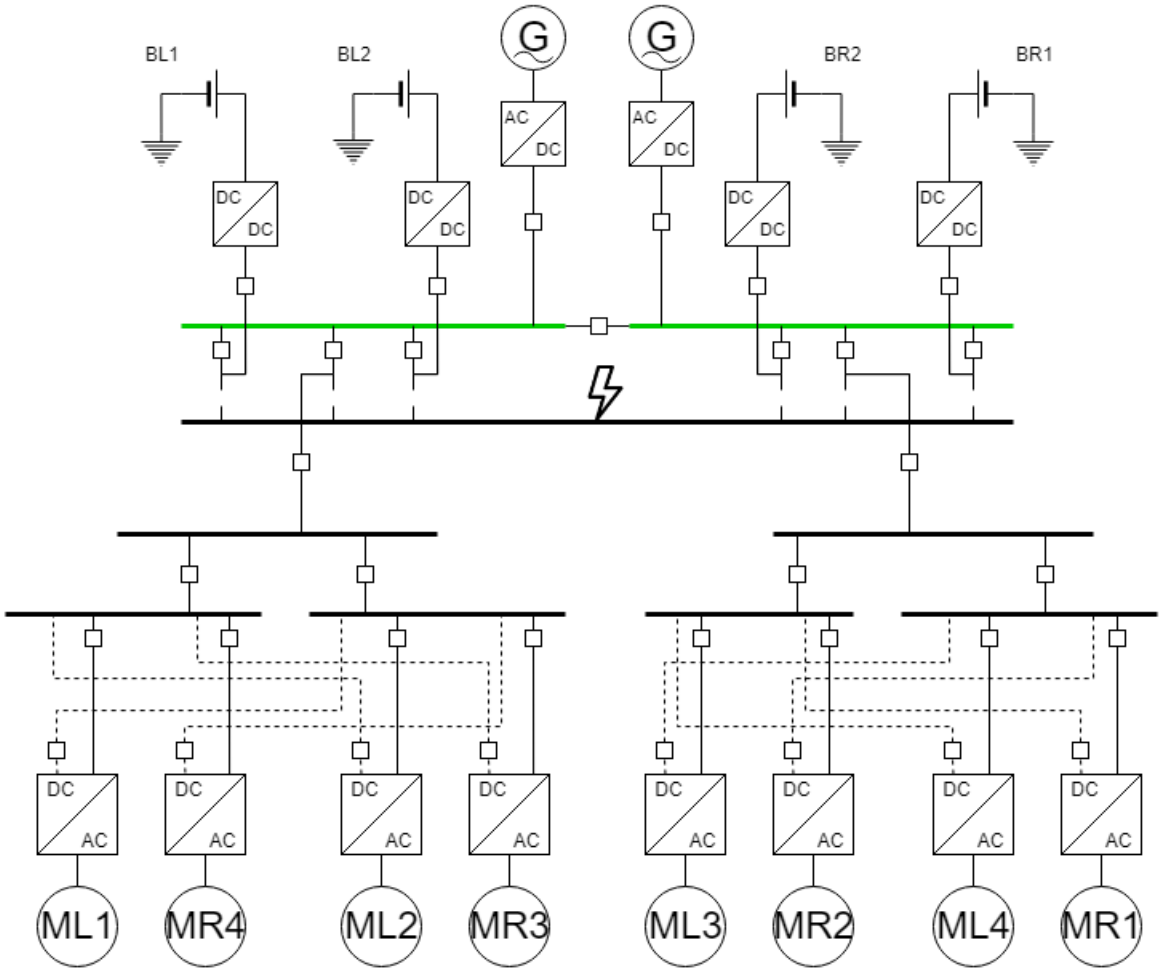

Figure F.6: Fault in the 4 battery bus at the lower battery bus.

F.3. Example grid fault analysis

Table F.1: Fault locations and corresponding breakers to be operated. [25]

Sl.no	Location of fault	Breakers to be operated
1	Phase A of generator G_{L1} shorted	Phase A breaker of G-CB
2	Three phases of generator G_{L1} shorted	All phase breakers of G-CB
3	Between AC–DC converter and TN1	AC–DC converter and TN2
4	Positive and ground between TN1 and TN2	TN1, TN2
5	Negative and ground between TN1 and TN2	TN1, TN2
6	Between MB3 and MB4	MB3, MB4 and TN1
7	Between MB1 and DB1	MB1, and DB2
8	Positive and ground between DB1 and DB2	DB1 and DB2
9	Negative and ground between DB1 and DB2	DB1 and DB2
10	Positive and negative between DB1 and DB2	DB1 and DB2
11	Between MB1 and MB2	MB1, MB2, MB3 and B2
12	Between MB2 and DB3	MB2 and DB4
13	Between MB1, MB2 and MB3	MB1, MB2, MB3
14	Positive and ground between DB3 and DB4	DB3 and DB4
15	Negative and ground between DB3 and DB4	DB3 and DB4
16	Positive and negative between DB3 and DB4	DB3 and DB4
17	Between MB5 and MB6	MB4, MB5 and MB6
18	Between MB5 and DB5	MB5, DB6
19	Between MB4, MB5 and MB6	MB4, MB5 and MB6
20	Positive and ground between DB5 and DB6	DB5 and DB6
21	Negative and ground between DB5 and DB6	DB5 and DB6
22	Positive and negative between DB5 and DB6	DB5 and DB6
23	Between MB6 and DB7	MB6 and DB7
24	Positive and ground between DB7 and DB8	DB7 and DB8
25	Negative and ground between DB7 and DB8	DB7 and DB8
26	Positive and negative between DB7 and DB8	DB7 and DB8
27	Between DB2 and DC–AC converter	DB1 and DC–AC converter
28	Between DB4 and DC–AC converter	DB3 and DC–AC converter
29	Between DB6 and DC–AC converter	DB5 and DC–AC converter
30	Between DB8 and DC–AC converter	DB7 and DC–AC converter
31	Between DC–AC converter and motor	M-CB and DC–AC converter
32	Internal fault in the motor	M-CB

Table F.2: Action of Circuit Breakers. [27]

S.no	Fault type	PFTA-1	PFTA-2
1	Generator Output terminals shorted	AC circuit breaker G1	AC circuit breaker G1
2	Front end active rectifier input A phase terminal shorted	A-phase CB of G1 - open	A-phase CB of G1 - open
3	Front end active rectifier input terminals shorted (2-phases)	all phase CB's of G1 - open	all phase CB's of G1 - open
4	Cable located between CB3 and CB4 is shorted	CB3, CB4	CB3, CB4
5	Cable located between CB5 and CB6 is shorted	CB5, CB6	CB5, CB6
6	Cable located between CB7 and CB8 is shorted	CB7, CB8	CB7, CB8
7	Cable located between CB9 and CB10 is shorted	CB9, CB10	CB9, CB10
8	DC/AC converter input terminals shorted in distribution network 1	CB3 and DC/AC converter	CB3 and DC/AC converter
9	DC/AC converter input terminals shorted in distribution network 2	CB5 and DC/AC converter	CB5 and DC/AC converter
10	DC/AC converter input terminals shorted in distribution network 3	CB7 and DC/AC converter	CB7 and DC/AC converter
11	DC/AC converter input terminals shorted in distribution network 4	CB9 and DC/AC converter	CB9 and DC/AC converter
12	Motor input terminals shorted	DC/AC converter	DC/AC converter
13	DC/DC converter input terminals shorted	DC/DC converter, B1	DC/DC converter and B1
14	DC/DC converter output terminals shorted	DC/DC converter, B2	DC/DC converter, B2
15	Short circuit between circuit breakers B2 and B3	B2 and B3	B2 and B3
16	Short circuit between circuit breaker B3 and main bus	B3, CB14, and CB15	B3, CB12, and CB13